NUMERICAL MODELING OF REACTIVITY EXCURSION ACCIDENTS IN SMALL LIGHT WATER REACTORS

Ph.D. Dissertation

Khaled Sayed Mahmoud

Department of Nuclear Techniques
Institute of Nuclear Techniques
Budapest University of Technology and Economics

Scientific Advisors
Szatmáry Zoltán, Dr. Sc.
Aszódi Attila, Dr.

Budapest, 2006

TO WHOM IT MAY CONCERN

We herby certify that this is a typical copy of the original Doctor Thesis of Mr. **Khaled Sayed Mahmoud** born in **December 13, 1968 Helwan, Egypt.**

Official Seal of the
Institute of Nuclear Techniques
Faculty of Natural Science
Budapest University of Technology and Economics

.

.....

..... :

"To the memory of my mother…"

Table of Contents

Table of Figures

List of Tables

Acknowledgments

First, I thank God for answering the prayers of many. He was faithful even when I was not. I acknowledge and praise Him for giving me the strength and wisdom necessary to accomplish this task.

This Ph.D. project is a fruit of this wonderful organized tree of cooperative work of the Nuclear Techniques Department, Institute of Nuclear Techniques that is being run by the faithful support of my Advisor Dr. Aszódi Attila I do thank him to provide the chance of updating my scientific skills in this excellent environment, many helpful discussions.

I do thank my Advisor Professor Szatmáry Zoltán who had save no effort to provide all of his scientific and technical experience available for me. I would like to thank him for the many fruitful discussions, cheerfully answering even my dumb questions, and for helping me to organize my thoughts in writing and reading this thesis. The years I spent in his companion have his own remarkable features had shaped a major part of my forthcoming career.

I do thank Professor Prof. Csom Gyula the Head of the System International Foundation to make funding of this project at the last one and half year possible.

All my deep respect and appreciation to the Hungarian Ministry of Education and the Egyptian Department General for Scholarships for funding this project. Special regards to Mr. András Tokai, Director of the International Coordination Department of Budapest University of Technology and Economics. I do thank the Egyptian cultural consoler of Egypt in Budapest Dr.Hesham Shafik for support and help.

For all of my colleagues and friends who helped me to overcome this period of time in Hungary I do thank them.

The permanent support of my dear wife and family members can never be thanked by words.

Chapter 1 Introduction

1.1. What is the Reactivity Excursion

Water moderator nuclear power plant generating electricity basically consists of a steam supply system, called the reactor core, and a turbo generator [1]. The primary energy in a nuclear power plant is generated by nuclear reactions induced by neutrons, which take place in the core of the reactor. This primary energy appears as heat that is transferred to water. The steam produced is then expanded in the turbine producing mechanical work which is used to produce electricity. The steam then condenses into water which is returned to the reactor core as feed water in a closed loop [2].

For the safety analysis of nuclear power plants, complex calculation models are used consisting of two modules: a neutronic module describing the neutron balance in the reactor core, and a thermal-hydraulic module simulating the heat transfer from the fuel to the water used as a coolant, and the various evaporation and condensation processes which take place in the reactor core and in the condenser systems. The coupling between these two modules is different for each code depending on the numerical schemes used to integrate the whole set of equations constituting the model of the plant [3]. These kinds of nuclear power plant models are too complicated for being applied to research reactors. The later require their own models.

One of the accidents to be analyzed using such calculation models is the reactivity accident or power excursion. The subject of the present thesis is to describe a model developed for this purpose for the Training and Research Reactor of the Budapest University of Technology and Economics, (BME-Reactor in the following). The root cause of the investigated hypothetical accident is not the subject of the thesis. We simply assume that, following a steady-state operation, some reactivity is inserted into the reactor and the safety rods fail to operate.

The conceivable effects of reactivity excursion accidents can vary widely from one reactor type to another and from one reactor design to another with a given type. Some reactors can be shown to be relatively immune to them. However, as a class, they include some of the most severe accidents that can be visualized. If the normal protection circuits on a reactor fail to operate or are ineffectual, a reactivity excursion can result in local to general core damage, and even release radioactive fission products. We mention in the next subsections some of the possible causes of such accident.

1.1.1. Uncontrolled Control Rod Withdrawal

This accident is frequently analyzed in safety reports, not because it is considered a probable one, but because it is easily defined and, if the initial conditions are properly chosen, defines the upper limit of the possible consequences of control rod malfunction. It may be visualized as the continuous withdrawal of control rods at their maximum attainable speed without regard for any warnings or stop signals which may be given by the reactor instrumentation. Consequently, one can think of some malfunction of the circuitry to the control rod drives which would prevent them from being turned off once they were set in motion.

1.1.2. Mechanical Failure of Control Rod or Control Rod System

Fail-safe mechanical design is an important consideration in limiting the amount of reactivity that can be added and the speed with which it can be added when a control rod fails mechanically. This can be handled by various design techniques of the control rods. Also, the cold water accident and the loss off coolant accident also can be a source of power excursion problems [4].

1.2. The Construction of the BME-Reactor

The BME-Reactor became critical in 1971. It is a tank type reactor, which is located on the site of the University. It is designed to be compact and safe and it is used mainly for neutron activation analysis, production of short-lived radioisotopes and for education and training. Its maximal thermal power is 100 kW. The cylinder-shaped tank is 1.4 m in diameter and filled with desalted water. The coolant level is 5750 mm. The reactor core is made up of 24 EK-10 type fuel assemblies, which contain 369 fuel rods altogether. Their active length is 500 mm. The fuel is 10% enriched uranium dioxide in magnesium matrix. Each regular fuel assembly contains 16 fuel rods arranged in a four by four square lattice with a pitch of 17.5 mm. The reactor core is moderated and cooled by light water. The reactor core is cooled by the natural convection of the coolant below 10 kW power. Over 10 kW, the coolant is forced at a volumetric flow 5.8 m3/h. The reflector is graphite surrounded by water [5, 6], see Figure 1.

The coolant enters into the tank at the bottom and is led off through a pipe at about 1200 mm above the top of the core. This means that a slightly forced buoyant flow can be observed while the cooling loop works, other details can be found in references [5, 7], see Figure 2.

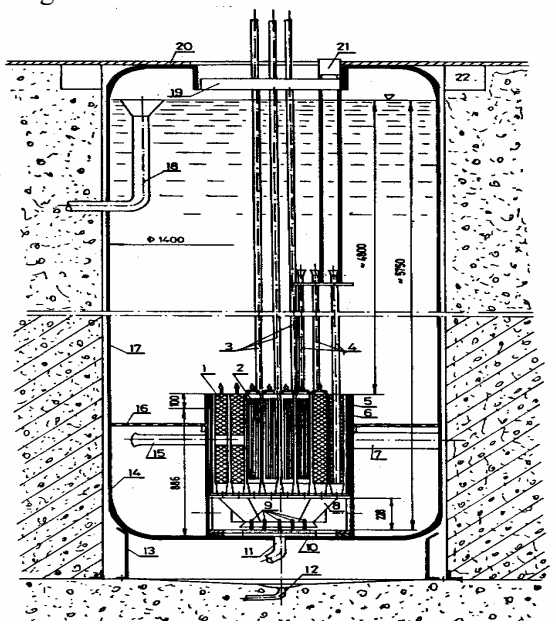

Figure 1. Vertical cross section of the BME-Reactor
1- Graphite Reflector Elements; 2-Fuel Assemblies; 3-Safety and Control Rods; 8-Diffuser; 9-Injectors; 11-Coolant Inlet

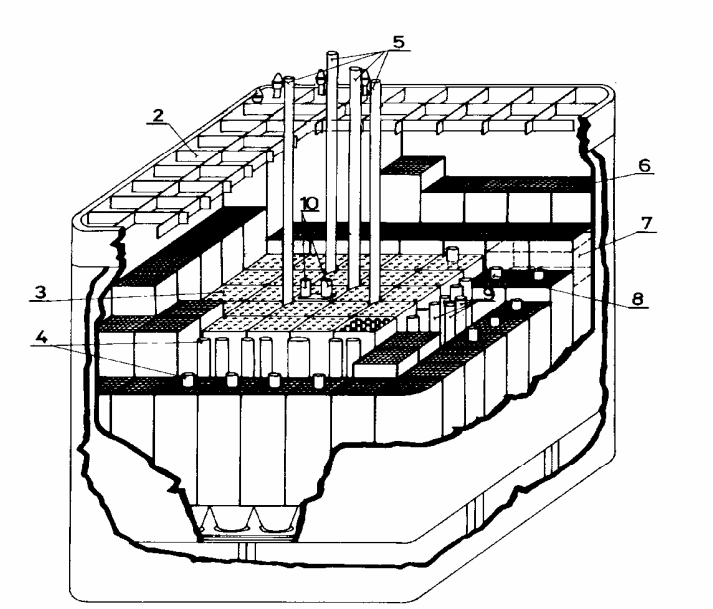

Figure 2. Structure of the BME-Reactor core
3-Fuel Assemblies; 5-Safety and Control Rods; 6- Graphite Reflector Elements

1.3. The System of Equations to be Solved

The training reactor, being located in the downtown of Budapest, has to satisfy special safety requirements, namely, it has to be inherently safe. It is required by the safety authority that the safety report of the reactor proved that such an accident could not lead to core damage and release of radioactive material. The former safety report written in 1996 used a combination of point reactor kinetic code REMEG and module HEATING of the SCALE 4.1 program system [7]. This study was accepted at that time but the excess reactivity may not be increased until the study is repeated by a more detailed and mathematically better founded computer model.

The actual excess reactivity of the reactor is 0.82 $ which means that no power excursion is possible in the strict sense of the word. In 1996, this excess reactivity value was estimated to be between 1.04 $ and 1.10 $. Such values would not allow serious reactivity accidents either. At the same time, certain irradiation experiments regularly performed at a power of 100 kW during 8 hours use up practically all this excess reactivity: 0,6 to 0,7 $ are lost due to the xenon and the temperature effects. Therefore, the control of the reactor becomes rather difficult during the last hours of the irradiations. Consequently, the excess reactivity needs to be increased to a value what the reactor had in 1980, i.e. near 1.2 $ in order to restore the original flexibility of the reactor operation.

The reactor can get permission for achieving this only if we are able to prove that even a prompt supercritical state of 1.2 $ can not result in a reactivity accident leading to core damage. It is trivial that it is not possible to check this statement experimentally at this reactor. Thus, we need a computer model simulating this accident. The first question that naturally arises is whether such a model is available in international

computer libraries. The answer is simply no because there are very few reactors operating with EK–10 type fuel elements (either research or training reactors). Such reactors were built in the former Soviet Union and socialist countries but most of them have been upgraded to higher powers by replacing the fuel rods with other types. For example, the 2 MW Budapest Research Reactor was upgraded to 5 MW in 1965 when the EK–10 fuel elements were replaced by tubular fuel clusters containing three coaxial tubes. This explains why no computer model is actually available for this particular fuel type, consequently, we had to develop our own model.

The second question is what kind of a computer model we need. A power excursion is stopped only by the feedback through the temperature coefficients (both Doppler and moderator). It follows from this that only a time dependent neutronic code with thermal-hydraulic feedback could be acceptable. Since the coolant flows axially leading to an axial variation of the temperature (as a function of the z-variable), the neutronic part of the model should solve at least the 1D space-time dependent equation. In this small core, the radial flux variations are important which cause a strong radial temperature dependence of the heat generation, too. The core has some asymmetry in x- and y-directions, thus, it is advisable to take into account the radial variations in x-y geometry. We come now to the final conclusion that we need a 3D space-time dependent model with thermal-hydraulic feedback. Similar codes at other reactors are based on the diffusion equation. This approximation should be sufficient for our case, too. There are codes which use finite elements while others use finite differences. The latter seemed to be simpler and more accurate because we could afford to put a mesh point in every elementary cell. We write the neutronic equation to be solved in the following form [8]:

$$\frac{1}{v_g}\frac{\partial \phi_g(\mathbf{r},t)}{\partial t} = \nabla\left(D_g(\mathbf{r})\nabla\phi_g(\mathbf{r})\right) - \Sigma_g^{\mathrm{t}}(\mathbf{r})\phi_g(\mathbf{r},t) + \sum_{\substack{g'=1 \\ g'\neq g}}^{G}\Sigma_{g'\to g}(\mathbf{r})\phi_{g'}(\mathbf{r},t) +$$

$$+ (1-\beta)\chi_g^{\mathrm{p}}\sum_{g'=1}^{G}\nu\Sigma_{g'}^{\mathrm{f}}(\mathbf{r})\phi_{g'}(\mathbf{r},t) + \sum_{m=1}^{M}\lambda_m\chi_{mg}C_m(\mathbf{r},t), \quad g=1,2,...,G \tag{1.1}$$

The notations are standard and they will be explained later. The concentrations of the M families of delayed neutron precursors are described by the set of equations:

$$\frac{\partial C_m(\mathbf{r},t)}{\partial t} = \beta_m\sum_{g=1}^{G}\nu\Sigma_g^{\mathrm{f}}(\mathbf{r})\phi_g(\mathbf{r},t) - \lambda_m C_m(\mathbf{r},t), \qquad m=1,2,...,M\,. \tag{1.2}$$

The thermal-hydraulic feedback is taken into account in the following way. The coolant flow is axial and is localized inside the fuel cluster. Therefore, it seemed to be sufficient to consider the flow inside a fuel channel, i.e. we neglect the cross-channel mixing. The heat transfer from the fuel to the coolant is described by the time dependent radial heat conduction equation [9] in radial geometry:

$$\rho C_p\frac{\partial T}{\partial t} = \frac{1}{r}\frac{\partial}{\partial r}\left(rk\frac{\partial T}{\partial r}\right) + \dot{q}_v \tag{1.3}$$

In two-phase flow the vapor and liquid move at the same velocity (no slip), and the lateral variations of properties in the flow channels can be neglected the flow conservation equation can takes the following form [10-12].

Conservation of mass:

$$\frac{\partial \rho_m}{\partial t} + \frac{\partial G_m}{\partial z} = 0 \tag{1.4}$$

Conservation of momentum:

$$\frac{\partial G_m}{\partial t} + \frac{\partial}{\partial z}\left(\frac{G_m^2}{\rho_m}\right) = -\frac{\partial P}{\partial z} - \frac{f G_m \mid G_m \mid}{2 D_e \rho_m} - \rho_m g \tag{1.5}$$

Conservation *of energy:*

$$\rho_m \frac{\partial h_m}{\partial t} + G_m \frac{\partial h_m}{\partial z} = \frac{q'' P_h}{\partial t} + \frac{\partial P}{\partial t} + \frac{G_m}{\rho_m}\left[\frac{\partial P}{\partial z} + \frac{f G_m \mid G_m \mid}{2 D_e \rho_m}\right] \tag{1.6}$$

The set of Equations (1.1)-(1.6) in addition to some constitutive equations represent the equations to be solved. We shall refer back to these equations later and they will be described in more detailed way.

1.4. Treatment of Time and Space Variables

For the time dependent of the previous equations, the fully implicit (backward) difference scheme is used to discretize the time variable, in both Equations (1.1) - (1.3) while the explicit (forward) difference scheme [13-16] has been used in Equations (1.4)-(1.6). For the spatial dependence, the three dimensional mesh cell centered formulation has been used in Equations (1.1)-(1.3), for the thermal-hydraulics Equations (1.4)-(1.6) a one dimensional mesh cell centered has been used to discretized the moderator enthalpy and density, Equations (1.4) and (1.6), while the mass flux is defined at the cell boundary, Equation (1.5). Also the mesh centered formulation is used also for the radial dependence of the heat conduction, Equation (1.3).

1.5. The Developed Integrated Neutronic/Thermal-hydraulic Code

A complete new 3D neutronic/thermal-hydraulic model has been developed and applied to simulate the power excursion accidents in the BME-Reactor induced by positively reactivity insertions. Validation of the code is beyond the scope of this thesis. In spite of this, we have tried to use any means for verifying the code by comparing the results of the code with the following:

- The start up experiment perturbed on the BME-Reactor was interpreted as quantitative verification.
- The point kinetic program REMEG [17, 7] developed for educative purposes. Of course, this can be only a qualitative verification.
- The sudden pressure reduction in the inlet pressure transient, for the thermal-hydraulic part only.

The group constants were calculated by WIMS-D4 code [18] while delayed neutron parameters were calculated using GRACE and THERMOS [19, 20]. This study together with the verifications represents the nuclear safety analysis of the BME-Reactor and will be included in the nuclear safety report of the BME-Reactor.

1.6. Structure of the Dissertation

Following the present introductory chapter, Chapter 2 gives a description, features and assumptions for some known previous reactivity excursion models. Chapter 3 outlines the basic iteration schemes for solving the 3D finite difference equations, namely, forward, backward and source iteration schemes which represent the basic tools used in this thesis. It gives the details of our new iterative scheme for solving the finite difference equation. The new scheme simplifies the treatment of the delayed neutron precursors and avoids the difficulties associated with the usual source iteration. Also, detailed study of the stability and the convergence of our scheme have been proved. Moreover, an analysis of the convergence of the Gauss-Siedel iteration and its effect on the eigenvalue were proved. Chapter 4 contains the thermal-hydraulics feedback calculations, cross-section generation and the coupling of the 3D-neutronic and thermal-hydraulic parts in addition to verification the thermal-hydraulic code for specific type of operational transient for BWR reactor type and the BME-Reactor, and the group constants generation. Chapter 5 contains the nuclear safety analysis of the BME-Reactor and verifications of the integrated neutronic/thermal-hydraulic code namely, the start up experiment and comparison with point reactor kinetic code REMEG. Also, the final results, conclusions and suggestions were included.

Each chapter is begin with the main target in short way and over with “discussion and conclusion” section to summarize its contents followed by “one step forward” section that links the next chapter as a brief introduction. Appendix A, gives a flow chart of the solution strategy of the integrated neutronic/thermal-hydraulic code.

1.7. Discussion and Conclusions

In conclusion, one can point out that this coupled neutronic/thermal-hydraulics analysis generally provides the following advantages:

- Predicting the core dynamics behavior and Safety of nuclear reactors.
- Establishing the full power output and transient and natural convection circulation behavior of the reactor.
- Determining the performance of the reactor system components.
- Influencing the flux distribution and the dynamic reactivity coefficients in the reactor core [21].

1.8. One Step Forward

Now we know the problem to be solved, why needs the reactor a coupled thermal-hydraulic neutronics model and what is it good for. The next chapter is a survey review the previous available models and techniques used to simulate the power excursion accidents using the coupled neutron/thermal-hydraulic calculation models.

Chapter 2 Reactivity Excursion Models

As explained in section 1.3, the accident analysis and reactor safety for the BME-Reactor require coupled neutron kinetic and thermal-hydraulic calculation. For severe core accident analysis the three-dimensional kinetic model is necessary to obtain the satisfactory transient results.

This chapter describes some of the existing coupled neutronic/thermal-hydraulic models which are available. All such models should solve a coupled set of equations representing both the neutronic and thermal-hydraulic fields.

2.1. Point Kinetic Dependent Models

Generally, the use of a large code requires a considerable amount of effort and skill with respect, in particular, to input preparation and output processing. This sometimes is hardly affordable by small research reactor operators, who are frequently required to perform transient analysis in order to deal with the safety review of proposed changes. Indeed, contrary to power reactors, research reactor operation is characterized by frequent core modifications, as required to respond to the changing experimental needs. Many models for coupled kinetics and thermal-hydraulics consider a point reactor [22]. In the following, examples of such models will be described.

2.1.1. REMEG Model

Since the REMEG Code [17] represent one tool of verifying our work which simulate the power excursion accident of the BME-Reactor and the related power safety requirements of it, we shall gave the description of this code in a brief way. Of course, comparisons with REMEG can give only a qualitative verification.

The physical-mathematical model of the REMEG program is composed of three sub-models:

1. The reactor kinetics equations.
2. The fuel temperature sub-model.
3. The coolant temperature sub-model.

In the following, the three sub-models are described.

a) Reactor kinetics

For the calculation of the energy released in the fuel the point kinetic equations are used:

$$\frac{dn(t)}{dt} = \frac{\beta}{\ell}[\rho(t) - 1] \cdot n(t) + \sum_{i=1}^{6} \lambda_{\mathrm{i}} C_{\mathrm{i}}(t) \tag{2.1}$$

$$\frac{dC_{\mathrm{i}}(t)}{dt} = \frac{\beta_{\mathrm{i}}}{\ell} n(t) - \lambda_{\mathrm{i}} C_{\mathrm{i}}(t), \quad \mathrm{i} = 1, 2, \ldots 6 \tag{2.2}$$

where

n Number of neutrons (which is proportional to the power generated in the fuel) [1/cm^3];

t Time [s];

β Total delayed neutron fraction [1];

ℓ Average neutron generation time [s];

ρ Reactivity [$];

λ_{i} Decay constant of the delayed neutrons belonging to the i$^{\mathrm{th}}$ group [1/s];

C_{i} Number of precursor nuclei of the delayed neutrons belonging to the i$^{\mathrm{th}}$ group [1/cm^3];

β_{i} Partial delayed neutron fraction of the i$^{\mathrm{th}}$ group [1].

The power generated in the reactor core (P_{k}) is proportional to the number of neutrons:

$$P_{\mathrm{k}}(t) = c_{\mathrm{k}} \cdot n(t) \tag{2.3}$$

where c_{k} is a properly chosen constant [Wcm^3].

The reactivity has three components:

$$\rho = \rho_{\mathrm{r}} + \rho_{\mathrm{f}} + \rho_{\mathrm{m}} \tag{2.4}$$

where

ρ_{r} Reactivity which can be inserted by removing the control rods (or by other means).

ρ_{f} Reactivity feedback from the change of the fuel temperature;

ρ_m Reactivity feedback from the change of the moderator (coolant) temperature.

We assume in the model that ρ_f and ρ_m are linear functions of the temperatures, i.e.:

$$\rho_f = c_D(T_f - T_{f,0}) \tag{2.5}$$

$$\rho_m = c_m(T_{ave} - T_{ave,0}) \tag{2.6}$$

where

$T_f(t)$ Average fuel temperature (as a function of time) [°C];

$T_{f,0}$ $T_f(t=0)$, i.e. fuel temperature at t = 0 (at the start of modeling) [°C];

c_D Doppler coefficient [$/K];

$T_{ave}(t)$ Average moderator (coolant) temperature (as a function of time) [°C];

$T_{ave,0}$ $T_{ave}(t=0)$, i.e. average moderator (coolant) temperature at t = 0 (at the start of modeling) [°C];

c_m Moderator temperature coefficient of the reactivity [$/K].

The model makes it possible to take into account the decay heat power (P_d) of the fission products. This component of the power has to be given by the user as a ratio to the initial total power. The total power released in the reactor core is always the sum of prompt and decay heat power:

$$P = P_k + P_d. \tag{2.7}$$

b) Fuel temperature

The fuel temperature sub-model calculates the heat transfer from the fuel through the cladding into the moderator. The gap between the fuel and the cladding is also taken into account; however its heat capacity is ignored. In addition to the convective heat the energy removed from the fuel by radiation (gamma- and heat radiation) and released in the moderator is also calculated. The ratio of this radiation power to the total one can be set by the user.

The fuel and cladding temperatures are calculated according to the following energy balance equations:

$$\mathrm{M_f} \cdot C_{\mathrm{pf}}[T_{\mathrm{f}}(t)]\frac{dT_{\mathrm{f}}(t)}{dt} = \eta P(t) - U_{\mathrm{fc}}[T_{\mathrm{f}}(t)] \cdot (T_{\mathrm{f}}(t) - T_{\mathrm{c}}(t)) \tag{2.8}$$

$$\mathrm{M_c} \cdot C_{\mathrm{pc}}[T_{\mathrm{c}}(t)]\frac{dT_{\mathrm{c}}(t)}{dt} = U_{\mathrm{fc}}[T_{\mathrm{f}}(t)] \cdot (T_{\mathrm{f}}(t) - T_{\mathrm{c}}(t)) - Q_{\mathrm{cm}}\ , \tag{2.9}$$

where

M_{f} Total mass of the fuel present in the reactor core [kg];

C_{pf} Specific heat of the fuel [J/kg/K];

T_{f} Average temperature of the fuel [°C];

η Ratio of the power released in the fuel to the total power [1];

U_{fc} Coefficient of the heat transfer from the fuel into the cladding, for the whole reactor core [W/K];

T_{c} Average temperature of the cladding [°C];

M_{c} Total mass of the cladding present in the reactor core [kg];

C_{pc} Specific heat of the cladding [J/kg/K];

Q_{cm} Heat transfer from the cladding into the moderator [J].

The changes of the heat transfer coefficient U_{fc}, and of the specific heats C_{pf} and C_{pc} with the fuel and cladding temperatures are taken into account in the model and they are calculated according to the following formulae:

$$U_{\mathrm{fc}} = (\mathrm{f}_0 + \mathrm{f}_1 \cdot T_{\mathrm{f}} + \mathrm{f}_2 \cdot T_{\mathrm{f}}^{\,2})\frac{\mathrm{F_b}}{\mathrm{d}}, \tag{2.10}$$

where

f_0 Zero order coefficient [W/K/m];

f_1 First order coefficient [W/K/m/°C];

f_2 Second order coefficient [W/K/m/°C^2];

$\mathrm{F_b}$ Area of the cladding inner surface, for the whole reactor core [m^2];

d Effective thickness of the gap between the fuel and cladding [m].

$$C_{\mathrm{pf}} = \mathrm{c}_{\mathrm{f0}} + \mathrm{c}_{\mathrm{f1}} \cdot T_{\mathrm{f}} + \mathrm{c}_{\mathrm{f2}} \cdot T_{\mathrm{f}}^{\,2}, \tag{2.11}$$

where

c_{f0} Zero order coefficient [J/kg/K];

c_{f1} First order coefficient [J/kg/K /°C];

c_{f2} Second order coefficient [J/kg/K /°C^2].

$$C_{pc} = c_{c0} + c_{c1} \cdot T_c + c_{c2} \cdot T_c^{\,2}, \tag{2.12}$$

where

c_{c0} Zero order coefficient [J/kg/K];

c_{c1} First order coefficient [J/kg/K /°C];

c_{c2} Second order coefficient [J/kg/K /°C^2].

c) Coolant temperature

The coolant (moderator) temperature is calculated according to the following energy balance equations:

$$M_m \cdot C_{pm}[T_{ave}(t)]\frac{dT_{ave}(t)}{dt} = Q_{cm} + (1-\eta)P(t) + \\ + W_{core} \cdot C_{pm}[T_{ave}(t)] \cdot (T_{out}(t) - T_{in}(t)) \tag{2.13}$$

where

M_m Total mass of the coolant (moderator) present in the reactor core [kg];

C_{pm} Specific heat of the coolant [J/kg/K];

T_{ave} Average coolant temperature (in the reactor core) [°C];

T_{out} Outlet coolant temperature [°C];

T_{in} Inlet coolant temperature [°C];

W_{core} Coolant mass flow rate (through the reactor core) [kg/s].

The heat transfer from the cladding into the coolant is calculated as follows:

$$Q_{cm} = U_{cm} \cdot (T_c - T_{ave}), \tag{2.14}$$

where

U_{cm} Coefficient of the heat transfer from the cladding into the coolant, for the whole reactor core [W/K].

The changes of the heat transfer coefficient U_{cm} and of the specific heat C_{pm} with the cladding and coolant temperatures are taken into account in the model and they are calculated according to the following formulae:

$$U_{cm} = \frac{(m_0 + m_1 \cdot T_{ave} + m_2 \cdot T_{ave}^2) \cdot (T_c - T_{ave})^{0.1} \cdot F_k}{(c_0 + c_1 \cdot T_c + c_2 \cdot T_c^2)^{0.24}}, \tag{2.15}$$

where

m_0 Zero order coefficient [W/K/m^2];

m_1 First order coefficient [W/K/m^2/°C];

m_2 Second order coefficient [W/K/m^2/°C^2];

F_k Area of the cladding outer surface, for the whole reactor core [m^2];

c_0 Zero order coefficient [1];

c_1 First order coefficient [1/°C];

c_2 Second order coefficient [1/°C^2].

$$C_{pm} = c_{m0} + c_{m1} \cdot T_{ave} + c_{m2} \cdot T_{ave}^2, \tag{2.16}$$

where

c_{m0} Zero order coefficient [J/kg/K];

c_{m1} First order coefficient [J/kg/K /°C];

c_{m2} Second order coefficient [J/kg/K /°C^2].

We assume that the average coolant temperature is equal to the mean of the inlet and outlet coolant temperatures, i.e.:

$$T_{ave} = \frac{T_{in} + T_{out}}{2}. \tag{2.17}$$

d) The coupled system of differential equations

The three sub-models described above contain all together 10 differential equations. The 10 unknown functions to be determined are the following:

$$P_k(t);\ \mathrm{C}_1(t),...,C_6(t);T_f(\mathrm{t});T_{ave}(\mathrm{t});T_c(\mathrm{t})$$

and the coupled system of differential equations to be solved:

$$\frac{dP_{\mathrm{k}}(t)}{dt}=\frac{\beta}{\ell}[\rho(t)-1]P_{\mathrm{k}}(t)+\sum_{i=1}^{6}\lambda_{\mathrm{i}}C_{\mathrm{i}}(t) \tag{2.18}$$

$$\frac{dC_{\mathrm{i}}(t)}{dt}=\frac{\beta_{\mathrm{i}}}{\ell_{\mathrm{i}}}P_{\mathrm{k}}(t)-\lambda_{\mathrm{i}}C_{\mathrm{i}}(t),\quad \mathrm{i}=1,2,...6 \tag{2.19}$$

$$\frac{dT_{\mathrm{f}}(t)}{dt}=\frac{\eta\cdot[P_{\mathrm{k}}(t)+P_{\mathrm{d}}(t)]-U_{\mathrm{f}}[T_{\mathrm{f}}(t)]\cdot[T_{\mathrm{f}}(t)-T_{\mathrm{c}}(t)]}{\mathrm{M}_{\mathrm{f}}\cdot C_{\mathrm{pf}}[T_{\mathrm{f}}(t)]} \tag{2.20}$$

$$\frac{dT_{\mathrm{c}}(t)}{dt}=\frac{U_{\mathrm{fc}}[T_{\mathrm{f}}(t)]\cdot[T_{\mathrm{f}}(t)-T_{\mathrm{c}}(t)]-U_{\mathrm{cm}}[T_{\mathrm{c}}(t),T_{\mathrm{ave}}(t)]\cdot[T_{\mathrm{c}}(t)-T_{\mathrm{ave}}(t)]}{\mathrm{M}_{\mathrm{c}}\cdot C_{\mathrm{pc}}[T_{\mathrm{c}}(t)]} \tag{2.21}$$

$$\frac{dT_{\mathrm{ave}}(t)}{dt}=\frac{U_{\mathrm{cm}}[T_{\mathrm{c}}(t),T_{\mathrm{ave}}(t)]\cdot[T_{\mathrm{c}}(t)-T_{\mathrm{ave}}(t)]+(1-\eta)\cdot[P_{\mathrm{k}}(t)+P_{\mathrm{d}}(t)]}{\mathrm{M}_{\mathrm{m}}\cdot C_{\mathrm{pm}}[T_{\mathrm{ave}}(t)]}-$$

$$-\frac{\mathrm{W}_{\mathrm{core}}\cdot C_{\mathrm{pm}}[T_{\mathrm{ave}}(t)]\cdot 2\cdot[T_{\mathrm{ave}}(t)-T_{\mathrm{in}}(t)]}{\mathrm{M}_{\mathrm{m}}\cdot C_{\mathrm{pm}}[T_{\mathrm{ave}}(t)]}. \tag{2.22}$$

The ρ(t) is an input function; the REMEG program allows a linear change in time for ρ(t). In stationary state the temperatures can be calculated by the following equations:

$$T_{\mathrm{ave}}=\frac{P}{2\cdot\mathrm{W}_{\mathrm{core}}\cdot C_{\mathrm{pm}}}+T_{\mathrm{in}} \tag{2.23}$$

$$T_{\mathrm{c}}=\frac{\eta P}{U_{\mathrm{cm}}}+T_{\mathrm{ave}} \tag{2.24}$$

$$T_{\mathrm{f}}=\eta P\left(\frac{1}{U_{\mathrm{fc}}}+\frac{1}{U_{\mathrm{cm}}}\right)+T_{\mathrm{in}}+\frac{P}{2\cdot\mathrm{W}_{\mathrm{core}}\cdot C_{\mathrm{pm}}}. \tag{2.25}$$

Since these equations involve the heat transfer coefficients and specific heats, which are functions of temperatures, this system of equations can be solved only in iterative way. The REMEG code determines the initial (stationary) temperatures by an iteration applying a relative error of 10^{-6}.

The program is used for the following purposes:

- Predicting the Core kinetics and thermal-hydraulic behavior of the BME-Reactor core during transients in a very simple mean.
- Educative purposes and for predicting the safety limits for reactivity insertion in a BME-Reactor because its importance from safety analysis as well as the reactor operation point of view [17].

Now the question arises why REMEG model is not good enough for simulating the power excursion accident of the BME-Reactor. The answer to this question summarized in the following points:

- A point kinetic model describes only the reactivity changes due to temperature changes by the temperature coefficients of reactivity. This is an approximation because the temperature is different in different points of the reactor. Therefore, a 3D neutronic model is necessary.
- The REMEG model does not take into account important phenomena such as coolant flow, boiling of the coolant, heat conduction from fuel to the clad …etc.

2.1.2. PARET Model

Limits for reactivity insertion in a reactor are important from safety analysis as well as the reactor operation point of view. Efforts have been made in the past to determine the reactivity insertion limits for various research reactors both experimentally and theoretically. In SPERT facility; many hundreds of transients were studied for a wide variety of cores, configurations and conditions. The SPERT cores ranged from MTR plate type fuel to Uo_2 fueled system representative of typical PWR cores and data for the safe reactivity insertion limits were obtained experimentally [23]. For carrying out rector transit studies theoretically, the PARET code was developed [24] as a part of SPERT program.

One-dimensional conductive heat transfer from the fuel to the clad and the convective heat transfer from the clad surface to the coolant is solved by this code for all of the specified number of nodes. The PARET code allows both the natural convective as well as the forced flow of the coolant in the hydrodynamic calculations. PARET code employs empirical convective heat transfer correlations in estimating the rate of heat transfer at the clad-moderator interface [23].

The coolant flow and the convective heat transfer problem was solved by employing the modified momentum integral model (MIM) in the PARET code which solves the governing mass, momentum and energy conservation equations along with the pressure balance equation for the entire domain of interest at each time step. The MIM model uses channel averaged mass flow rate in the momentum equation. Also, the coolant properties once evaluated at some reference pressure are assumed temperature dependent only for the first step and the same values are used throughout the rest of calculations. Time step control was varied to achieve an optimum CPU run time.

PARET code was developed to predict the course of nondestructive reactivity accidents in reactor core. In PARET code, the reactor dynamic has been modeled using the point reactor equations with continuous reactivity feedback from the thermal and hydrodynamic model. The point reactor assumption has been found valid especially for small cores [23].

The sensitivity of various safety parameters, affecting the reactivity insertion limits imposed by clad melting temperature for a typical pool type research reactor, has been investigated. The analysis was done for low enriched uranium (LEU) core with scram disabled conditions. The temperature coefficients of fuel and coolant, void/density coefficient and β_{eff} were individually varied and the reactor behavior for different ramp reactivity transients was studied. The ramp reactivity insertions was ranged from 1.6 to 2 \$/0.5 sec and peak power, maximum fuel, clad and coolant temperature were determined. Results show that peak power decreases with an increase in the Doppler coefficient of reactivity. However, it rises with an increase in the reactivity insertion. Also, peak power decreases with an increase in the void coefficient of reactivity. With a decrease in the void coefficient of reactivity, the maximum fuel and clad temperatures show a non-linear rise. Also, the power and temperature peaks in the transient are sensitive to the values of β_{eff} [23].

2.1.3. Lumped-Parameter Model

Thermal-hydraulics is computed on the basis of a one-, or multi-dimensional core description. Lumped parameters models for thermal-hydraulics are generally considered only for qualitative studies of reactor dynamics. Relevant examples can be found in standard texts [8], and include the Newton's law of cooling model, the adiabatic model, and the constant power removal model. In these simplified models temperature effects are accounted for through a single effective temperature for the whole core.

The temperature effects are described by considering two distinct temperature regions, corresponding respectively to the coolant and the fuel [22]. This enables reactivity feedback to include all the major contributions, namely, moderator temperature/density effects and fuel temperature effects. In line with the point model concept, coolant temperature and fuel temperature are both assumed to be functions separable in space and time.

The space dependence is postulated to be the static distribution corresponding to a one-dimensional (in the axial direction) core. This model is computationally economic, can be implemented with little numerical and development effort, and provides predictions with an accuracy sufficient for practical purposes. The model can accommodate the usual transient initiators, e.g. loss of flow or reactivity insertion. The model considers only the severe case of unprotected reactivity insertion transients. However, as it will become apparent, the model can easily adapted to analyze also other types of transient. Note that in reactivity transients the inserted reactivity needs to be

pre-specified in the model, hence, in analyzing practical situations some neutronic calculations will be required first. Thus, the proposed model does not circumvent the need of using neutronic codes [22].

In this model a typical pool-type research reactor with MTR-type fuel elements of rectangular geometry, cooled and moderated with light water was selected as a reference reactor. A one-dimensional core is considered, consisting of a cooling channel and a fuel plate. Incompressible slug flow is assumed to take place on the plate surface through a constant heat transfer coefficient determined from Dittus-Boelter correlation for turbulent-flow convection. The core inlet temperature (or pool temperature) is normally a constant specified as an input parameter. Feedback effects are induced by changes of coolant density (due to temperature changes), changes of coolant temperature (spectrum effects only), and changes of fuel temperature (Doppler effects) [22].

It can be concluded that the lumped-parameter model able to predict with simple means the behavior of a small research reactor core during transient conditions. The model is based on a lumped parameters description of both the kinetics (point model) and thermal-hydraulics. The model was applied to the analysis of unprotected transients induced by an insertion of reactivity. However, the model can be easily adapted to analyze also other types of transients. The model provides a reasonably accurate means for determining the transient behavior of a research reactor, provided that no significant vapor generation takes place in the core.

The model was demonstrated to be applicable for various reactivity insertion rates, up to insertions as high as 1.5 $. A simple criterion on the applicability range of the model is suggested, namely, the model can be used to provide reasonably accurate predictions as long as $T_{out} < T_{sat}$, i.e. no bulk boiling occurs in the core [22].

2.2. Finite Difference in Space and Time Models

Solutions techniques for the multigroup form of the time-dependent diffusion equation in one or more space dimensions can be divided into two broad categories. Indirect solution techniques include the well-known time-synthesis [25], space-time synthesis [26], and quasistatic [27] methods. These methods are characterized by relatively small computational time requirements. Direct solutions techniques, which comprise the second category, solve the equations by finite differencing them in space and time.

The WIGLE [28, 29] method represents successful application of direct methods to the one dimensional problem. The TWIGL method [30] is a successful extension of WIGLE to two dimensions, but it would become prohibitively time-consuming. The TWIGL program uses a specified θ-method [16] of time-differencing with the fluxes at each time step being determined by the cyclic Chebyshev polynomial iterative method [15] to solve the two-dimensional neutron group equations.

In the core dynamics of TWIGL code the fluid dynamics is modeled for only single-phase liquid water. This is satisfactory for analyzing many PWR transients since in normal operation and even for many abnormal situations; insignificant amounts of steam voids are present. This code could also be used to do conservation safety calculations for those accidents (like the fuel element ejection accident) where it is accept of that the inclusion of steam void feedback would reduce the calculated severity of the accident. A single-phase model requires the solution of the conservation of mass and energy (if the mass flux is assumed constant at its steady state value only an energy equation would have to be solved) under the assumption that pressure can be considered constant in space and time (or equivalently that the pressure derivatives are negligible) [21].

2.3. Nodal Models

In this section some models which using nodal expansion method for treating the neutron physics field of equations are presented.

2.3.1. NLSANMT/COBRA-IV

Based on the semi-analytical nodal expansion method and nonlinear iteration strategy [31, 32] a three-dimensional neutron kinetic code NLSANMT is developed, and coupled with the widely used subchannel thermal-hydraulic transient analysis code COBRA-IV [33, 34] to form the integrated NLSANMT/ COBRA-IV code system for PWR core transient calculations [35].

In this model [35], the neutron kinetic and mathematical model of the code NLSANMT, the features and status of the integrated NLSANMT/COBRA-IV system are described. A demonstration application to rod ejection accident analysis is presented using the OECD NEACRP PWR hot zero power full core rod ejection benchmark problems [36-38]. The NLSANMT/COBRA-IV solution shows good agreement with the reference solutions, even if one node per assembly and one channel per assembly are used.

The subchannel thermal-hydraulic steady-state and transient analysis code COBRA-IV is a well verified code widely used in nuclear industry, which is the extended version of the COBRA-III subchannel analysis code developed at the Pacific Northwest Laboratory [33, 34]. The COBRA-IV code can compute the flow and enthalpy distributions in nuclear fuel rod bundles and core for both steady-state and transient conditions.

In the COBRA-IV code the two-phase flow is assumed to be incompressible, homogeneous and thermal-equilibrium, but thermally expandable. The conservation equations for mass, energy, axial and transverse momentum conservation can be solved

by two numerical methods, implicit method and explicit method. COBRA-IV is very flexible for modeling a reactor core and fuel assemblies. A flow channel in the COBRAIV model can be a subchannel or a lumped channel representing an entire fuel assembly.

In addition, COBRA-IV also solves the heat conduction equations for nuclear fuel rods to compute the rod internal temperature distribution and the rod surface heat fluxes, in which the effects of radial and axial conduction and temperature dependence of them al conductivity are considered. The method of Weighted Residuals (MWR) using orthogonal collocation is applied in radial direction and the finite difference method is used for time derivatives and axial space derivatives [35].

NLSANMT and COBRA-IV are coupled to form the integrated code system NLSANMT/COBRA-IV for PWR core transient analysis through a module for controlling the data transfer between the two codes. Each one of the two codes is otherwise left intact. The inputs of the NLSANMT and the COBRA-IV remain unaffected by the integration, and are read in only once at the beginning of a case of coupled analysis [39].

In the NLSANMT/COBRA-IV code, the NLSANMT reactor core model is very flexible that an assembly can be divided into a node or some nodes in radial direction. Accordingly each node is represented as a coolant channel in the COBRA-IV model, but the axial meshing can differ from NLSANMT. An interface module is used for controlling the data transfer and interpolation for axial direction between the two codes. On the one hand the module calls the COBRA-IV for coolant density, coolant temperature and fuel temperature feedback calculations during the NLSANMT feedback iterations of a neutronic calculation. On the other hand the power distribution calculated by NLSANMT is transferred to COBRA-IV for thermal-hydraulic calculation. During each time step an iteration calculation between NLSANMT and COBRA-IV is performed till power distribution converges and the code interface can use the COBRA-IV feedback based on the most updated power distribution.

The coupled NLSANMT/COBRA-IV code system has been used to simulate rod ejection accidents. For example, the OECD NEACRP PWR hot zero power full core rod ejection benchmark problems have been analyzed. The results are presented in the next section [35].

As a conclusion, the three-dimensional neutron kinetic nodal code NLSANMT based on the nonlinear iteration semi-analytical nodal expansion method has been coupled with the subchannel thermal-hydraulic steady-state and transient analysis code COBRA-IV to form the integrated code NLSANMT/COBRA-IV for PWR core transient analysis. An application of the coupled code system to the OECD NEACRP PWR hot zero power full core rod ejection benchmark problems shows that good agreement with the reference solution is obtained, even when one node per assembly and one channel per assembly are used.

2.3.2. KIKO3D/ ATHLET

A VVER-440 type nuclear power plant has a number of special features (e.g.: hexagonal fuel assembly arrangement, the shroud of the assemblies, the horizontal heat exchanger), and hence, the analytic tools of such a reactor system can be different from those of PWR of western design. Therefore, special hexagonal three-dimensional dynamic codes were developed for the safety analyses of VVER reactors. KIKO3D [40] is one of the new three-dimensional reactor dynamics programs for coupled neutron kinetics and thermal-hydraulics calculation of VVER type pressurized water reactor cores. The code has been developed in the KFKI Atomic Energy Research Institute. For solving the time dependent neutronic equations, a new nodal method has been developed which is general enough for the geometry, the symmetries of the nodes, and the concrete form of the neutronic equations to be solved inside the nodes (transport or diffusion equation). Only the linear anisotropy of the neutron flux on the node boundaries is utilized. Generalized response matrices for the time dependent problem are defined [41].

Main applications of KIKO3D are the calculations of asymmetric reactivity initiated accidents in the core, e.g. control rod ejection, start-up of inoperable loop, inadvertent control rod withdrawal. It was already used in the AGNES (Advanced General and New Evaluation of Safety) [42] project for the safety reassessment calculations of NPP Paks [43].

The neutron-physical algorithm was verified by well-known international mathematical benchmarks. The neutron-physical and thermo-hydraulical validation of the program was performed in the frame of the AER international VVER co-operation by the definition of new hexagonal VVER-440 type benchmark problems. It is important to have the ability to do best-estimate calculations with multidimensional neutron kinetics models coupled to sophisticated system thermal-hydraulic codes (RELAP, ATHLET etc.) The embedding of the KIKO3D three-dimensional model into the ATHLET system transient code [44] allows best estimate simulations of interactions between reactor core behavior and plant dynamics. To qualify the prediction of the calculation tool, the VVER-specific data-bases are also important, and hence, a main circulation pump trip transient measured at NPP Paks was also used during the validation process.

As a conclusion, a three-dimensional reactor dynamics program—KIKO3D—for coupled neutron kinetics and thermal-hydraulics calculation of VVER type pressurized water reactor cores has been developed and benchmarked. For the solution of the time dependent neutronic equations, a general nodal method was used, which was applied for the special case of rectangular and hexagonal homogenized nodes in the KIKO3D program. The accuracy of the assumed approximations has been validated against rectangular and hexagonal benchmark problems. The systematic solution and the comparative analysis of the presented benchmark series validated the adequacy of the KIKO3D models for analyzing transients in VVER reactors. Results of other independent codes verified the neutron kinetic solution. The agreement was good even when relatively large time steps were used; this was due to the factorization method.

The selected results demonstrated the capabilities of KIKO3D for safety analysis of VVER power plants. It is a best estimate code, however, methods for conservative modification of the desired parameters has been developed in it. Solution of the realistic benchmark problems made an extensive analysis and improvement of some parts of the thermal-hydraulic model necessary. The final results were reliable and the accuracy of the safety-related parameters was satisfactory [41].

2.3.3. TRAC-PF1/NEM

The reactivity insertion accidents (RIA) in pressurized water reactors (PWR) have been identified as a significant safety concern. Realistic numerical simulations of such transients require detailed three-dimensional (3-D) thermal-hydraulic and more rigorous 3-D core dynamic models to better describe the space-time effects involved. Recent advances in computer technology make possible the incorporation of full 3-D modeling of reactor core into system transient codes. The real application of these complex integrated safety codes to reactivity transient and accident analyses using the actual nuclear power plant (NPP) operational data requires also an efficient cross-section generation methodology. The methodology must be capable of covering the whole range of core conditions during different transients. To address these issues a closely coupled transient 3-D neutronics (NEM)/thermal-hydraulic PWR analysis code using TRAC-PF1 was developed at the Pennsylvania State University (PSU). Although further improvements are being implemented in TRAC-PF1/NEM, this code has reached the level suitable for direct industry applications [45].

Among current best-estimate system transient codes TRAC-PF1 has a 3-D thermal-hydraulic analysis capability [46]. A modified version of TRAC-PF1/MOD2 v.5.4 is currently being used at PSU. This version incorporates a 1-D decay heat model that dynamically computes the decay heat axial shape during the transient. The code calculates general transient two-phase coolant conditions in one, two, or three dimensions using a realistic six-equation, two-fluid, and finite difference model. This six-equation model, in conjunction with specialized empirical models for a variety of PWR primary- and secondary-loop components and control systems, allows TRAC-PF1/MOD2 v.5.4 to accurately model both mild and severe thermal-hydraulic transients.

An accurate 3-D transient neutronics model based on the Nodal Expansion Method (NEM) was developed and integrated into TRAC-PF1 [47]. The NEM spatial model is based on the transverse integrated procedure. Two levels of approximation are used: fourth-degree transverse-integrated flux representation and quadratic leakage approximation. The nodal coupling relationships are expressed in a partial current formulation. The time dependence of the neutron flux is approximated by a first order, fully implicit, finite-difference scheme, whereas the time dependence of the neutron precursor distributions is modeled by a linear time-integrated approximation. The coarse-mesh rebalances and asymptotic extrapolation methods are used to accelerate convergence of the iterative solution process. Several benchmark problems were used to assess the NEM model in both steady state and transient conditions [47, 48]. Very good agreement was obtained among the reference results and those from NEM. The

coupling of the NEM neutronics to TRAC-PF1 has made use of the local thermal-hydraulic description to simulate the core response during a transient.

TRAC-PF1/NEM employs an improved semi-implicit neutronics/thermal-hydraulic coupling scheme. At the beginning of a time step, TRAC-PF1/MOD2 first performs its prepass stage, where fluid-state-dependent material properties and heat-transfer coefficients are calculated based on thermal-hydraulic conditions at the end of the previous time step. Then in the outer iteration stage, the multidimensional fluid-dynamic equations are solved using previous time-step fuel-rod heat fluxes. Then, the 3-D transient NEM neutronics model calculates the present time-step nodal power distribution using cross-section-dependent feedback parameters based on present time-step fluid conditions and previous time-step fuel-rod temperatures. Finally, in the postpass stage, the new nodal power distribution is used in the numerical solution of the heat-conduction equations. To ensure symmetry between the 3-D thermal-hydraulics vessel, the heat structure, and the neutronics core model proper radial and axial nodding and mapping schemes have to be developed for a given reactor and for a given transient [45].

Results from several PWR studies show a good accuracy in both steady state power distribution predictions and transient power evolution. The coupled TRAC- PF1/NEM performs well during simulations where different feedback effects are significant. TRAC-PF1 has a full 3-D thermal-hydraulic description of the vessel flow and is, therefore, able to resolve local effects that would be impossible to study with less sophisticated codes based on a parallel coolant channel model. The coupled TRAC-PF1/NEM methodology combines the 3-D thermal-hydraulic models of TRAC-PF1 with a fully transient 3-D neutronics simulation of the core. The code is supplemented by an efficient and flexible cross-section generation procedure.

The calculations performed demonstrate that TRAC-PF1/NEM resolves local and system interaction effects in a reasonable amount of computational time. All these features make the PSU version of TRAC-PF1/NEM capable of modeling PWR reactivity transients where an accurate 3-D simulation is required [45].

2.4. Discussion and Conclusion

After these comparisons between the different coupled neutronic/thermal-hydraulics we conclude that:

- Coupled point reactor kinetics and thermal-hydraulics codes permit to predict with simple means the behavior of a small research reactor core during transient conditions.

- Limits for reactivity insertion in a reactor are important from safety analysis as well as the reactor operation point of view.

- Direct finite difference methods are the most straightforward approach to the accurate solution of the space time kinetics problem, and these methods are characterized by fairly definite error bounds.

- The incorporation of full 3D modeling of the reactor core into system transient codes allows best-estimate simulations of interactions between reactor core behavior and plant dynamics.

- The three dimensional feature permits extremely flexible nodding of the reactor vessel and, thus, more realistic simulations.

- Most of the models discussed are strongly dependent on the special features of the reactors the behavior of which they simulate. Therefore, we have used only methodic ideas applied in them for developing our own model.

2.5. One Step Forward

In the next chapter we shall treat the three-dimensional neutron dynamics of BME-Reactor, of course, this study is an essential part of the required coupled 3D neutronic/thermalhydraulic analysis of the BME-Reactor during transient conditions.

Chapter 3 A 3D-Time Dependent Neutron Diffusion Model

Fast codes, capable of dealing with three-dimensional geometries, are needed to be able to simulate spatially complicated transients in nuclear power reactors. We established a new model for solving the 3-dimensional time dependent multi-group neutron diffusion equation which simplifies the treatment of the delayed neutron precursors, overcome the difficulties associated with the normal source iteration techniques, also the stability and the convergent of the model have been proved, and we show also that our model converges in the Gauss Seidel iteration.

3.1. Direct Finite Difference Methods

Numerical solutions of the coupled time-dependent transport and precursor equations for reactor kinetics problems of practical interest are prohibitively difficult, so approximate methods are employed. This thesis is concerned with the most common approximation to the time-dependent transport equation i.e., the time dependent few group diffusion equation that have been developed for the purpose of analyzing nuclear reactor transients that occur on time scales of milliseconds to ten's of seconds. The derivation of the diffusion equation from the continuous energy transport equation is described in details in number of references [8, 49-50].

The various methods for calculating the spatial neutron flux distribution (finite difference, nodal, finite element, synthesis, etc.) can be extended to calculate the space-time neutron flux distribution by adding a neutron density time derivative, distinguishing between prompt and delayed neutron sources in the neutron balance equation and appending equations to calculate the delayed neutron precursor densities (e.g., Equations (1.1) and (1.2)). Writing the group fluxes and precursor densities at every spatial point (e.g., mesh point, node) as a column vector $\boldsymbol{\psi}$, and writing the terms of the multigroup neutron and delayed neutron precursor balance equations at each spatial point as a matrix $\mathbf{H}$, the space-time neutron kinetics equations can be written as a coupled set of ordinary differential equations [51]:

$$\mathbf{H}\boldsymbol{\psi} = \dot{\boldsymbol{\psi}} \tag{3.1}$$

Direct finite difference methods are the most straightforward approach to the accurate solution of the space time kinetics problem, and these methods are characterized by fairly definite error bounds [52]. The primary advantage of finite

difference methods is that the complex nonlinear partial differential equations can be expressed in difference form to obtain algebraic expressions [4, 53]. In this section we shall concentrate on the direct finite difference methods for solving the time-dependant neutron diffusion equations along their time-dependent delayed neutrons precursor counterparts.

Finite difference methods: Transient finite difference methods are simply the extension of the well known procedures for solving the static diffusion equation to the time-dependent case. To obtain an acceptable accuracy, the finite difference mesh spacing must be in the order of the smallest group-wise diffusion length. For many reactor problems of interest this requirement results in the use of tremendous number of mesh boxes, and hence unknowns, that must be solved for. For large multi-dimensional models the resulting computer resource requirements are often prohibitively large [4].

The BME-Reactor to be described consists of several homogeneous regions: core, graphite reflector, water reflector. For the description of this reactor (see Section 1.2), the x-y-z geometry is the most adequate. In the finite difference method, this system is covered by a 3D mesh so that every region boundary should be a mesh plane. The finite-difference equations are obtained by integrating Equation (1.1) for regions around every all points. The derivation of our finite-difference equation is not the subject of the present thesis because we use standard methods [54].

3.1.1. Explicit Integration: Forward-Difference Method

The simplest approximate solution to Equation (3.1) is obtained by a simple forward difference algorithm,

$$\boldsymbol{\psi}(p+1) = \boldsymbol{\psi}(p) + \Delta t \mathbf{H}(p) \tag{3.2}$$

where argument p denotes the value at time step t_p, and p+1 denotes $t_{p+1} = t_p + \Delta t$. This algorithm is simple enough but unfortunately suffers from a problem of numerical stability, which requires the use of such small time i.e., very time consuming in the calculations. The nature of this problem is seen by considering an expansion of $\psi(p)$ in terms of the eigenfunctions of the operator $\mathbf{H}$:

$$\boldsymbol{\psi}(p) = \sum_n a_n \boldsymbol{\Omega}_n \tag{3.3}$$

where $\boldsymbol{\Omega}_n$ is the eigenfunctions belonging to eigenvalues ω_n

$$\mathbf{H}\boldsymbol{\Omega}_n = \omega_n \boldsymbol{\Omega}_n \tag{3.4}$$

Substituting Equation (3.3) into Equation (3.2) yields

$$\boldsymbol{\psi}(p+1) = \sum_n a_n (1+\omega_n \Delta t)\boldsymbol{\Omega}_n \tag{3.5}$$

The condition for numerical stability is that the fundamental mode $\boldsymbol{\Omega}_1$ grows more rapidly than the harmonics $\boldsymbol{\Omega}_n, n \geq 2$. This requires that

$$\left|1+\omega_1 \Delta t\right| > \left|1+\omega_n \Delta t\right|, \qquad \text{n} \geq 2 \tag{3.6}$$

To ensure this, $\left|\omega_n \Delta t\right|$ must be much less than unity. The magnitude of the fundamental eigenvalue has the order 0.1 sec^{-1}, except for highly supercritical transients, in which case small time steps is to be used in any case. Numerical studies have shown that Δt necessary for convergence should be less than the reciprocal of all $v_g \Sigma_g^{\text{a}}$ which can be 10^{-4} sec for the thermal group while it can be less than 10^{-7} sec for fast groups. Thus $\Delta t < 10^{-7}$ sec may be required for stability. When the time derivative terms for epithermal groups are assumed to vanish $\Delta t < 10^{-4}$ sec may be required [51]. If the mesh for finite difference approximately is fine even smaller Δt is required.

3.1.2. Implicit Integration: Backward-Difference Method

The numerical stability problem associated with the forward scheme can be eliminated by the backward-difference algorithm:

$$\boldsymbol{\psi}(p+1) = [\mathbf{I} - \Delta t \mathbf{H}(p+1)]^{-1} \boldsymbol{\psi}(p) \tag{3.7}$$

An extension of the type of Equation (3.3) substituted into Equation (3.7) yields

$$\left|(1-\Delta t \omega_1)^{-1}\right| > \left|(1-\Delta t \omega_n)^{-1}\right|, \qquad \text{n} \geq 2 \tag{3.8}$$

The method is unconditionally stable if $0 > \text{Re}\{\omega_1\} > \text{Re}\{\omega_n\}$, $\text{n} \geq 2$. For $\text{Re}\{\omega_1\} > 0$, the stability requirement is determined by the requirement that $\boldsymbol{\psi}(p+1)$ be a positive vector, which necessitates that

$$\left|\Delta t\right| < \frac{1}{\omega_1} \tag{3.9}$$

This requirement is restrictive only for large ω_1 that correspond to fast transients where small time steps would be necessary in any case.

The difficulty with the backward-difference method arises from the necessity of inverting a matrix at each time step. Thus, although much larger time steps may be taken with the implicit method than with the explicit method, the computation time needed for the matrix inversions is large. The size of the time step used in the backward-difference method is usually limited by the effect of truncation error of order Δt^2 upon the accuracy of the solution rather than by numerical stability [51].

3.1.3. Source Iteration

The standard methods of the numerical solution of the multigroup neutron diffusion equation are based on the outer-inner iteration strategy in which the discrete form of neutron diffusion equations is solved groupwise by means of inner iterations stopped when either their number achieves a value assumed for each group or a given convergence criterion is fulfilled. Completing the cycle of inner iterations in all groups corresponds to single outer iteration for which the fission sources are recalculated. Usually Chebyshev polynomial acceleration techniques [15, 55] are used for increasing the rate of convergence of outer iterations [53, 56].

3.2. POWEX-K Iteration Scheme

In this chapter, we develop a three-dimensional space-time-dependent neutron diffusion code POWEX-K (The POWEX-K Code name is referred to following: POWer EXcursion-Khaled) for simulating power excursion accidents. The process involves some thermal-hydraulic feedback through the heat transfer from the fuel to the water used as coolant. These feedbacks play an important role in the reactivity transients of nuclear power reactors. However, we consider in the present section only the neutron-physical aspects of the transient.

Our earlier investigations [57, 58] for the 2D time dependent calculations for the BME-Reactor based on different finite difference schemes, showed that only the backward difference scheme is applicable for handling the time dependence of complicated transients.

The POWEX-K code is designed as a part of integrated neutronic/thermal-hydraulic code for simulating power excursion accidents of the Training Reactor of the Budapest University of Technology and Economics as an essential part of investigating the inherent safety analysis of the reactor. WIMS-D4 code [18] and GRACE and THERMOS codes [19, 20] are used to calculate the group constants and delayed neutron parameters, respectively.

3.2.1. Steady State Calculations, Spatial Discretization

Although the reactivity accidents are described by a space-time dependent code, we need a steady state neutron diffusion model, too. The reasons are the following:

- For the time dependent calculations, we need initial values for the neutron flux and delayed neutron precursor concentrations. Since we shall assume that the reactivity accidents are initiated by some stepwise reactivity change with respect to a stationary state, the flux and delayed neutron precursor concentrations are calculated for this initial state by a steady-state program.
- The value of reactivity step inducing the power excursion accident can be best calculated by a steady state diffusion program. We return to this point later.

The next section deals with the discretization of the time variable. In order to simplify that section, we discuss the spatial discretization in the present one. The time-dependent program uses exactly the same finite differencing scheme as the steady state program; the spatial discretization applies to both steady state and time-dependent programs.

In multigroup diffusion theory, the initial critical state of the reactor can be described by:

$$-\nabla\left(D_g(\mathbf{r})\nabla\phi_g(\mathbf{r})\right)+\Sigma_g^{\mathrm{t}}(\mathbf{r})\phi_g(\mathbf{r})-\sum_{\substack{g'=1\\g'\neq g}}^{G}\Sigma_{g'\to g}(\mathbf{r})\phi_{g'}(\mathbf{r})=\frac{1}{k_{eff}}\chi_g^{\mathrm{p}}\sum_{g'=1}^{G}\nu\Sigma_{g'}^{\mathrm{f}}(\mathbf{r})\phi_{g'}(\mathbf{r}) \tag{3.10}$$

where $g=1,2,...,G$

The notations are:

$\mathbf{r}$	Spatial coordinate;
G	Total number of energy groups;
g	Group index;
$\phi_g(\mathbf{r})$	Space dependent neutron fluxes [n/cm^2/sec];
$D_g(\mathbf{r})$	Neutron diffusion coefficients [cm];
$\Sigma_g^{\mathrm{t}}(\mathbf{r})$	Total cross section [cm^{-1}];
$\Sigma_{g'\to g}(\mathbf{r})$	Slowing down cross section [cm^{-1}];
$\nu\Sigma_{g'}^{\mathrm{f}}(\mathbf{r})$	Fission cross section [cm^{-1}];
χ_g^{p}	Prompt neutron fission spectrum;
k_{eff}	Criticality eigenvalue.

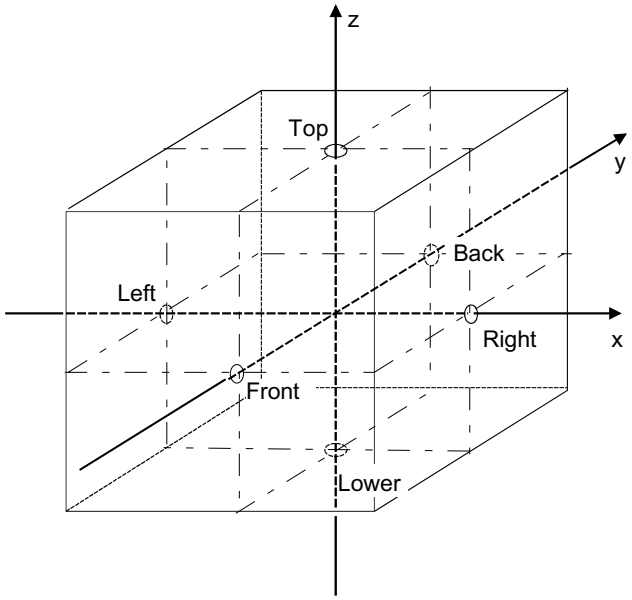

Figure 3. The Octants around a mesh points

Our next task now is to discretize the spatial dependence of this equation and then to solve it. Equation (3.10) is discretized by using the mesh-cell-centered formulation. We assume a rectangular mesh defined by a series of parallel planes perpendicular to each of the three coordinate directions. The actual finite difference equations are obtained by using the seven-point scheme.

After discretization, vector function $\mathbf{\Phi}(\mathbf{r})$ becomes a vector of length $G \times N$ the elements. N is the number of cells in the finite difference mesh (i.e. $N = N_x N_y N_z$) where N_x, N_y, N_z are the number of mesh lines in x, y and z directions, respectively. The elements of the vector are ordered so that first come all group fluxes for mesh point 1, followed by all group fluxes for mesh point 2, and so on. Figure 3 shows a mesh point. Let its subscripts be *ijk* according to the coordinates x, y, z, respectively. The figure shows the planes drawn perpendicularly to the coordinate axes at half way between the neighboring mesh points. The faces of the resulting hexahedron are identified by the expressions “Left”, “Right”, “Front”, “Back”, “Top”, and “Lower” as shown in Figure 3. The planes parallel to the x–y, x–z, and y–z planes cut the hexahedron into eight octants. The octants are numbered (not shown in Figure 3), and the group constants belonging to an individual octant are identified by superscripts indicating the number of the octant. Now, Equation (3.10) is discretized by integrating it for all octants. The integral of the leakage term $\nabla\left(D_g(\mathbf{r})\nabla\phi_g(\mathbf{r})\right)$ for group g and mesh point *ijk* is approximated by [59]:

$$s_{g,ijk}\left(\Phi_{g,i,j,k-1}-\Phi_{g,ijk}\right)+b_{g,ijk}\left(\Phi_{g,i,j,k+1}-\Phi_{g,ijk}\right)+c_{g,ijk}\left(\Phi_{g,i,j-1,k}-\Phi_{g,ijk}\right)+$$
$$+h_{g,ijk}\left(\Phi_{g,i,j+1,k}-\Phi_{g,ijk}\right)+r_{g,ijk}\left(\Phi_{g,i-1,j,k}-\Phi_{g,ijk}\right)+u_{g,ijk}\left(\Phi_{g,i+1,j,k}-\Phi_{g,ijk}\right)$$

where

$$s_{g,ijk} = \frac{D_g^1 \Delta X_{ijk}^{\text{Left}} \Delta Y_{ijk}^{\text{Back}} + D_g^2 \Delta X_{ijk}^{\text{Right}} \Delta Y_{ijk}^{\text{Back}} + D_g^3 \Delta X_{ijk}^{\text{Right}} \Delta Y_{ijk}^{\text{Front}} + D_g^4 \Delta X_{ijk}^{\text{Left}} \Delta Y_{ijk}^{\text{Front}}}{4\Delta Z_{ijk}^{\text{Top}}}$$

$$b_{g,ijk} = \frac{D_g^5 \Delta X_{ijk}^{\text{Left}} \Delta Y_{ijk}^{\text{Back}} + D_g^6 \Delta X_{ijk}^{\text{Right}} \Delta Y_{ijk}^{\text{Back}} + D_g^7 \Delta X_{ijk}^{\text{Right}} \Delta Y_{ijk}^{\text{Front}} + D_g^8 \Delta X_{ijk}^{\text{Left}} \Delta Y_{ijk}^{\text{Front}}}{4\Delta Z_{ijk}^{\text{Lower}}}$$

$$c_{g,ijk} = \frac{D_g^4 \Delta X_{ijk}^{\text{Left}} \Delta Z_{ijk}^{\text{Top}} + D_g^3 \Delta X_{ijk}^{\text{Right}} \Delta Z_{ijk}^{\text{Top}} + D_g^7 \Delta X_{ijk}^{\text{Right}} \Delta Z_{ijk}^{\text{Lower}} + D_g^8 \Delta X_{ijk}^{\text{Left}} \Delta Z_{ijk}^{\text{Lower}}}{4\Delta Y_{ijk}^{\text{Front}}}$$

$$h_{g,ijk} = \frac{D_g^1 \Delta X_{ijk}^{\text{Left}} \Delta Z_{ijk}^{\text{Top}} + D_g^2 \Delta X_{ijk}^{\text{Right}} \Delta Z_{ijk}^{\text{Top}} + D_g^6 \Delta X_{ijk}^{\text{Right}} \Delta Z_{ijk}^{\text{Lower}} + D_g^5 \Delta X_{ijk}^{\text{Left}} \Delta Z_{ijk}^{\text{Lower}}}{4\Delta Y_{ijk}^{\text{Back}}}$$

$$r_{g,ijk} = \frac{D_g^3 \Delta Y_{ijk}^{\text{Front}} \Delta Z_{ijk}^{\text{Top}} + D_g^2 \Delta Y_{ijk}^{\text{Back}} \Delta Z_{ijk}^{\text{Top}} + D_g^7 \Delta Y_{ijk}^{\text{Front}} \Delta Z_{ijk}^{\text{Lower}} + D_g^6 \Delta Y_{ijk}^{\text{Back}} \Delta Z_{ijk}^{\text{Lower}}}{4\Delta X_{ijk}^{\text{Right}}}$$

$$u_{g,ijk} = \frac{D_g^4 \Delta Y_{ijk}^{\text{Front}} \Delta Z_{ijk}^{\text{Top}} + D_g^1 \Delta Y_{ijk}^{\text{Back}} \Delta Z_{ijk}^{\text{Top}} + D_g^8 \Delta Y_{ijk}^{\text{Front}} \Delta Z_{ijk}^{\text{Lower}} + D_g^5 \Delta Y_{ijk}^{\text{Back}} \Delta Z_{ijk}^{\text{Lower}}}{4\Delta X_{ijk}^{\text{Left}}}$$

The superscripts at the diffusion constant (D_g) indicate the numbers of the octants.
The integral of the leakage term $\nabla\left(D_g(\mathbf{r})\nabla\phi_g(\mathbf{r})\right)$ becomes:

$$r_{g,ijk}\Phi_{i+1,j,k} + c_{g,ijk}\Phi_{i,j+1,k} + s_{g,ijk}\Phi_{i,j,k+1} + u_{g,ijk}\Phi_{i-1,j,k} + h_{g,ijk}\Phi_{i,j-1,k} + b_{g,ijk}\Phi_{i,j,k-1} - e_{g,ijk}\Phi_{ijk}$$

with

$$e_{g,ijk} = r_{g,ijk} + c_{g,ijk} + s_{g,ijk} + u_{g,ijk} + h_{g,ijk} + \mathrm{b}_{g,ijk}\,.$$

Each of the term contains products of the form $\Sigma_g(\mathbf{r})\phi_g(\mathbf{r})$ their integral is approximated as follows:

$$\int \Sigma_g(\mathbf{r})\phi_g(\mathbf{r})\mathrm{d}V \cong \phi_{g,ijk}\sum_{\alpha=1}^{8}\Sigma_g^{\alpha}V_{\alpha}\,.$$

The sum for α go through all octants. V_α is the volume of octant α. In this way, we reach finally the following approximation for the integral of Equation (3.10) for group $g = 1,2,...,G$:

$$\Phi_{ijk,\lambda+1} = \left[e_{ijk} + A_{ijk} - \frac{1}{k_{eff}} \chi^{\mathrm{p}} F_{ijk} \right]^{-1} \bullet \left\{ r_{ijk}\Phi_{i+1,j,k,\lambda} + c_{ijk}\Phi_{i,j+1,k,\lambda} + s_{ijk}\Phi_{i,j,k+1,\lambda} + u_{ijk}\Phi_{i-1,j,k,\lambda+1} + h_{ijk}\Phi_{i,j-1,k,\lambda+1} + b_{ijk}\Phi_{i,j,k-1,\lambda+1} \right\} \tag{3.11}$$

where

$$A_{ijk} = \begin{cases} \sum_{g=1}^{4} \phi_{g,ijk} \sum_{\alpha=1}^{8} \nu\Sigma_g^{\alpha,\mathrm{t}} V_\alpha & g' = g \\ -\sum_{g=1}^{4} \phi_{g,ijk} \sum_{\alpha=1}^{8} \nu\Sigma_{g'\to g}^{\alpha} V_\alpha & g' \neq g \end{cases};$$

$$F_{ijk} = \sum_{g=1}^{4} \phi_{g,ijk} \sum_{\alpha=1}^{8} \nu\Sigma_g^{\alpha,\mathrm{f}} V_\alpha .$$

In Equation (3.11), we have omitted subscript *g* for simplicity.

It can be seen from this finite-difference scheme that no special treatment is built in the program for the control rods. The latter would require, for example, logarithmic boundary conditions which are not included in the program. The reason is simple: power excursion is possible only when all control rods are out of the core. Consequently, it is sufficient to write such a time-dependent code which assumes that the diffusion equation is valid in all mesh points. As to the steady-state code, it is always applied to critical or near critical states, thus, the presence of the control rods needs to be simulated. This happens in the following way: the absorption cross section is perturbed in the mesh points lying in the actual space of the control rods so that the reactor became critical (or had the required reactivity). This approximate way of simulating the control rods has an influence only on the initial flux of the time-dependent calculation. The time-dependent flux "forgets" very fast the initial flux profile. Therefore, the calculated time-dependent flux becomes correct near the maximal power of a power excursion accident.

Equation (3.11) shows that the steady-state program uses the point Gauss Seidel algorithm for every energy group separately. When this iteration converges for all groups g, the fission source and k_{eff} are recalculated and the iteration formula (3.11) is applied again. This means that we apply the classical inner and outer iteration schemes for the steady-state program. The corresponding running times are short as compared with those of the time-dependent program. However, this inner-outer iteration scheme would lead to very long running times. Therefore, a new iteration scheme was developed for it (see next section).

The group constants and material properties are calculated by using WIMS-D4 [18]. They are listed in Table 1 for room temperature. The delayed neutron constants were calculated by using GRACE and THERMOS codes [19, 20]. They are listed in Table 2. As an illustration, the thermal flux distributions in x and z directions obtained by the steady-state code are shown in Figures 4 and 5 at two different positions of the core (near core center and near reflector) at full reactor power 100 kW.

Table 1. Material properties for the static calculations (using WIMS-D4)

Material 1 (Core)					
Group Type	Group	D [cm]	Σ^a [cm^{-1}]	Σ^r [cm^{-1}]	$\nu\Sigma^f$ [cm^{-1}]
Fast Groups	1	2.36E+00	1.16E-03	8.16E-02	1.87E-03
	2	9.07E-01	6.07E-04	1.04E-01	5.40E-04
	3	6.64E-01	9.68E-03	1.02E-01	6.96E-03
Thermal Group	4	2.26E-01	6.42E-02	0.00E+00	9.95E-02
Material 2 (Moderator)					
Fast Groups	1	2.89E+00	8.23E-04	9.63E-02	0.00E+00
	2	1.14E+00	1.39E-05	1.60E-01	0.00E+00
	3	6.09E-01	1.01E-03	1.59E-01	0.00E+00
Thermal Group	4	1.43E-01	1.91E-02	0.00E+00	0.00E+00
Material 3 (Reflector)					
Fast Groups	1	2.08E+00	2.60E-06	2.89E-02	0.00E+00
	2	8.94E-01	2.40E-06	1.59E-02	0.00E+00
	3	7.13E-01	2.33E-05	9.32E-03	0.00E+00
Thermal Group	4	5.45E-01	1.39E-03	0.00E+00	0.00E+00

Table 2. Delayed neutron precursor constants for dynamic calculations

Precursor index	1	2	3	4	5	6
β_i	2.67E-04	1.71E-03	1.54E-03	3.10E-03	9.06E-04	3.30E-04
λ_i [sec^{-1}]	1.24E-02	3.05E-02	1.11E-01	3.01E-01	1.14E+00	3.01E+00

Group index	1	2	3	4
χ^p	7.50E-01	2.50E-01	0.00E+00	0.00E+00
v [cm/sec]	1.94E+09	3.79E+08	5.31E+06	2.79E+05
χ^m	0.7497	0.2503	0	0

p (prompt), m=1,2,…,6 (Core width 50 cm, reflector thickness 20 cm)

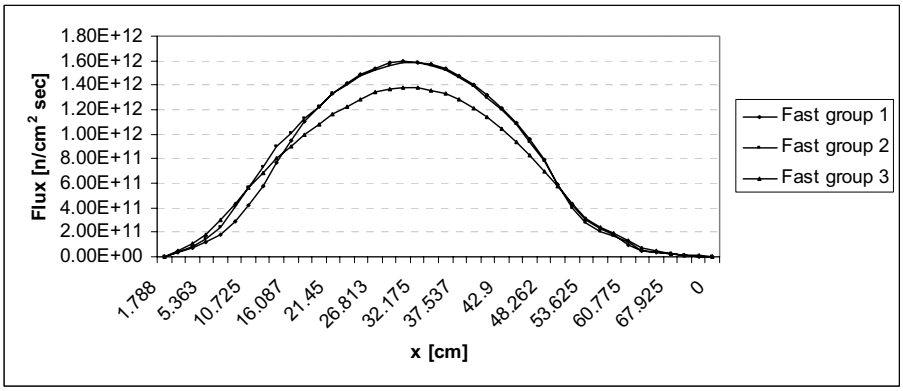

(a)

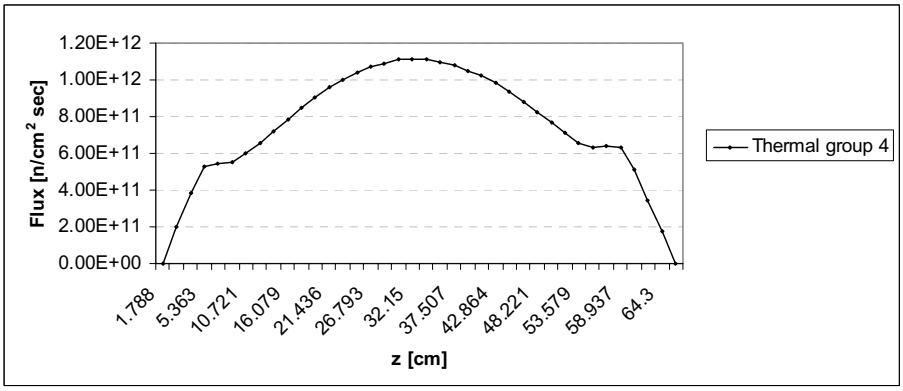

(b)

Figure 4. Steady state flux distribution near the core center
a) Fast, b) Thermal

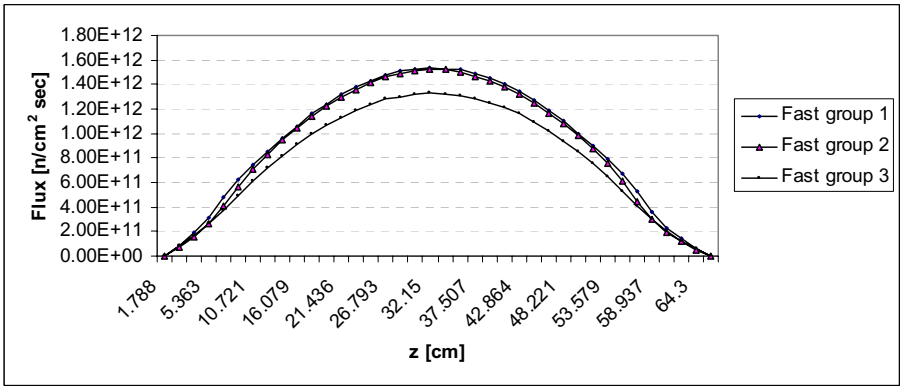

(a)

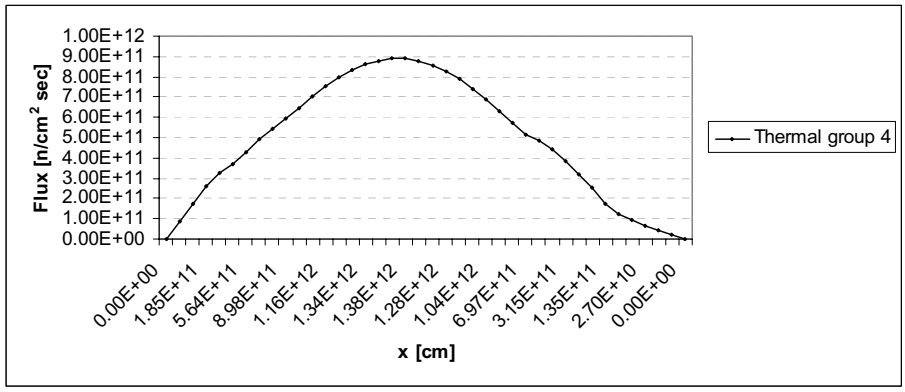

(b)

Figure 5. Steady state flux distribution near reflector
a) Fast, b) Thermal

3.2.2. Basic Equations of POWEX-K Scheme

The BME-Reactor dynamics under transient conditions is modeled using the few-group neutron diffusion equation [60]:

$$\frac{1}{v_g}\frac{\partial \phi_g(\mathbf{r},t)}{\partial t} = \nabla\left(D_g(\mathbf{r})\nabla\phi_g(\mathbf{r})\right) - \Sigma_g^{\mathrm{t}}(\mathbf{r})\phi_g(\mathbf{r},t) + \sum_{\substack{g'=1 \\ g'\neq g}}^{G}\Sigma_{g'\to g}(\mathbf{r})\phi_{g'}(\mathbf{r},t) +$$

$$+ (1-\beta)\chi_g^{\mathrm{p}}\sum_{g'=1}^{G}\nu\Sigma_{g'}^{\mathrm{f}}(\mathbf{r})\phi_{g'}(\mathbf{r},t) + \sum_{m=1}^{M}\lambda_m\chi_{mg}C_m(\mathbf{r},t), \quad g=1,2,...,G \tag{3.12}$$

The notations will be explained later. The concentrations of the M families of delayed neutron precursors are described by the set of equations:

$$\frac{\partial C_m(\mathbf{r},t)}{\partial t} = \beta_m\sum_{g=1}^{G}\nu\Sigma_g^{\mathrm{f}}(\mathbf{r})\phi_g(\mathbf{r},t) - \lambda_m C_m(\mathbf{r},t), \qquad m=1,2,...,M \tag{3.13}$$

For notational convenience, we recast the coupled set of diffusion and delayed neutron precursors Equations (3.12) and (3.13) into matrix form:

$$\mathbf{V}^{-1}\frac{\partial \mathbf{\Phi}(\mathbf{r},t)}{\partial t} = \nabla\left(\mathbf{D}(\mathbf{r})\nabla\mathbf{\Phi}(\mathbf{r},t)\right) - \mathbf{A}\mathbf{\Phi}(\mathbf{r},t) + (1-\beta)\boldsymbol{\chi}\mathbf{F}^{\mathrm{T}}(\mathbf{r})\mathbf{\Phi}(\mathbf{r},t) + \sum_{m=1}^{M}\boldsymbol{\chi}_m\lambda_m C_m(\mathbf{r},t) \tag{3.14}$$

$$\frac{\partial C_m(\mathbf{r},t)}{\partial t} = \beta_m\mathbf{F}^{\mathrm{T}}(\mathbf{r})\mathbf{\Phi}(\mathbf{r},t) - \lambda_m C_m(\mathbf{r},t), \qquad m=1,2,...,M \tag{3.15}$$

where

t Time [sec];

m Delayed neutron family index;

M Total number of delayed neutron families;

$\mathbf{\Phi}(\mathbf{r},t)$ Vector of space and time dependent neutron fluxes [n/cm^2/sec]:

$$\mathbf{\Phi}(\mathbf{r},t)=\begin{bmatrix}\phi_1(\mathbf{r},t)\\ \vdots \\ \phi_G(\mathbf{r},t)\end{bmatrix}; \tag{3.16a}$$

$C_m(\mathbf{r},t)$ Space and time dependent delayed neutron precursor concentration for delayed neutron family m [atom/cm^3];

$\mathbf{V}^{-1}$ Diagonal matrix of inverse neutron velocities averaged for the energy groups [sec/cm]:

$$\left[\mathbf{V}^{-1}\right]_{gg}=\frac{1}{v_g}\ ; \tag{3.16b}$$

$\mathbf{D}$ Diagonal matrix of the neutron diffusion coefficients [cm]:

$$\left[\mathbf{D}\right]_{gg}=D_g\,; \tag{3.16c}$$

$\mathbf{A}$ Total cross section plus slowing down matrix [cm^{-1}]:

$$\left[\mathbf{A}\right]_{g,g'}=\begin{cases}\Sigma_g^{\mathrm{R}}+\Sigma_g^{\mathrm{a}} & g'=g\\ -\Sigma_{g'\to g} & g'\neq g\end{cases}; \tag{3.16d}$$

χ Vector of the prompt neutron fission spectrum:

$$\left[\chi\right]_g=\chi_g^{\mathrm{p}}; \tag{3.16e}$$

$\mathbf{F}$ Vector of neutron production cross sections [cm^{-1}]:

$$\left[\mathbf{F}\right]_g=\nu\Sigma_g^{\mathrm{f}}; \tag{3.16f}$$

χ_m Vector of the neutron spectrum for delayed neutron precursor family m:

$$\left[\chi_m\right]_g=\chi_{mg}\,; \tag{3.16g}$$

β_m Delayed neutron fraction for family *m;*

β Total delayed neutron fraction, $\beta = \sum_{m=1}^{M} \beta_m$;

λ_m Decay constant for delayed neutron precursor family *m* [$\sec^{-1}$].

Superscript "T" denotes matrix transpose.

3.2.3. Solution of the Basic Equations

We solve Equations (3.14) and (3.15) by using the backward finite difference approximation for the time derivative [60]. The spatial derivatives are approximated by the usual finite difference scheme for XYZ-geometry.

3.2.4. Time Difference Equations

We take Equations (3.14) and (3.15) and form the finite difference equations for the time variable. A fully-implicit (i.e. backward) finite difference approximation of Equations (3.14), (3.15) is [60]:

$$\mathbf{V}^{-1}\frac{\mathbf{\Phi}(\mathbf{r},t_\ell)-\mathbf{\Phi}(\mathbf{r},t_{\ell-1})}{\Delta t_\ell} = \nabla\big(\mathbf{D}\nabla\mathbf{\Phi}(\mathbf{r},t_\ell)\big)+$$

$$+[-\mathbf{A}+(1-\beta)\boldsymbol{\chi}\mathbf{F}^{\mathrm{T}}(\mathbf{r})]\mathbf{\Phi}(\mathbf{r},t_\ell)+\sum_{m=1}^{M}\boldsymbol{\chi}_m\lambda_m C_m(\mathbf{r},t_\ell) \qquad (3.17)$$

Here, $\Delta t_\ell = t_\ell - t_{\ell-1}$ ($\ell = 1, 2, \ldots$). Similarly, Equation (3.15) becomes:

$$\frac{C_m(\mathbf{r},t_\ell)-C_m(\mathbf{r},t_{\ell-1})}{\Delta t_\ell} = \beta_m\mathbf{F}^{\mathrm{T}}\mathbf{\Phi}(\mathbf{r},t_\ell)-\lambda_m C_m(\mathbf{r},t_\ell)\,. \qquad (3.18)$$

The precursor concentration at the advanced time step can be expressed as follows:

$$C_m(\mathbf{r},t_\ell) = (1+\Delta t_\ell\lambda_m)^{-1}(C_m(\mathbf{r},t_{\ell-1})+\Delta t_\ell\beta_m\mathbf{F}^{\mathrm{T}}(\mathbf{r})\mathbf{\Phi}(\mathbf{r},t_\ell))\,. \qquad (3.19)$$

Substitution of Equation (3.19) into Equation (3.17) yields:

$$-\nabla\big(\mathbf{D}\nabla\mathbf{\Phi}(\mathbf{r},t_\ell)\big)+\left[\frac{1}{\Delta t_\ell}\mathbf{V}^{-1}+\mathbf{A}-(1-\beta)\boldsymbol{\chi}\mathbf{F}^{\mathrm{T}}-\sum_{m=1}^{M}\frac{\lambda_m\Delta t_\ell\beta_m}{1+\Delta t_\ell\lambda_m}\boldsymbol{\chi}_m\mathbf{F}^{\mathrm{T}}\right]\mathbf{\Phi}(\mathbf{r},t_\ell) =$$

$$=\frac{1}{\Delta t_\ell}\mathbf{V}^{-1}\mathbf{\Phi}(\mathbf{r},t_{\ell-1})+\sum_{m=1}^{M}\frac{\boldsymbol{\chi}_m\lambda_m}{1+\Delta t_\ell\lambda_m}C_m(\mathbf{r},t_{\ell-1})\,. \qquad (3.20)$$

The left hand side of Equation (3.20) contains the unknown fluxes at time step ℓ while the right hand side contains quantities computed for the previous time step. Operators A, D, and $\boldsymbol{\chi}_m\mathbf{F}^{\mathrm{T}}$ depend on space variable **r** and on time variable t_ℓ. This latter dependence is slight because it is due to the thermal-hydraulical feedbacks only. For simplicity, the time dependence will not be indicated in the following equations unless it is necessary for clarity.

3.2.5. Reformulation of the Spatial Difference Equations

As done in section 3.2.1 Equation (3.20) can spatially discretized by the same way. We form diagonal matrices $\mathbf{S}_{ijk}$, $\mathbf{B}_{ijk}$, $\mathbf{C}_{ijk}$, $\mathbf{H}_{ijk}$, $\mathbf{R}_{ijk}$, and $\mathbf{U}_{ijk}$ from these coefficients. For example:

$$\left\lfloor \mathbf{S}_{ijk} \right\rfloor_{gg} = s_{g,ijk} .$$

The other matrices are defined analogously. In these notations, the integral of the leakage term $\nabla(\mathbf{D}\nabla\boldsymbol{\Phi})$ becomes:

$$\mathbf{R}_{ijk}\boldsymbol{\Phi}_{i+1,j,k} + \mathbf{C}_{ijk}\boldsymbol{\Phi}_{i,j+1,k} + \mathbf{S}_{ijk}\boldsymbol{\Phi}_{i,j,k+1} + \mathbf{U}_{ijk}\boldsymbol{\Phi}_{i-1,j,k} + \mathbf{H}_{ijk}\boldsymbol{\Phi}_{i,j-1,k} + \mathbf{B}_{ijk}\boldsymbol{\Phi}_{i,j,k-1} - \mathbf{E}_{ijk}\boldsymbol{\Phi}_{ijk}$$

with

$$\mathbf{E}_{ijk} = \mathbf{R}_{ijk} + \mathbf{C}_{ijk} + \mathbf{S}_{ijk} + \mathbf{U}_{ijk} + \mathbf{H}_{ijk} + \mathbf{B}_{ijk} .$$

In this way, we form matrices $\mathbf{V}_{ijk}$, $\mathbf{A}_{ijk}$ and $\boldsymbol{\chi}_m\mathbf{F}^{\mathrm{T}}_{ijk}$ for every mesh point *ijk* (cf. Equations (3.16.d) and (3.16.f)). We reach finally the following approximation for the integral of Equation (3.20):

$$\left[\frac{1}{\Delta t_\ell}\mathbf{V}^{-1}_{ijk} + \mathbf{E}_{ijk} + \mathbf{A}_{ijk} - (1-\beta)\boldsymbol{\chi}\mathbf{F}^{\mathrm{T}}_{ijk} - \sum_{m=1}^{M}\frac{\lambda_m \Delta t_\ell \beta_m}{1+\Delta t_\ell \lambda_m}\boldsymbol{\chi}_m\mathbf{F}^{\mathrm{T}}_{ijk}\right]\boldsymbol{\Phi}_{ijk}(t_\ell) =$$

$$= \mathbf{R}_{ijk}\boldsymbol{\Phi}_{i+1,j,k}(t_\ell) + \mathbf{C}_{ijk}\boldsymbol{\Phi}_{i,j+1,k}(t_\ell) + \mathbf{S}_{ijk}\boldsymbol{\Phi}_{i,j,k+1}(t_\ell) + \mathbf{U}_{ijk}\boldsymbol{\Phi}_{i-1,j,k}(t_\ell) +$$

$$+ \mathbf{H}_{ijk}\boldsymbol{\Phi}_{i,j-1,k}(t_\ell) + \mathbf{B}_{ijk}\boldsymbol{\Phi}_{i,j,k-1}(t_\ell) + \frac{1}{\Delta t_\ell}\mathbf{V}^{-1}_{ijk}\boldsymbol{\Phi}_{ijk}(t_{\ell-1}) + \sum_{m=1}^{M}\frac{\boldsymbol{\chi}_m\lambda_m}{1+\Delta t_\ell\lambda_m}C_{m,ijk}(t_{\ell-1}) \qquad (3.21)$$

The left hand side of this equation contains only terms belonging to the actual time step t_ℓ and to mesh point *ijk* while the right hand side contains only terms belonging either to the former time step or to the neighboring mesh points. In order to solve this equation, a rather large matrix ought to be inverted which, however, is too large for direct inversion. We have chosen the iteration technique for this reason. Our former equation naturally yields an iteration formula:

$$\boldsymbol{\Phi}_{ijk,\lambda+1}(t_\ell)=\left[\frac{1}{\Delta t_\ell}\mathbf{V}_{ijk}^{-1}+\mathbf{E}_{ijk}+\mathbf{A}_{ijk}-(1-\beta)\boldsymbol{\chi}\mathbf{F}_{ijk}^{\mathrm{T}}-\sum_{m=1}^{M}\frac{\lambda_m\Delta t_\ell\beta_m}{1+\Delta t_\ell\lambda_m}\boldsymbol{\chi}_m\mathbf{F}_{ijk}^{\mathrm{T}}\right]^{-1}\bullet$$

$$\bullet\Big\{\ \mathbf{R}_{ijk}\boldsymbol{\Phi}_{i+1,j,k,\lambda}(t_\ell)+\mathbf{C}_{ijk}\boldsymbol{\Phi}_{i,j+1,k,\lambda}(t_\ell)+\mathbf{S}_{ijk}\boldsymbol{\Phi}_{i,j,k+1,\lambda}(t_\ell)+$$

$$+\mathbf{U}_{ijk}\boldsymbol{\Phi}_{i-1,j,k,\lambda+1}(t_\ell)+\mathbf{H}_{ijk}\boldsymbol{\Phi}_{i,j-1,k,\lambda+1}(t_\ell)+\mathbf{B}_{ijk}\boldsymbol{\Phi}_{i,j,k-1,\lambda+1}(t_\ell)+$$

$$+\frac{1}{\Delta t_\ell}\mathbf{V}^{-1}\boldsymbol{\Phi}_{ijk}(t_{\ell-1})+\sum_{m=1}^{M}\frac{\boldsymbol{\chi}_m\lambda_m}{1+\Delta t_\ell\lambda_m}C_{m,ijk}(t_{\ell-1})\ \Big\}\qquad(3.22)$$

where we have introduced subscript λ as the iteration counter.

The iteration sweeps through the mesh in the sense of increasing subscripts i*, j, k*. As it can be seen from Equation (3.22), we apply the *Gauss-Seidel* method: when the iteration is done for some mesh point, the former fluxes are replaced by the new iterates. That is why λ stands in some terms while $\lambda+1$ stands in others. The convergence of this iteration scheme is studied in the next section: it will be shown that the iteration is always convergent for subcritical reactor states while, for supercritical states, it is convergent only if time step Δt_ℓ is sufficiently small. It can bee seen that Equation (3.22) tends to the steady state Equation (3.11) if we take $\Delta t_\ell \to 0$.

Since this program is meant for simulating reactivity accidents, the initial fluxes and delayed neutron precursor concentrations at $t=0$ are calculated by a static three-dimensional neutron diffusion code using the same group constants as the dynamic code.

The method has been found unconditionally stable. Due to the backward scheme, the time step is limited only by the speed of change of the neutron fluxes. Thus, relatively large time steps may be used for slow processes. However, they should be of the order of milliseconds for power excursion accidents. The drawback of this backward scheme consists in that we have to perform iteration in every time step. However, the method requires a relatively great number of iterations only for the first time step (i.e. at the stiff transient from the static state to the time-dependent state) but, after that, only few iteration steps (1 to 5) are needed for satisfying the convergence criteria [60].

3.3. The Iterative Scheme and its Stability

Since our iteration formula (3.22) deviates from the usual source iteration, we have to study its convergence [60].

3.3.1. The Iteration Matrix

As the iteration proceeds, the flux iterates $\mathbf{\Phi}_{ijk,\lambda}(t_\ell)$ will approach the exact solution of Equation (3.21) if the iteration is convergent at all. Let us denote the latter by dropping the iteration counter λ: $\mathbf{\Phi}_{ijk}(t_\ell)$. In order to simplify the derivations, we study the simple Gauss-iteration first. The effects of the Gauss-Seidel scheme will be studied later. Consequently, we rewrite Equation (3.22) as follows:

$$\left[\frac{1}{\Delta t_\ell}\mathbf{V}_{ijk}^{-1}+\mathbf{E}_{ijk}+\mathbf{A}_{ijk}-(1-\beta)\boldsymbol{\chi}\mathbf{F}_{ijk}^{\mathrm{T}}-\sum_{m=1}^{M}\frac{\lambda_m\Delta t_\ell\beta_m}{1+\Delta t_\ell\lambda_m}\boldsymbol{\chi}_m\mathbf{F}_{ijk}^{\mathrm{T}}\right]\mathbf{\Phi}_{ijk,\lambda+1}(t_\ell)=$$

$$=\mathbf{R}_{ijk}\mathbf{\Phi}_{i+1,j,k,\lambda}(t_\ell)+\mathbf{C}_{ijk}\mathbf{\Phi}_{i,j+1,k,\lambda}(t_\ell)+\mathbf{S}_{ijk}\mathbf{\Phi}_{i,j,k+1,\lambda}(t_\ell)+\mathbf{U}_{ijk}\mathbf{\Phi}_{i-1,j,k,\lambda}(t_\ell)+$$

$$+\mathbf{H}_{ijk}\mathbf{\Phi}_{i,j-1,k,\lambda}(t_\ell)+\mathbf{B}_{ijk}\mathbf{\Phi}_{i,j,k-1,\lambda}(t_\ell)+\frac{1}{\Delta t_\ell}\mathbf{V}^{-1}\mathbf{\Phi}_{ijk}(t_{\ell-1})+\sum_{m=1}^{M}\frac{\boldsymbol{\chi}_m\lambda_m}{1+\Delta t_\ell\lambda_m}C_{m,ijk}(t_{\ell-1}) \qquad (3.23)$$

Note that the essential difference consists in that the iteration counter $\lambda+1$ was replaced by λ at the right hand side. Introduce the error term of the iterate No. λ:

$$\boldsymbol{\delta}_{ijk,\lambda}=\mathbf{\Phi}_{ijk}(t_\ell)-\mathbf{\Phi}_{ijk,\lambda}(t_\ell) \qquad (3.24)$$

We can get an iteration formula for it if we subtract Equation (3.23) from Equation (3.21):

$$\left[\frac{1}{\Delta t_\ell}\mathbf{V}_{ijk}^{-1}+\mathbf{E}_{ijk}+\mathbf{A}_{ijk}-(1-\beta)\boldsymbol{\chi}\mathbf{F}_{ijk}^{\mathrm{T}}-\sum_{m=1}^{M}\frac{\lambda_m\Delta t_\ell\beta_m}{1+\Delta t_\ell\lambda_m}\boldsymbol{\chi}_m\mathbf{F}_{ijk}^{\mathrm{T}}\right]\boldsymbol{\delta}_{ijk,\lambda+1}=\mathbf{R}_{ijk}\boldsymbol{\delta}_{i+1,j,k,\lambda}+$$

$$+\mathbf{C}_{ijk}\boldsymbol{\delta}_{i,j+1,k,\lambda}+\mathbf{S}_{ijk}\boldsymbol{\delta}_{i,j,k+1,\lambda}+\mathbf{U}_{ijk}\boldsymbol{\delta}_{i-1,j,k,\lambda}+\mathbf{H}_{ijk}\boldsymbol{\delta}_{i,j-1,k,\lambda}+\mathbf{B}_{ijk}\boldsymbol{\delta}_{i,j,k-1,\lambda} \qquad (3.25)$$

We remind that, in these formulae, all vectors (like $\boldsymbol{\delta}_{ijk,\lambda}$, $\boldsymbol{\chi}$, $\mathbf{F}_{ijk}$, etc.) have G components and all matrices (like $\mathbf{V}$, $\mathbf{E}_{ijk}$, $\mathbf{A}_{ijk}$, $\mathbf{R}_{ijk}$, etc.) are of size $G\times G$ where G is the number of neutron energy groups. In order to simplify notations, we introduce some hyper-vectors and hyper-matrices. We order the mesh points ijk in some way (e.g. in increasing order of the subscripts), and form hyper-vector $\boldsymbol{\Delta}_\lambda$ such that:

$$\left[\boldsymbol{\Delta}_\lambda\right]_{ijk}=\boldsymbol{\delta}_{ijk,\lambda}. \qquad (3.26a)$$

Now define the following diagonal hyper-matrices whose diagonal blocks are given by:

$$\left[\hat{\mathbf{A}}\right]_{ijk} = \mathbf{E}_{ijk} + \mathbf{A}_{ijk}$$

and

$$\left[\hat{\mathbf{V}}\right]_{ijk} = \mathbf{V}\,. \tag{3.26b}$$

Neutron production is described by hyper-matrix $\hat{\mathbf{P}}$:

$$\left[\hat{\mathbf{P}}\boldsymbol{\Delta}_{\lambda}\right]_{ijk} = \left[(1-\beta)\boldsymbol{\chi}\mathbf{F}_{ijk}^{\mathrm{T}} + \sum_{m=1}^{M}\frac{\lambda_m \Delta t_\ell \beta_m}{1+\Delta t_\ell \lambda_m}\boldsymbol{\chi}_m \mathbf{F}_{ijk}^{\mathrm{T}}\right]\boldsymbol{\delta}_{ijk,\lambda}\,. \tag{3.26c}$$

Finally, hyper-matrix $\hat{\mathbf{W}}$ reproduces the right hand side of Equation (3.25):

$$\begin{aligned}\left[\hat{\mathbf{W}}\boldsymbol{\Delta}_{\lambda}\right]_{ijk} = {} & \mathbf{R}_{ijk}\boldsymbol{\delta}_{i+1,j,k,\lambda} + \mathbf{C}_{ijk}\boldsymbol{\delta}_{i,j+1,k,\lambda} + \mathbf{S}_{ijk}\boldsymbol{\delta}_{i,j,k+1,\lambda} + \\ & + \mathbf{U}_{ijk}\boldsymbol{\delta}_{i-1,j,k,\lambda} + \mathbf{H}_{ijk}\boldsymbol{\delta}_{i,j-1,k,\lambda} + \mathbf{B}_{ijk}\boldsymbol{\delta}_{i,j,k-1,\lambda}\end{aligned} \tag{3.26d}$$

Hyper-matrix $\hat{\mathbf{W}}$ is not diagonal. Its actual form depends on way the mesh points *ijk* are ordered. Later, we shall need the static spectrum:

$$\boldsymbol{\chi}_{\mathrm{s}} = (1-\beta)\boldsymbol{\chi} + \sum_{m=1}^{M}\beta_m\boldsymbol{\chi}_m \tag{3.26e}$$

and the static fission operator:

$$\left[\hat{\mathbf{P}}_{\mathrm{s}}\boldsymbol{\Delta}_{\lambda}\right]_{ijk} = \boldsymbol{\chi}_{\mathrm{s}}\mathbf{F}_{ijk}^{\mathrm{T}}\boldsymbol{\delta}_{ijk,\lambda}\,. \tag{3.26f}$$

In these notations, Equation (3.25) has the form:

$$\left[\frac{1}{\Delta t_\ell}\hat{\mathbf{V}}^{-1} + \hat{\mathbf{A}} - \hat{\mathbf{P}}\right]\boldsymbol{\Delta}_{\lambda} = \hat{\mathbf{W}}\boldsymbol{\Delta}_{\lambda-1}$$

or

$$\boldsymbol{\Delta}_{\lambda} = \left[\frac{1}{\Delta t_{\ell}} \hat{\mathbf{V}}^{-1} + \hat{\mathbf{A}} - \hat{\mathbf{P}} \right]^{-1} \hat{\mathbf{W}} \boldsymbol{\Delta}_{\lambda-1} . \tag{3.27}$$

The iteration is convergent if this error vector tends to zero for $\lambda \to +\infty$. In order to find the conditions of this, we have to analyze the eigenvalues of the iteration matrix: the iteration will be convergent if $|\mu| < 1$ for all of the eigenvalues μ. Let us consider the eigenvalue equation:

$$\left[\frac{1}{\Delta t_{\ell}} \hat{\mathbf{V}}^{-1} + \hat{\mathbf{A}} - \hat{\mathbf{P}} \right]^{-1} \hat{\mathbf{W}} \boldsymbol{\varphi} = \mu \, \boldsymbol{\varphi}$$

or

$$\frac{1}{\mu} \hat{\mathbf{W}} \boldsymbol{\varphi} = \left[\frac{1}{\Delta t_{\ell}} \hat{\mathbf{V}}^{-1} + \hat{\mathbf{A}} - \hat{\mathbf{P}} \right] \boldsymbol{\varphi} \tag{3.28}$$

Where $\boldsymbol{\varphi}$ is the eigenvector belonging to eigenvalue μ. It can be simply seen that the iteration matrix has only non-negative elements. Consequently, the theorem of Frobenius holds for it: the multiplicity of the largest eigenvalue is one, it is real, and the corresponding eigenvector has only positive elements. In the following, we shall find that particular eigenvalue.

3.3.2. Linear Perturbation Formula for the Eigenvalue

The shape of Equation (3.28) is similar to that of the static eigenvalue equation. This observation allows calculating eigenvalue μ by linear perturbation theory. We rewrite first the static eigenvalue equation in our notations. It can be seen from Equations (3.17) and (3.18) that we get the static (i.e. time-independent) equation by letting Δt_{ℓ} tend to infinity. We do this in Equation (3.21):

$$\left[\mathbf{E}_{ijk} + \mathbf{A}_{ijk} - \frac{1}{k_{\text{eff}}} \boldsymbol{\chi}_{\text{s}} \mathbf{F}^{\text{T}}_{ijk} \right] \boldsymbol{\Phi}_{ijk} = \mathbf{R}_{ijk} \boldsymbol{\Phi}_{i+1,j,k} + \mathbf{C}_{ijk} \boldsymbol{\Phi}_{i,j+1,k} + \mathbf{S}_{ijk} \boldsymbol{\Phi}_{i,j,k+1} + \mathbf{U}_{ijk} \boldsymbol{\Phi}_{i-1,j,k} +$$
$$+ \mathbf{H}_{ijk} \boldsymbol{\Phi}_{i,j-1,k} + \mathbf{B}_{ijk} \boldsymbol{\Phi}_{i,j,k-1}$$

where $\boldsymbol{\chi}_{\text{s}}$ is the static fission spectrum defined by Equation (3.26e). We have introduced k_{eff} according to the sense. If we form hyper-vector $\boldsymbol{\varphi}_{\text{s}}$ from the $\boldsymbol{\Phi}_{ijk}$ vectors just as we formed hyper-vector $\boldsymbol{\Delta}_{\lambda}$ before, the latter equations can be rewritten in the following condensed form:

$$\hat{\mathbf{W}}\boldsymbol{\varphi}_s = \left[\hat{\mathbf{A}} - \frac{1}{k_{\text{eff}}}\hat{\mathbf{P}}_s\right]\boldsymbol{\varphi}_s . \tag{3.29}$$

If we compare this with Equation (3.28), we can see that these equations are really similar. The theorem of Frobenius holds for this equation, too. Let k_{eff} be that particular eigenvalue for which all elements of $\boldsymbol{\varphi}_s$ are positive. We shall show that Equation (3.28) is only a perturbation of Equation (3.29), thus, the μ obtained below by perturbation theory will be the largest eigenvalue we are looking for.

In our notations, the finite difference form of the static adjoint diffusion equation is the following:

$$\hat{\mathbf{W}}\boldsymbol{\psi}^+ = \left[\hat{\mathbf{A}}^{\mathrm{T}} - \frac{1}{k_{\text{eff}}}\hat{\mathbf{P}}_s^{\mathrm{T}}\right]\boldsymbol{\psi}^+ \tag{3.30}$$

where, as before, superscript "T" means transpose of the matrix. For the static eigenvalue k_{eff}, we have the well known formula:

$$\frac{1}{k_{\text{eff}}} = \frac{\left(\boldsymbol{\psi}^+, \left[\hat{\mathbf{A}} - \hat{\mathbf{W}}\right]\boldsymbol{\varphi}_s\right)}{\left(\boldsymbol{\psi}^+, \hat{\mathbf{P}}_s\boldsymbol{\varphi}_s\right)}$$

Where $(\boldsymbol{\psi},\boldsymbol{\varphi})$ is the inner product of hyper-vectors $\boldsymbol{\psi}$ and $\boldsymbol{\varphi}$. When the operators (hyper-matrices) are perturbed by $\delta\hat{\mathbf{A}}$, $\delta\hat{\mathbf{W}}$, and $\delta\hat{\mathbf{P}}$, respectively, the perturbation of k_{eff} is:

$$\delta\frac{1}{k_{\text{eff}}} = \frac{\left(\boldsymbol{\psi}^+, \left[\delta\hat{\mathbf{A}} - \delta\hat{\mathbf{W}} - \frac{1}{k_{\text{eff}}}\delta\hat{\mathbf{P}}\right]\boldsymbol{\varphi}_s\right)}{\left(\boldsymbol{\psi}^+, \hat{\mathbf{P}}_s\boldsymbol{\varphi}_s\right)} \tag{3.31}$$

The operators perturbations can be obtained by comparing Equations (3.28) and (3.29):

$$\delta\hat{\mathbf{A}} = \frac{1}{\Delta t_\ell}\hat{\mathbf{V}}^{-1} + \hat{\mathbf{A}} - \hat{\mathbf{A}} = \frac{1}{\Delta t_\ell}\hat{\mathbf{V}}^{-1} \tag{3.32a}$$

$$\delta\hat{\mathbf{W}} = \frac{1}{\mu}\hat{\mathbf{W}} - \hat{\mathbf{W}} = \left(\frac{1}{\mu} - 1\right)\hat{\mathbf{W}} \tag{3.32b}$$

$$\delta\hat{\mathbf{P}} = \hat{\mathbf{P}} - \hat{\mathbf{P}}_s .$$

The latter can be obtained by means of Equations (3.26c), (3.26e), and (3.26f):

$$\left[\left(\hat{\mathbf{P}}-\hat{\mathbf{P}}_{\mathrm{s}}\right)\boldsymbol{\varphi}\right]_{ijk}=\left[(1-\beta)\boldsymbol{\chi}+\sum_{m=1}^{M}\frac{\lambda_m\Delta t_\ell\beta_m}{1+\Delta t_\ell\lambda_m}\boldsymbol{\chi}_m-\boldsymbol{\chi}_{\mathrm{s}}\right]\mathbf{F}_{ijk}^{\mathrm{T}}\boldsymbol{\Phi}_{ijk}=$$

$$=-\sum_{m=1}^{M}\frac{\beta_m}{1+\Delta t_\ell\lambda_m}\boldsymbol{\chi}_m\mathbf{F}_{ijk}^{\mathrm{T}}\boldsymbol{\Phi}_{ijk}\,. \tag{3.32c}$$

Finally, the perturbation of the static eigenvector is:

$$\delta\frac{1}{k_{\mathrm{eff}}}=1-\frac{1}{k_{\mathrm{eff}}}\,. \tag{3.32d}$$

Substituting these perturbations in Equation (3.31), we get the following:

$$1-\frac{1}{k_{\mathrm{eff}}}=\frac{\left(\boldsymbol{\psi}^{+},\left[\frac{1}{\Delta t_\ell}\hat{\mathbf{V}}^{-1}-\left(\frac{1}{\mu}-1\right)\hat{\mathbf{W}}-\frac{1}{k_{\mathrm{eff}}}\left(\hat{\mathbf{P}}-\hat{\mathbf{P}}_{\mathrm{s}}\right)\right]\boldsymbol{\varphi}_{\mathrm{s}}\right)}{\left(\boldsymbol{\psi}^{+},\hat{\mathbf{P}}_{\mathrm{s}}\boldsymbol{\varphi}_{\mathrm{s}}\right)}\,.$$

In order to simplify this formula, we introduce the following notations:

$$\Lambda=\frac{(\boldsymbol{\psi}^{+},\hat{\mathbf{V}}^{-1}\boldsymbol{\varphi}_{\mathrm{s}})}{(\boldsymbol{\psi}^{+},\hat{\mathbf{P}}_{\mathrm{s}}\boldsymbol{\varphi}_{\mathrm{s}})}\,, \tag{3.33a}$$

$$a=\frac{(\boldsymbol{\psi}^{+},\hat{\mathbf{W}}\boldsymbol{\varphi}_{\mathrm{s}})}{(\boldsymbol{\psi}^{+},\hat{\mathbf{P}}_{\mathrm{s}}\boldsymbol{\varphi}_{\mathrm{s}})}\,, \tag{3.33b}$$

$$\beta_m^{\mathrm{eff}}=\beta_m\frac{(\boldsymbol{\psi}^{+},\hat{\mathbf{P}}_m\boldsymbol{\varphi}_{\mathrm{s}})}{(\boldsymbol{\psi}^{+},\hat{\mathbf{P}}_{\mathrm{s}}\boldsymbol{\varphi}_{\mathrm{s}})} \tag{3.33c}$$

with

$$\left[\hat{\mathbf{P}}_m\boldsymbol{\varphi}\right]_{ijk}=\boldsymbol{\chi}_m\mathbf{F}_{ijk}^{\mathrm{T}}\boldsymbol{\Phi}_{ijk}\,.$$

These quantities have common names in reactor physics: Λ is the generation time, β_m^{eff} is the effective delayed neutron fraction for delayed-neutron precursor family m. Finally, we get after some algebra:

$$\frac{1}{\mu}-1=\frac{\dfrac{\Lambda}{\Delta t_\ell}+\dfrac{1}{k_{\text{eff}}}\displaystyle\sum_{m=1}^{M}\frac{\beta_m^{eff}}{1+\Delta t_\ell\lambda_m}-\rho}{a}.$$

Here,

$$\rho=1-\frac{1}{k_{\text{eff}}} \tag{3.33d}$$

is the reactivity. The numerator in the right hand side recalls the inhour equation. In order to enhance this similarity, we introduce further notations:

$$\alpha_{\text{c}}=\frac{\beta_{\text{eff}}}{\Lambda},\qquad \omega=\frac{1}{\Delta t_\ell},\qquad \beta_{\text{eff}}=\sum_{m=1}^{M}\beta_m^{\text{eff}} \tag{3.33e}$$

Leading to:

$$\frac{1}{\mu}-1=\frac{\dfrac{\omega}{\alpha_{\text{c}}}+\omega\displaystyle\sum_{m=1}^{M}\frac{\beta_m^{\text{eff}}/\beta_{\text{eff}}}{\omega+\lambda_m}-\frac{\rho}{\beta_{\text{eff}}}}{a/\beta_{\text{eff}}}. \tag{3.34}$$

We have taken into account that $k_{\text{eff}}\approx 1$. The numerical value of a is usually some tens, β_{eff} is somewhat less than 10^{-2}, thus, the absolute value of the right hand side is a small number. Therefore, μ is usually positive and close to unity. For very small values of ω, μ can be negative. We discuss such cases later but, for the time being, assume that μ is positive. As we have stated above, the iteration is convergent only if μ is less than unity, or, in other words, the right hand side is positive:

$$\frac{\omega}{\alpha_{\text{c}}}+\omega\sum_{m=1}^{M}\frac{\beta_m^{\text{eff}}/\beta_{\text{eff}}}{\omega+\lambda_m}>\frac{\rho}{\beta_{\text{eff}}}. \tag{3.35}$$

This is the condition of convergence we were looking for. It is trivially satisfied for subcritical reactor states since $\rho < 0$. However, Inequality (3.35) does not hold for sufficiently small values of ω if $\rho > 0$. This means that the iteration is not necessarily convergent for supercritical states. Let ω_0 be that value of ω for which Inequality (3.35) goes over into equality:

$$\frac{\omega_0}{\alpha_{\text{c}}}+\omega_0\sum_{m=1}^{M}\frac{\beta_m^{\text{eff}}/\beta_{\text{eff}}}{\omega_0+\lambda_m}=\frac{\rho}{\beta_{\text{eff}}}.$$

This formula is nothing else than the inhour equation. Thus, ω_0 is the reactor period $\left(=\ln 2/T_{2x}\right)$. It allows writing the convergence condition in a very simple form:

$$\Delta t_\ell < \Delta t_{\max} = \frac{1}{\omega_0}. \tag{3.36}$$

This inequality constitutes a sufficient condition of convergence for supercritical reactor states. As a matter of fact, it is trivially satisfied because we need to choose such values of Δt_ℓ for which $\omega_0 \Delta t_\ell$ is significantly less than unity. Otherwise, the finite-difference approximation according to Equations (3.17) and (3.18) would be rather inaccurate.

As to negative values of μ, they can occur for ω values much less than ω_0 i.e. for time steps Δt_ℓ much greater than $\Delta t_{\max}$. We are not interested in such cases because the result of the eventually convergent iteration will be too inaccurate.

Consequently, the iteration is always convergent for well formulated problems. If we meet convergence problems, this is sure sign of that our time steps are too large. Such difficulties can appear when fast reactor transients are investigated [60].

3.4. Analysis of the Convergence of the Gauss-Seidel Iteration

Gauss Seidel method applied to the classic iteration makes the iteration convergent faster, but our iteration matrix is not classic therefore we have to prove that Gauss Seidel method is also accelerate convergent inside our model.

As a conclusion of our considerations, we have to analyze the effects of the Gauss-Seidel iteration on the eigenvalue of the iteration matrix. We shall follow the line of reasoning of Reference [15]. In Section 3.3.1, we have started from Equation (3.23) instead of Equation (3.22). In order to study the Gauss-Seidel iteration, we return to the latter. Divide hyper-matrix $\hat{\mathbf{W}}$ in two parts:

$$\hat{\mathbf{W}} = \hat{\mathbf{W}}_{\text{lower}} + \hat{\mathbf{W}}_{\text{upper}}$$

where the matrices on the right hand side contain the elements of $\hat{\mathbf{W}}$ below and above the main diagonal, respectively. Introduce the notations:

$$\hat{\boldsymbol{\alpha}} = \left[\frac{1}{\Delta t_\ell} \hat{\mathbf{V}}^{-1} + \hat{\mathbf{A}} - \hat{\mathbf{P}} \right]^{-1} \hat{\mathbf{W}}_{\text{lower}}$$

$$\hat{\boldsymbol{\beta}} = \left[\frac{1}{\Delta t_\ell} \hat{\mathbf{V}}^{-1} + \hat{\mathbf{A}} - \hat{\mathbf{P}} \right]^{-1} \hat{\mathbf{W}}_{\text{upper}} .$$

It is straightforward to derive that the error term satisfies the following equation instead of Equation (3.27):

$$\boldsymbol{\Delta}_\lambda = \hat{\boldsymbol{\beta}} \boldsymbol{\Delta}_\lambda + \hat{\boldsymbol{\alpha}} \boldsymbol{\Delta}_{\lambda-1}$$

or

$$\boldsymbol{\Delta}_\lambda = \left(\hat{\mathbf{I}} - \hat{\boldsymbol{\beta}} \right)^{-1} \hat{\boldsymbol{\alpha}} \boldsymbol{\Delta}_{\lambda-1} . \tag{3.37}$$

In the actual notations, the iteration studied above can be rewritten as follows:

$$\boldsymbol{\Delta}_\lambda = \left(\hat{\boldsymbol{\alpha}} + \hat{\boldsymbol{\beta}} \right) \boldsymbol{\Delta}_{\lambda-1} \tag{3.38}$$

(cf. Equation (3.28)).

We have now to calculate the eigenvalue of the iteration given by Equation (3.37). Let us write the eigenvalue equation corresponding to Equation (3.38):

$$(\hat{\boldsymbol{\alpha}} + \hat{\boldsymbol{\beta}}) \mathbf{Z} = \mu \mathbf{Z} . \tag{3.39}$$

Here, $\mathbf{Z}$ is a hyper-vector whose blocks have G elements: $\mathbf{Z} = \text{Col}[\mathbf{z}_1 \ldots \mathbf{z}_N]$. The iteration matrix is written in terms blocks of size $G \times G$:

$$\hat{\boldsymbol{\alpha}} + \hat{\boldsymbol{\beta}} = \begin{bmatrix} 0 & \boldsymbol{\alpha}_1 & 0 & 0 & & & 0 \\ \boldsymbol{\beta}_1 & 0 & \boldsymbol{\alpha}_2 & 0 & & & \vdots \\ 0 & \boldsymbol{\beta}_2 & 0 & \boldsymbol{\alpha}_3 & & & \\ & & \ddots & \ddots & \ddots & & \\ & & & & & \boldsymbol{\beta}_{N-1} & 0 \end{bmatrix} .$$

In terms of these notations, the eigenvalue Equation (3.39) can be rewritten as follows:

$$\nu \mathbf{z}_1 - \boldsymbol{\alpha}_1 \mathbf{z}_2 = 0$$

$$-\boldsymbol{\beta}_{\ell-1} \mathbf{z}_{\ell-1} + \nu \mathbf{z}_\ell - \boldsymbol{\alpha}_\ell \mathbf{z}_{\ell+1} = 0 \qquad (\ell = 2, 3, ..., N\text{-}1) \tag{3.39a}$$

$$-\boldsymbol{\beta}_{N-1} \mathbf{z}_{N-1} + \nu \mathbf{z}_N = 0$$

Let us now formulate the eigenvalue Equation (3.38) in terms of the blocks:

$$\left(\hat{\mathbf{I}}-\hat{\boldsymbol{\beta}}\right)^{-1}\hat{\boldsymbol{\alpha}}\hat{\mathbf{y}}=\nu\hat{\mathbf{y}} \tag{3.40}$$

where $\hat{\mathbf{y}}=\mathrm{Col}[\mathbf{y}_1 \ldots \mathbf{y}_N]$. Rewrite this in terms of the blocks:

$$\nu\mathbf{y}_1-\boldsymbol{\alpha}_1\mathbf{y}_2=0$$

$$-\nu\boldsymbol{\beta}_{\ell-1}\mathbf{y}_{\ell-1}+\nu\mathbf{y}_\ell-\boldsymbol{\alpha}_\ell\mathbf{y}_{\ell+1}=0, \qquad (\ell=2,3,\ldots,N\text{-}1)$$

$$-\nu\boldsymbol{\beta}_{N-1}\mathbf{y}_{N-1}+\nu\mathbf{y}_N=0$$

Divide the ℓ^{th} row by $\nu^{(\ell-1)/2}$:

$$\frac{-\boldsymbol{\beta}_{\ell-1}\mathbf{y}_{\ell-1}}{\nu^{\frac{\ell-3}{2}}}+\frac{\mathbf{y}_\ell}{\nu^{\frac{\ell-3}{2}}}-\frac{\boldsymbol{\alpha}_\ell\mathbf{y}_{\ell+1}}{\nu^{\frac{\ell-1}{2}}}=0\,. \tag{3.41}$$

Introduce the substitution:

$$\mathbf{y}_\ell=\nu^{\frac{\ell-2}{2}}\mathbf{x}_\ell$$

and then get

$$-\boldsymbol{\beta}_{\ell-1}\mathbf{x}_{\ell-1}+\sqrt{\nu}\mathbf{x}_\ell-\boldsymbol{\alpha}_\ell\mathbf{x}_{\ell+1}=\mathbf{0}\,.$$

If it is compared with Equation (39a), it is clear that $\mu=\sqrt{\nu}$ or:

$$\nu=\mu^2\,.$$

We have thus shown that ν<1 because we know that μ<1. More is true: ν<μ<1. This means that the Gauss-Seidel iteration converges in our case, too [60].

3.5. Results of Sample Calculations

Figures 6 and 7 are showing the results of some sample calculations. The reactor was assumed as critical for $t < 0$ at a power of 100 kW. The steady-state flux and delayed neutron precursors calculated for this state were taken as initial values for the time-dependent calculation simulating a power excursion. It was assumed that the sudden reactivity change of 1.2 \$ happened at $t = 0$.

The group constants don't change during this transient test, also no feedback calculations are taken into account. As expected, this perturbation caused severe flux raise in the reactor. Figure 6 shows the total power of BME-Reactor as a function of time. The power rises following a rapid exponential trend with short period, within short period the power rises to almost 198.3 MW.

The spatial dependence of fast and thermal fluxes for the 1st fast energy group and 4th thermal energy group are shown in Figure 7 and Figure 8 at two different places of the core (near the reflector, and near the core centre) and at different time steps. The figures show that the flux increases as the time increase. This will not be the case if we take the thermal-hydraulic feedback into account.

In the real reactor, the rising temperatures have strong feedback effects on the reactivity leading to a decrease of the power within some tenth of seconds. It will be the subject of the next chapter how these temperature feedbacks are taken into account.

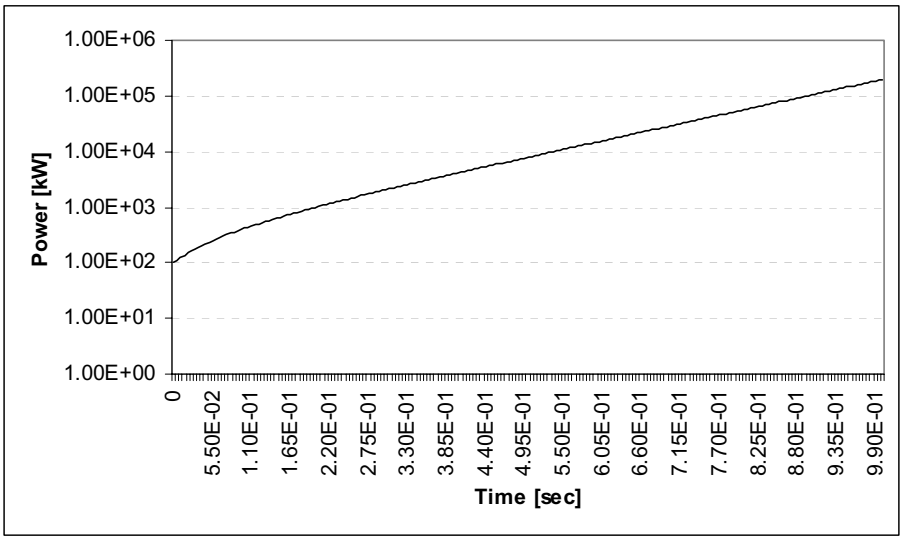

Figure 6. Time behavior of power for ramp reactivity 1.2 \$ without feedback

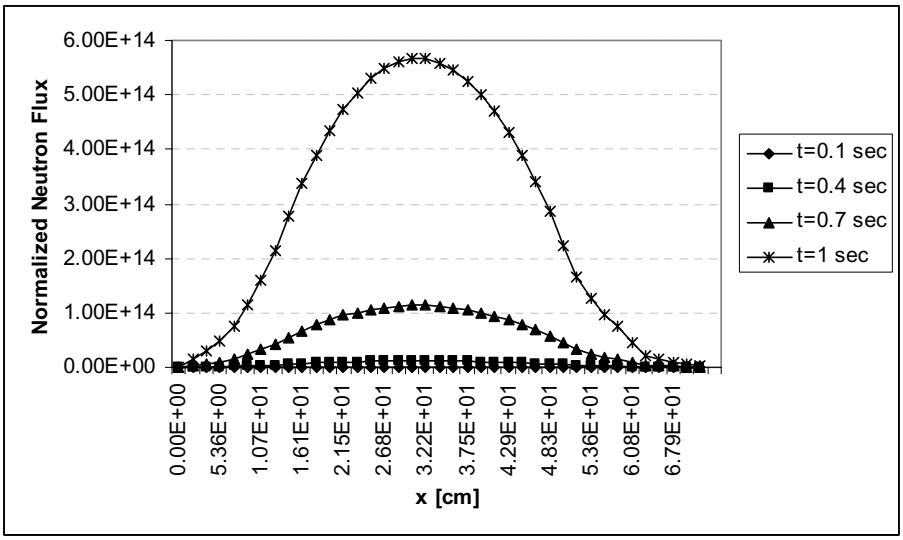

(a)

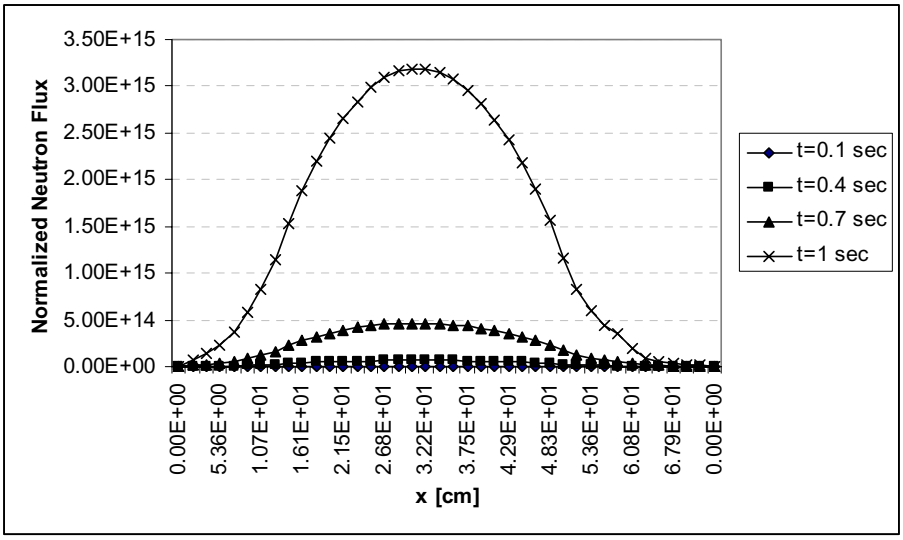

(b)

Figure 7. Spatial dependence of the fast flux in the hottest channel for 1.2 $ without feedback
a) Near Reflector , b) Near Core Center

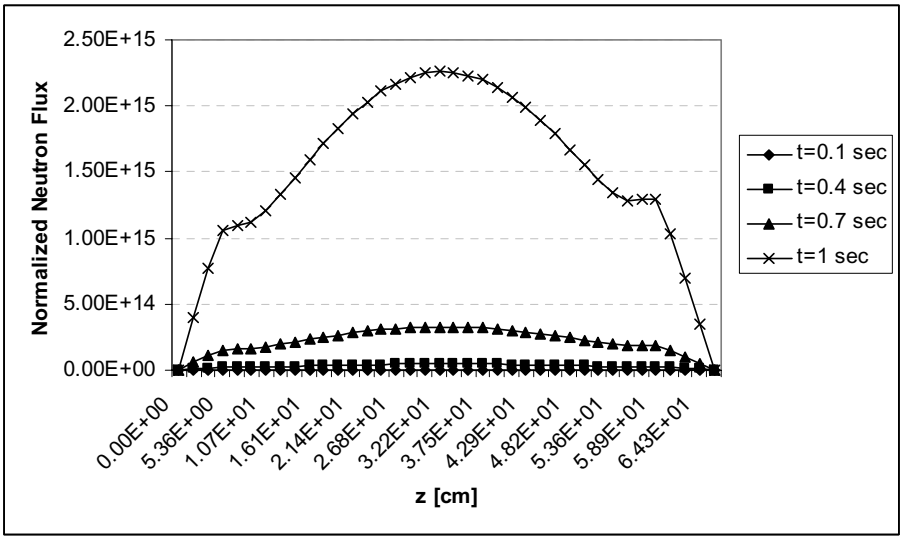

(a)

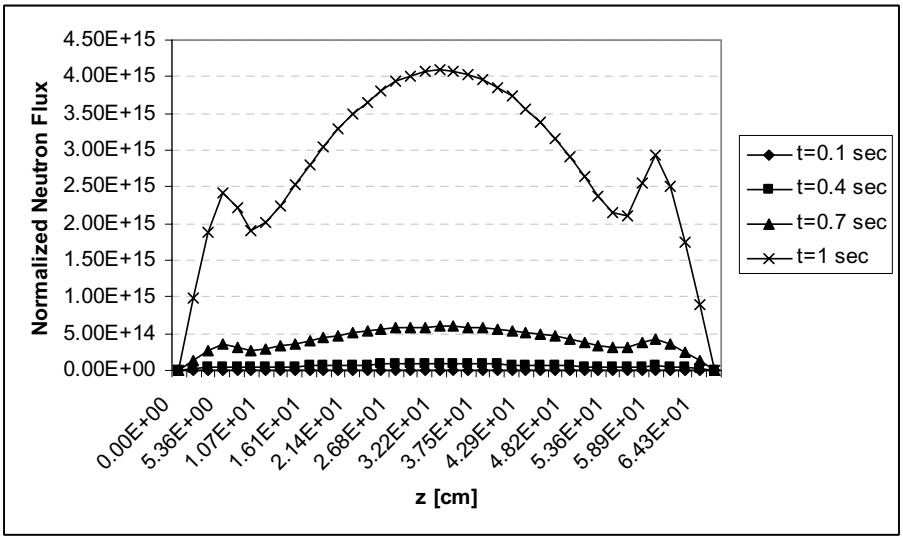

(b)

Figure 8. Axial dependence of the thermal flux in the hottest channel for 1.2 $ without feedback
a) Near Reflector, b) Near Core Center

3.6. Discussion and Conclusion

The conclusions of our studies can be summarized as follows:

- Fast codes, capable of dealing with three-dimensional geometries, are needed to be able to simulate spatially complicated transients in nuclear power reactors.
- The study of power excursion accidents needs accurate predictions of the neutron space-time dependent flux.
- For simulating a reactivity accident in the BME-Reactor, the backward difference scheme can be used to give stable, convergent and accurate results.
- Neutronic code POWEX-K has been developed based on the new iterative scheme which simplifies treatment of delayed neutron precursor concentrations and omits the difficulties associated with the usual source iteration.
- The new iterative scheme of the solution is convergent if the time steps are chosen to be less than the reciprocal of the reactor period. This is a condition which is naturally satisfied for all well formulated problems.
- Gauss Seidel method is accelerating convergent inside our model.

3.7. One Step Forward

Up to now we developed a model solves the 3D few group neutron diffusion equations without any feedback effects taken into account in the calculations. This model still needs thermal-hydraulic part to give predicated results, see Figure 8. Thus, a coupled neutronic/thermal-hydraulic code has to be build and fuel and moderator feedbacks effects should take into account. See next chapter.

Chapter 4 Thermal-hydraulics Feedback Calculations

A coupled 3D neutronic/thermal-hydraulic integrated code for the purpose of simulating the power excursion accidents due to positive reactivity insertions has been developed, which models the BME-Reactor core neutron dynamics using the 3D multigroup time dependent neutron diffusion equations (utilizing our new technique, see previous chapter) and models the thermal-hydraulic response of the BME-Reactor using a simple two phase model so called (Momentum Integral model MI) with reactivity feedbacks due to coolant and fuel temperature.

4.1. Introduction

In the present chapter, we develop a coupled three-dimensional neutronic/thermal-hydraulic model for simulating power excursion accident in the BME-Reactor. The process involves some thermal-hydraulic feedback through the heat transfer from the fuel to the water used as coolant, condensation and evaporation which take place in the reactor core and in the condenser system. These feedbacks play an important role in the reactivity transients of nuclear power reactors [22, 61].

4.2. POWEX-K/MI Model

This section contains all mathematical and physical models used in POWEX-K/MI model. Although the tests and the verification of the integrated code POWEX-K/MI comes later in chapter 5, (the POWEX-K-code is briefly discussed in Section 3.2 and, the MI name referred to the thermal–hydraulic module of the coupled code which basically depend on the so called Momentum Integral model [10-12]).

The model to be developed in this section contains equations describing the basic processes relevant to BME-Reactor dynamics, namely, the reactor physics model, the thermal heat conduction model, and the hydrodynamic model.

4.2.1. The Reactor Physics Model (POWEX-K)

The BME-dynamics can be described using Equations (3.14) and (3.15):

$$\mathbf{V}^{-1}\frac{\partial \mathbf{\Phi}(\mathbf{r},t)}{\partial t} = \nabla\big(\mathbf{D}(\mathbf{r})\nabla\mathbf{\Phi}(\mathbf{r},t)\big) - \mathbf{A}\mathbf{\Phi}(\mathbf{r},t) + (1-\beta)\boldsymbol{\chi}\mathbf{F}^{\mathrm{T}}(\mathbf{r})\mathbf{\Phi}(\mathbf{r},t) + \sum_{m=1}^{M}\boldsymbol{\chi}_m\lambda_m C_m(\mathbf{r},t) \tag{4.1}$$

$$\frac{\partial C_m(\mathbf{r},t)}{\partial t} = \beta_m \mathbf{F}^{\mathrm{T}}(\mathbf{r})\boldsymbol{\Phi}(\mathbf{r},t) - \lambda_m C_m(\mathbf{r},t), \qquad m = 1,2,...,M \tag{4.2}$$

In section 3.2 we introduced the code POWEX-K which solves Equations (4.1) and (4.2) using the backward finite difference approximation for time derivatives. The spatial derivatives are approximated by the usual finite difference scheme [59]. We have developed a new iterative scheme for solving the 3D time dependent few-group neutron diffusion equation which simplifies the treatment of the delayed neutron precursors. It overcomes the difficulties associated with the normal source iteration techniques [60]. Our iteration formula (3.22) reads as follow:

$$\boldsymbol{\Phi}_{ijk,\lambda+1}(t_\ell) = \left[\frac{1}{\Delta t_\ell}\mathbf{V}_{ijk}^{-1} + \mathbf{E}_{ijk} + \mathbf{A}_{ijk} - (1-\beta)\boldsymbol{\chi}\mathbf{F}_{ijk}^{\mathrm{T}} - \sum_{m=1}^{M}\frac{\lambda_m \Delta t_\ell \beta_m}{1+\Delta t_\ell \lambda_m}\boldsymbol{\chi}_m \mathbf{F}_{ijk}^{\mathrm{T}}\right]^{-1} \bullet$$

$$\bullet \Big\{ \mathbf{R}_{ijk}\boldsymbol{\Phi}_{i+1,j,k,\lambda}(t_\ell) + \mathbf{C}_{ijk}\boldsymbol{\Phi}_{i,j+1,k,\lambda}(t_\ell) + \mathbf{S}_{ijk}\boldsymbol{\Phi}_{i,j,k+1,\lambda}(t_\ell) +$$

$$+ \mathbf{U}_{ijk}\boldsymbol{\Phi}_{i-1,j,k,\lambda+1}(t_\ell) + \mathbf{H}_{ijk}\boldsymbol{\Phi}_{i,j-1,k,\lambda+1}(t_\ell) + \mathbf{B}_{ijk}\boldsymbol{\Phi}_{i,j,k-1,\lambda+1}(t_\ell) +$$

$$+ \frac{1}{\Delta t_\ell}\mathbf{V}^{-1}\boldsymbol{\Phi}_{ijk}(t_{\ell-1}) + \sum_{m=1}^{M}\frac{\boldsymbol{\chi}_m \lambda_m}{1+\Delta t_\ell \lambda_m} C_{m,ijk}(t_{\ell-1}) \Big\} \tag{4.3}$$

Fuel temperature, moderator density, fission product poisons, and fuel burn-up are examples of feedback mechanisms that influence reactor dynamics. Feedback mechanisms can be distinguished by the response time to the changes occurring in the system. Fuel temperature and moderator density have time constants of order of seconds. They are hours for fission product poisons and weeks or months for fuel burn-up. Since the power excursion transient is very fast, we may assume that only the fuel and moderator temperatures (consequently the moderator density as well) are the significant feedback mechanisms. These feedbacks are taken into account by recalculating the few-group constants at each time step for each node.

4.2.2. Sub-channel Thermal-hydraulic Model (MI)

The heat transfer model MI inside the fuel region is based on one-dimensional radial heat conduction. The conservation equations are written for on dimensional axial homogeneous upward flow through the channel. On the other hand, constitutive equations as heat transfer coefficient, friction factor are used taking into account the geometry as well as the convection regime (forced or natural). In the following, we shall discuss the basic models and equations used in the reactor physics model, fuel model, and hydrodynamic model [62].

a) Fuel Heat Conduction Model

(1) Differential Equations

In MI model, we solve the one-dimensional conductive heat transfer from the fuel to the clad and the convective heat transfer from the clad to the coolant for nuclear fuel rods in order to compute the rod internal temperature distribution and the rod surface heat fluxes. Assuming only radial conduction, the equation governing the temperature distribution within the fuel pellet can be written as [63]

$$\rho_F C_{pF} \frac{\partial T_F}{\partial t} = \frac{1}{r} \frac{\partial}{\partial r} \left(r k_F \frac{\partial T_F}{\partial r} \right) + \dot{q}_v \tag{4.4}$$

while for the cladding with no internal heat generation the equation is written:

$$\rho_C C_{pC} \frac{\partial T_C}{\partial t} = \frac{1}{r} \frac{\partial}{\partial r} \left(r k_C \frac{\partial T_C}{\partial r} \right) \tag{4.5}$$

In EK-10 type fuel rod, there is no gap between the fuel pellet and the clad, hence the accompanied set of boundary conditions for Equations (4.4) and (4.5) are given by:

$$\left. \frac{\partial T_F}{\partial r} \right|_{r=0} = 0 \qquad \text{and} \qquad - k_C \left. \frac{\partial T_C}{\partial r} \right|_{r=r_{co}} = h[T_{co}(t) - T_m(t)]$$

where,

T_m	Moderator temperature [K];
T_F	Fuel pellet temperature [K];
T_C	Clad temperature [K];
r_{co}	Clad outside radius [m];
T_{co}	Clad outside surface temperature [K];
$\rho_F C_{pF}$	Fuel pellet heat capacity [J/m^3 K];
$\rho_C C_{pC}$	Clad heat capacity [J/m^3 K];
k_f	Fuel pellet thermal conductivity [W/m K];
k_c	Clad thermal conductivity [W/m K];
h	Convective heat transfer coefficient [W/m^2 K];
$\dot{q}_v$	Pellet volumetric heat generation [W/m^3].

The heat conduction and energy conservation equation are coupled at the interface between the clad and the coolant.

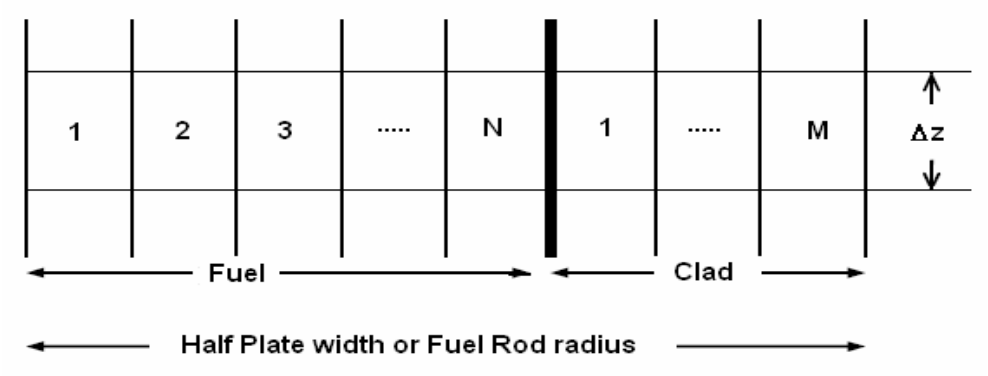

Figure 9. Radial fuel region nodalisation

(2) Finite Difference Equations

In transient thermal calculation the unit cell is represented as shown in Figure 9. For each node a heat balance is made, neglecting axial heat transfer in solid. By applying a first order implicit finite difference formula to Equations (4.4) and (4.5), the terms of Equation (4.4) at each node, Figure 9, at time $t = t + \Delta t$ are then given by:

$$\frac{\partial}{\partial r}\left[k(T)\frac{\partial T}{\partial r}\right] \approx \frac{1}{2\Delta r^2}\left[\left(k_{i+1}^n + k_{i+1}^n\right)T_{i+1}^{n+1} - \left(k_{i+1}^n + 2k_i^n + k_{i-1}^n\right)T_i^{n+1} + \left(k_i^n + k_{i-1}^n\right)T_{i-1}^{n+1}\right] \quad (4.6)$$

$$\frac{k(T)}{r}\frac{\partial T}{\partial r} \approx \frac{k_i^n}{2r\Delta r}\left[T_{i+1}^{n+1} - T_{i-1}^{n+1}\right] \quad (4.7)$$

$$\rho C(T)\frac{\partial T}{\partial t} = \frac{\rho C_i^n}{\Delta t}\left[T_i^{n+1} - T_i^n\right] \quad (4.8)$$

where *n* is the time index, *i* is the radial index, and $r = (i-1)\Delta r$.

Substituting from Equations (4.6)-(4.8) into Equation (4.4) yields:

$$\frac{\rho C_i^n}{\Delta t}\left[T_i^{n+1}-T_i^n\right]=\frac{1}{2\Delta r^2}\left[\left(k_{i+1}^n+k_i^n\right)T_{i+1}^{n+1}-\left(k_{i+1}^n+2k_i^n+k_{i-1}^n\right)T_i^{n+1}+\left(k_i^n+k_{i-1}^n\right)T_{i-1}^{n+1}\right]+$$
$$\frac{k_i^n}{2r\Delta r}\left[T_{i+1}^{n+1}-T_{i-1}^{n+1}\right]+\dot{q}_v(n,i,j) \tag{4.9}$$

By rearranging Equation (4.9) we get:

$$\left[-\frac{\alpha_{ba}\Delta t}{\Delta r^2}+\frac{\alpha\Delta t}{2(i-1)\Delta r^2}\right]T_{i-1}^{n+1}+\left[\frac{2\alpha_{ce}\Delta t}{\Delta r^2}+1\right]T_i^{n+1}+$$
$$\left[-\frac{\alpha_{fo}\Delta t}{\Delta r^2}-\frac{\alpha\Delta t}{2(i-1)\Delta r^2}\right]T_{i+1}^{n+1}=T_i^n+\frac{\alpha\dot{q}_v(n,i,j)\Delta t}{k_i^n} \tag{4.10}$$

Equation (4.10) can be written in the compact form

$$A_iT_{i-1}^{n+1}+B_iT_i^{n+1}+E_iT_{i+1}^{n+1}=G_i^n \tag{4.11}$$

where

$$A_i=\left[-\frac{\alpha_{ba}\Delta t}{\Delta r^2}+\frac{\alpha\Delta t}{2(i-1)\Delta r^2}\right], \tag{4.12.i}$$

$$B_i=\left[\frac{2\alpha_{ce}\Delta t}{\Delta r^2}+1\right], \tag{4.12-ii}$$

$$E_i=\left[-\frac{\alpha_{fo}\Delta t}{\Delta r^2}-\frac{\alpha\Delta t}{2(i-1)\Delta r^2}\right], \tag{4.12-iii}$$

$$G_i^n=T_i^n+\frac{\alpha\dot{q}_v(n,i,j)\Delta t}{k_i^n}. \tag{4.12.iv}$$

and

$$\alpha=\frac{k_i^n}{\rho C_i^n},$$
$$\alpha_{ba}=\frac{\left(k_i^n+k_{i-1}^n\right)}{2\rho C_i^n},$$
$$\alpha_{ce}=\frac{\left(k_{i+1}^n+2k_i^n+k_{i-1}^n\right)}{4\rho C_i^n}, \tag{4.13}$$
$$\alpha_{fo}=\frac{\left(k_{i+1}^n+k_i^n\right)}{2\rho C_i^n}.$$

$$T_i^{n+1} = T_i(t+\Delta t); \quad T_i^n = T_i(t) \tag{4.14}$$

where

$$\dot{q}_v(n,i,j) = \begin{cases} \mathrm{E_f} \sum_{g=1}^{4} \Sigma_\mathrm{f} \Phi^g(n,i,j) \quad [\mathrm{W/m^3}], & i = 1,...,N \\ 0, & i = N+1, M \end{cases} \tag{4.15}$$

where

$\mathrm{E_f}$	Energy per fission [W sec/fission];
Σ_f	Macroscopic fission cross section [1/m];
Φ^g	Group flux [fission/$\mathrm{m^2}$sec];
N	Maximum radial fuel subdivisions;
M	Maximum radial fuel and clad subdivisions;
g	Energy group index;
$\dot{q}_v(n,i,j)$	Heat generation in the i^{th} fuel radial node and the j^{th} axial mesh at time n.

Equation (4.15) represents the interface between the neutronic field and the heat generation in the fuel heat conduction process. It shows that no chemical reactions inside the fuel pellet and between the pellet and the clad are taken into account. Finally, we obtain the following matrix instead of Equation (4.11) which is easily solved using the THOMAS algorithm [64] as follows:

$$\begin{bmatrix} B_1 & E_1 & 0 & 0 & 0 & 0 & 0 & 0 \\ A_2 & B_2 & E_2 & 0 & 0 & 0 & 0 & 0 \\ . & . & . & . & . & . & . & . \\ 0 & 0 & A_i & B_i & E_i & 0 & 0 & 0 \\ . & . & . & . & . & . & . & . \\ 0 & 0 & 0 & A_N & B_N & E_N & 0 & 0 \\ . & . & . & . & . & . & . & . \\ 0 & 0 & 0 & 0 & 0 & 0 & A_M & B_M \end{bmatrix} \begin{bmatrix} T_1^{n+1} \\ T_2^{n+1} \\ . \\ T_i^{n+1} \\ . \\ T_N^{n+1} \\ . \\ T_M^{n+1} \end{bmatrix} = \begin{bmatrix} G_1^n \\ G_2^n \\ . \\ G_i^n \\ . \\ G_N^n \\ . \\ G_M^n \end{bmatrix} \tag{4.16}$$

The solution of the equation system (4.16) is derived as follows:

$$T_M^{n+1} = X_M, \quad T_i^{n+1} = X_i - Y_i . T_{i+1}^{n+1}, \quad i = M-1,...,2$$

$$\mathrm{Y_1} = E_1/B_1, \quad Y_i = \mathrm{E_i}/(B_i - A_i Y_{i-1}), \quad i = 2,..., M-1, M$$

$$X_1 = G_1^n/B_1, \quad X_i = (G_i^n - A_i X_{i-1})/(B_i - A_i Y_{i-1}), \quad i = 2,..., M-1, M$$

In the calculation of this thesis, the core was subdivided into 30 axial and 10 radial nodes per channel. Heat transfer in each fuel element is determined on the basis of one dimensional conduction solution up to 29 axial sections. The moderator in each axial section is not subdivided radially but it is assumed to be adequately represented by an average bulk temperature and average fluid properties. For the heat transfer across the clad-coolant interface, local flow and temperature dependant correlations was used.

(3) Thermal Conductivity and Heat Capacity Approximations

The thermal conductivity of solids is mainly a function of temperature, and can be determined experimentally for most metals. In case of nuclear fuels, the situation is more complicated because the thermal conductivity also becomes a function of radiation because of change of the chemical and physical properties of nuclear materials [21].

For EK-10 fuel material type (Fuel: uranium dioxide; Fuel enrichment 10%; Uranium content: 80 gm/fuel rod; Magnesium content: 37 gm/fuel rod) the thermal conductivity as a function of temperature is based on data of reference [7]:

$$k^{fuel} = 0.2895\,(157.146 - 0.0225\,\mathrm{T_f}) + 0.711(33.9563 - 0.118343\,\mathrm{T_f} + 0.00012743\,\mathrm{T_f^2}) \tag{4.17}$$

The aluminum alloy was used to manufacture the EK-10 type fuel element cladding has the thermal conductivity as a function of temperature of the following form:

$$k^{cladd} = -0.0000606061\ (-2325.28 + \mathrm{T_c})\,(1543.98 + \mathrm{T_c}) \tag{4.18}$$

Where T is the temperature in Kelvin, and k is the thermal conductivity in [W/m K]. Also the heat capacity of the fuel as a function of temperature is:

$$C_p^{fuel} = -0.00041238\,(-1287.95 + T_f)\,(124.413 + T_f) + 0.2895\,(884.831 + 0.409543T_f + 0.0001132T_f^2) \tag{4.19}$$

and for the cladding material the heat capacity is:

$$C_p^{clad} = 905.58 - 0.189027\,T_c + 0.0006199\,\mathrm{T_c^2} \tag{4.20}$$

where T_f, T_c are the fuel and clad temperatures and C_p is the heat capacity in [J/kg K]. See Figure (10)(a-d) for the temperature distributions of the different thermal properties for both fuel and clad used in the BME-Reactor.

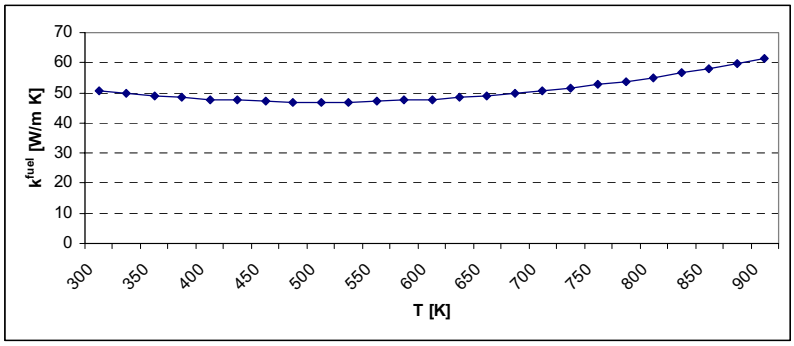

a) Fuel thermal conductivity

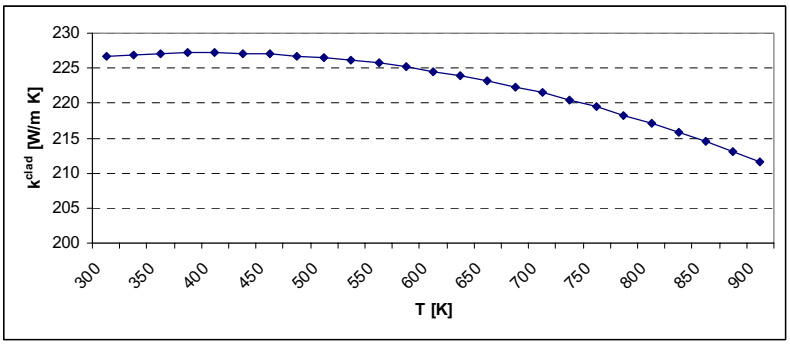

b) Clad thermal conductivity

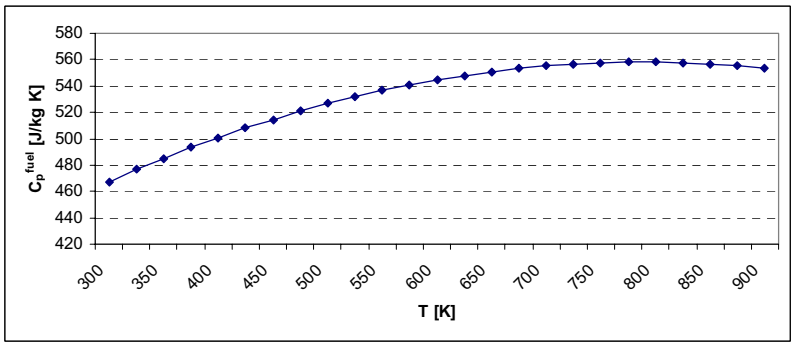

c) Fuel specific heat

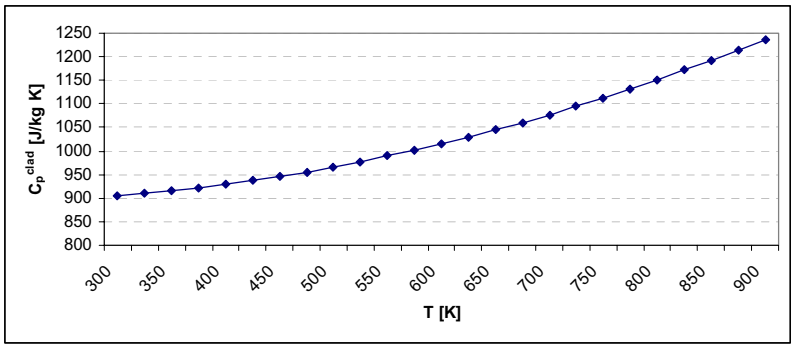

d) Clad specific heat

Figure10. Thermal properties of the BME- Reactor.

b) Hydrodynamic Model

By neglecting the lateral variation of fluid properties and velocity, and, assuming in two-phase flow the vapor and liquid move at the same velocity (no slip), the conservation equations of mass, momentum and energy for a single heated channel can be written in the following form:

"Conservation of mass"

$$\frac{\partial \rho_m}{\partial t} + \frac{\partial G_m}{\partial z} = 0 \tag{4.21}$$

"Conservation of momentum"

$$\frac{\partial G_m}{\partial t} + \frac{\partial}{\partial z}(G_m^2 / \rho_m) = -\frac{\partial P}{\partial z} - \frac{\phi_{\ell_o}^2 (f/\rho)\,|G_m|\,G_m}{2D_e} - \rho_m g \tag{4.22}$$

"Conservation of Energy"

$$\rho_m \frac{\partial H_m}{\partial t} + G_m \frac{\partial H_m}{\partial z} = \frac{\partial P}{\partial z} + \frac{q'' P_h}{A_z} + \frac{G_m}{\rho_m}\left[\frac{\partial P}{\partial z} + \frac{\phi_{\ell_o}^2 (f/\rho)\,|G_m|\,G_m}{2D_e}\right] \tag{4.23}$$

where,

A_z	Channel flow area [m^2];	t	Time [sec];
g	Gravitational acceleration [m/sec^2];	f	Friction factor;
G	Mass flux [kg/m^2 sec];	H	Enthalpy [J/kg];
q''	Heat flux [W/m^2];	P_h	Heated perimeter [m];
$\phi_{\ell_o}^2$	Two phase friction multiplication factor;	z	Axial distance [m];
D_e	Equivalent hydraulic diameter [m];	ρ	Density [kg/m^3].

Under the assumption that the liquid and vapor can be considered as a homogeneous mixture, the above equations are applicable for two phase flow as well as for single phase flow [10-12].

(1) Momentum Integral Model

The MI model (MI) [10-12] is originally developed for boiling water reactors in which the two-phase in which the two-phase is assumed to be one-dimensional vertical, incompressible, homogeneous flow with no slip, thermal-equilibrium but thermally expandable. In the actual calculations, no steam phase will appear. In this model, the sonic effects are neglected. The thermal expansion and enthalpy transport are preserved. The general mass, momentum, and energy equations are used in the form proposed by KAZIMI [10].

In the MI code module, the coolant flow and convective heat transfer problem are described by employing the momentum integral model (MI) [10-12] which solves the governing mass, momentum and energy Equations (4.21)-(4.23) for the entire domain of interest at each time step. The MI model has been found valid especially for small cores and very low coolant velocity like occurring in the BME-Reactor. The MI code can compute the flow and enthalpy distribution in nuclear fuel rod bundles and core for both steady and transient conditions. MI code is very flexible for modeling a reactor core and fuel assemblies.

(2) Differential Equations

It is assumed that the fluid to be incompressible (i.e., $\partial\rho/\partial p = 0$). For this case the equation of state for density, assumed differentiable only with respect to H_m :

$$\rho_m = \rho_m(H_m, \mathrm{p}^*) \tag{4.24}$$

where p^* is a reference pressure. From the mass Equation (4.21) we have

$$\frac{\partial G_m}{\partial z} = -\left(\frac{\partial \rho_m}{\partial H_m}\right)\left(\frac{\partial H_m}{\partial t}\right) \tag{4.25}$$

Integrate the momentum Equation (4.22) over the channel and define G_{avg} as the average mass velocity we have:

$$\frac{\partial G_{avg}}{\partial t} = \frac{1}{L}\left(\Delta P - F\right) \tag{4.26}$$

with

$$\Delta \mathrm{P} = -\int_0^L \frac{\partial \mathrm{P}}{\partial z} dz = \mathrm{P}_{\mathrm{inlet}} - \mathrm{P}_{\mathrm{outlet}}\,, \tag{4.26.i}$$

$$G_{avg} = \frac{1}{L}\int_0^L G_m dz\,, \tag{4.26.ii}$$

$$F = \left(\frac{G_m^2}{\rho_m}\right)_{\mathrm{outlet}} - \left(\frac{G_m^2}{\rho_m}\right)_{\mathrm{inlet}} + \int_0^L \frac{\phi_{\ell_o}^2 (f/\rho)\,|G_m|\,G_m}{2D_e} dz + \int_0^L \rho_m g dz\,. \tag{4.26.iii}$$

where ΔP is the pressure drop and F is the friction factor.

By neglecting the pressure and friction terms in the energy Equation (4.23) we get:

$$\rho_m \frac{\partial H_m}{\partial t} + G_m \frac{\partial H_m}{\partial z} = \frac{q'' P_h}{A_z} \tag{4.27}$$

The equations we need to solve are Equations (4.25), (4.26) and (4.27).

(3) Finite Difference Equations

Using a staggered mesh where $(G_m)_j^n$ is defined at the cell boundary, $(H_m)^n_{j-\frac{1}{2}}$ and $(\rho_m)^n_{j-\frac{1}{2}}$ are defined at the center of cell. Then, finite difference Equation (4.27) yields [11]:

$$(H_m)^{n+1}_{j+\frac{1}{2}} = (H_m)^n_{j+\frac{1}{2}} + \frac{\Delta t}{(\rho_m)^n_{j-\frac{1}{2}} \Delta z}\left[(G_m)^n_{j+1} \frac{(H_m)^n_{j+\frac{3}{2}} - (H_m)^n_{j+\frac{1}{2}}}{2} + (G_m)^n_j \frac{(H_m)^n_{j+\frac{1}{2}} - (H_m)^n_{j-\frac{1}{2}}}{2} \right] + \frac{(q'')^n_{j+\frac{1}{2}} P_h \Delta t}{(A_z (\rho_m)^n_{j-\frac{1}{2}})} \tag{4.28}$$

Here, j is the axial index, and n is the time index as before. Combining Equations (4.25) and (4.27) rearranging and finite differencing yields:

$$\left(1 + \frac{1}{\rho_m}\frac{d\rho_m}{dH_m} H_m\right)\frac{\partial G_m}{\partial z} = -\frac{1}{\rho_m}\left(\frac{d\rho_m}{dH_m}\right)\left[\frac{q'' P_h}{A_z} - \frac{\partial G_m H_m}{\partial z}\right] \tag{4.29}$$

Converting the above equation into a finite difference form yields [11]:

$$1+\left(\frac{H_m}{\rho_m}\frac{d\rho_m}{dH_m}\right)_{j+\frac{1}{2}}\frac{(G_m)_{j+1}-(G_m)_j}{\Delta z}=-\left(\frac{1}{\rho_m}\frac{d\rho_m}{dH_m}\right)_{j+\frac{1}{2}}\bullet$$
$$\left[\frac{(q'')^n_{j+\frac{1}{2}}\cdot P_h}{A_z}-\frac{(G_m)_{j+1}\dfrac{(H_m)_{j+\frac{1}{2}}+(H_m)_{j-\frac{1}{2}}}{2}-(G_m)_j\dfrac{(H_m)_{j+\frac{1}{2}}+(H_m)_{j-\frac{1}{2}}}{2}}{\Delta z}\right] \tag{4.30}$$

By rearranging the last equation we get:

$$(G_m)_{j+1}=(\alpha_j(G_m)_j+\beta_j) \tag{4.31}$$

where

$$\alpha_j=\frac{1+\left(\frac{1}{\rho_m}\frac{d\rho_m}{dH_m}\right)_{j+\frac{1}{2}}\left[\frac{(H_m)_{j+\frac{1}{2}}-(H_m)_{j-\frac{1}{2}}}{2}\right]}{1+\left(\frac{1}{\rho_m}\frac{d\rho_m}{dH_m}\right)_{j+\frac{1}{2}}\left[\frac{(H_m)_{j+\frac{1}{2}}-(H_m)_{j+\frac{3}{2}}}{2}\right]}, \tag{4.32.i}$$

$$\beta_j=\frac{\left(\frac{1}{\rho_m}\frac{d\rho_m}{dH_m}\right)_{j+\frac{1}{2}}\left[\frac{(q'')_{j+\frac{1}{2}}\cdot P_h}{A_z}\Delta z\right]}{1+\left(\frac{1}{\rho_m}\frac{d\rho_m}{dH_m}\right)_{j+\frac{1}{2}}\left[\frac{(H_m)_{j+\frac{1}{2}}-(H_m)_{j+\frac{3}{2}}}{2}\right]}. \tag{4.32.ii}$$

All the above values are referred to the new time step i.e., n+1. Equation (4.26) can be changed into:

$$(G_{avg})^{n+1}=(G_{avg})^n+\frac{\Delta t}{L}(\Delta P^n-F^n) \tag{4.33}$$

From the initial conditions, the enthalpy distribution $(H_m)_{j+1}$ at a new time step can always be calculated by means of Equation (4.28). If $(G_m)_1$ is specified the mass flux distribution can be known from Equation (4.31) and the pressure at the outlet of the

channel can be calculated. But, if the pressure drop is given, G_{avg} at new time step can be obtained from Equation (4.33) and, by the following relation, the value of $(G_m)_1$ can be calculated:

$$(G_m)_1^{n+1} = \frac{1}{\hat{\gamma}^{n+1}}(G_{avg}^{n+1} - \hat{\delta}^{n+1}) \tag{4.34}$$

where

$$\hat{\gamma}^{n+1} = \frac{1}{2N}\sum_{j=1}^{N}\left(\gamma_j^{n+1} + \gamma_{j-1}^{n+1}\right)$$

$$\hat{\delta}^{n+1} = \frac{1}{2N}\sum_{j=1}^{N}\left(\delta_j^{n+1} + \delta_{j-1}^{n+1}\right)$$

and

$$\gamma_j^{n+1} = \alpha_j^{n+1}\gamma_{j-1}^{n+1}, \qquad \gamma_o = 1$$

$$\delta_j^{n+1} = \alpha_j^{i+1}\delta_{j-1}^{n+1} + \beta_j, \quad \delta_o = 0$$

The numerical limitation of the momentum integral model is that:

$$\Delta t \le \Delta z / |U_m| \tag{4.35}$$

where $U_m = \dfrac{G_m}{\rho_m}$ is the mean transport velocity [m/sec].

In Equation (4.31), the parameter $(d\rho_m / dH_m)_{j+\frac{1}{2}}$ is evaluated by the following equation:

$$\left(\frac{d\rho_m}{dH_m}\right)_{j+\frac{1}{2}} = \frac{(\rho_m)_{j-1} - (\rho_m)_j}{(H_m)_{j-1} - (H_m)_j} \tag{4.36}$$

The primary reason for doing so is to avoid the drastic change of the derivative if boiling begins.

When, for a given power distribution inside the core, the thermal-hydraulic module computes the average fuel, clad and coolant temperatures for every mesh point of the finite difference scheme, we are able to calculate the few-group constants of the 3D diffusion equation. (If necessary, we can recalculate the power distribution leading the new temperatures for which the few-group constants can be recalculated and so on until convergence is reached. But, this iteration has been found superfluous in practice). These few-group constants can be obtained by an asymptotic slowing-down and thermalization code (WIMS-D4 -4D in our case). The thermal-hydraulic feedback is taken into account via the recalculation of the few-group constants.

It is needless to say that WIMS-D4 is not run in the framework of the model POWEX-K/MI but the few-group constants are calculated once for ever for some selected values of the fuel, clad and coolant temperatures. We thus obtain tables of the few-group constants with three entries which allow interpolating the few-group constants for every particular set of these three temperatures. We reach now an important point. We reach now to an important point. The range and the selected values of the temperatures should enclose those temperatures which will occur during the studied power excursions. Preliminary calculations have shown that the following temperature ranges would be sufficient:

- From room temperature to 100 °C for the coolant temperature;
- From room temperature to 1600 °C for the fuel temperature;
- From room temperature to 500 °C for the clad temperature.

If, in the actual calculations, anyone of these temperatures gets out of these ranges, we have to enlarge the range of the pre-calculated few-constants. Especially critical is the range of the coolant temperature. Fortunately enough, such cases did not occurred in the actual calculations.

The solution is completely determined by considering the closure relationships, the initial and boundary conditions. The initial distributions of $G_m(z,t)$, $H_m(z,t)$ are assumed as known from the steady state solutions [10]. The heat flux $q''(z,t)$ in a reactor is dependent on the coolant and fuel thermal conditions. Hence, the specification of $q''(z,t)$ is obtained from the effects of the neutronic response and the transient heat conduction in the fuel. The boundary conditions for solving the momentum equation are to be specified as $G_m(0,t)$ at the inlet and $P_m(L,t)$ at the outlet. In the actual calculations we shall assume that the inlet and outlet pressures are specified, see Table 3.

(4) Preliminary Test for the Thermal-hydraulic part

This momentum integral model (MI-Model) have been checked for some types of transients, we show here one of these namely, the sudden pressure reduction in the inlet pressure transient for BWR channel whose outlet is maintained at constant pressure which used as a test of the thermal-hydraulic part, it is compared with the expected behavior histories of normalized flow rate $G_m(z,t)/G_m(0,0)$ mentioned in details in some references [10-12] and a typical results have been obtained, see Figure 11, 12 also we apply the same transient for the BME-Reactor, Figure 13. We can see the averaging trend in this model, i.e., the local mass flux tends to spread out across the whole channel. Table 3 shows the channel geometry properties and the initial and boundary conditions applied for the transient calculations for both BWR and BME-reactor.

The transient condition:

$$P_{in}(t) - P_{out} = 0.5\left[P_{in}(0) - P_{out}\right]\left(1 + e^{-400t}\right) \tag{4.37}$$

Table 3. Channel geometry properties and operating conditions

Operating Condition	**Symbol**	**BWR**	**BME**	**Units**
Channel length	L	3.05	0.5	m
Rod diameter	D	0.0127	0.01	m
Pitch	P	0.01595	0.017	m
Flow area for rod	A_z	0.000128	0.00021	m^2
Equivalent diameter	D_e	0.013	0.027	m
Initial linear heat	q'_o	16.40	0.542	kW/m
Inlet mass flux	G_{inlet}	2302	21.46	kg/m^2 s
Inlet pressure	P_{inlet}	6.96	0.00157	MPa
Outlet pressure	P_{outlet}	6.90	0.00150	MPa
Inlet enthalpy	H_{inlet}	1225.5	84.0	kJ/kg

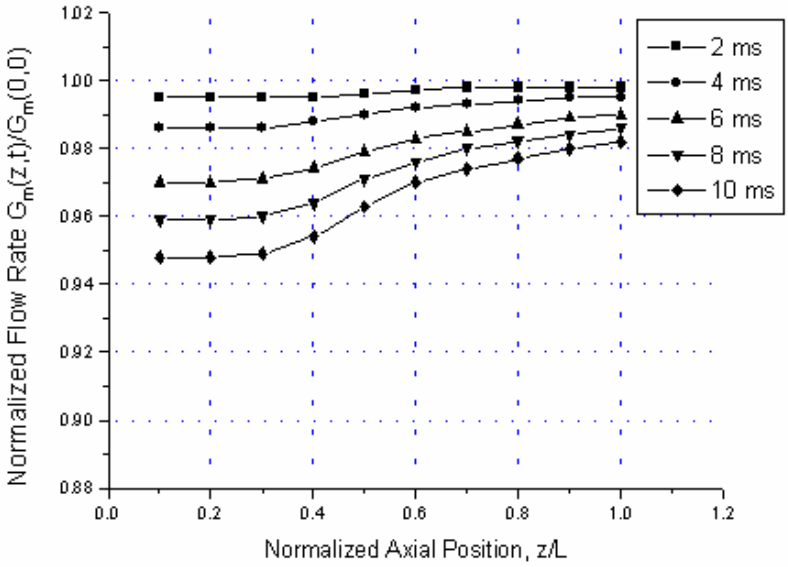

Figure 11. Short-term responses of the BWR inlet pressure transient using MI-code.

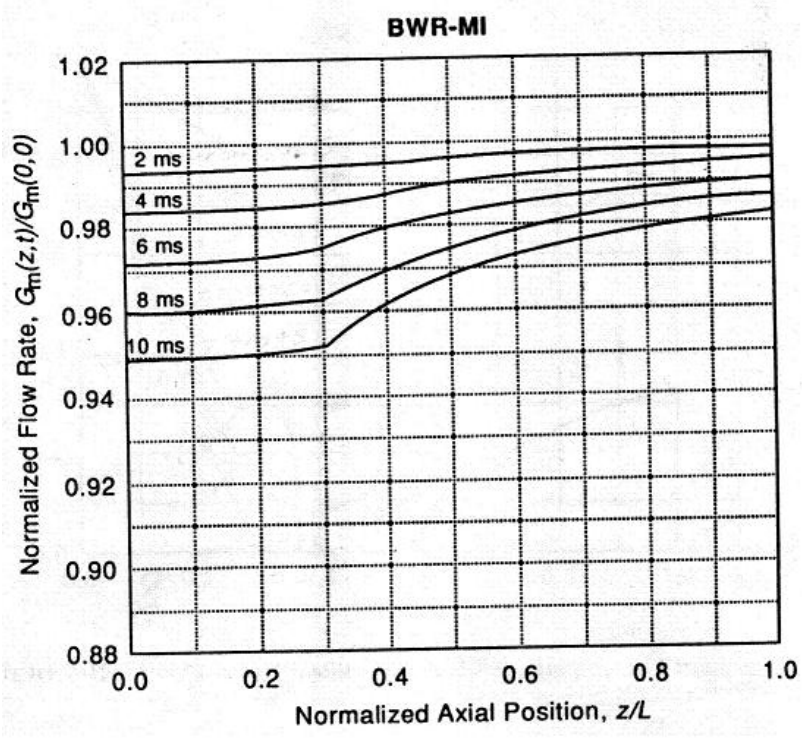

Figure 12. Short-term responses of the BWR inlet pressure transient. [Ref. 10-12]

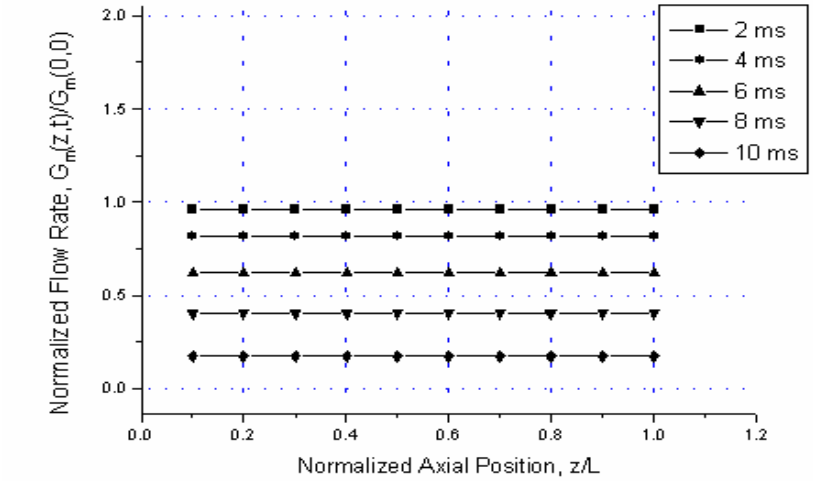

Figure 13. Short-term responses of the BME-Reactor inlet pressure transient.

c) Heat Transfer Closure Relationship

(1) Evaluation of the Turbulent Friction Factor and the Two Phase Friction Multipliers

A commonly encountered expression for the friction factor is the McAdams approximation for a smooth tube where $30{,}000 < \mathrm{Re} < 1{,}000{,}000$

$$f = 0.184\,\mathrm{Re}^{-0.2} \tag{4.38}$$

where Re is Reynolds number defined by:

$$\mathrm{Re} = \frac{G_m D_e}{\mu} \tag{4.39}$$

where μ is the dynamic viscosity [kg/m sec].

Martinelli-Nelson [65] dealt with steam-water data. Their basic assumption was that the two phase multiplier $\phi_{\ell_o}^2$ can be related to the flow quality at any given pressure. Thermodynamic equilibrium and a turbulent-turbulent flow regime were assumed to exist. Jones [66] developed an empirical approximation to the Martinelli-Nelson $\phi_{\ell_o}^2$ for water. Martinelli-Nelson included a synthesized flow rate effect, his correlation were used:

$$\phi_{\ell_o}^2 = \Omega(p, G_m)\left\{1.2\left[\left(\frac{\rho_\ell}{\rho_v}\right)-1\right]x^{0.824}\right\}+1.0 \tag{4.40}$$

where

$$\Omega(p, G_m) = \begin{cases} 1.36 + 0.0005p + 0.1\left(\dfrac{G_m}{10^6}\right) - 0.000714p\left(\dfrac{G_m}{10^6}\right) & \text{for } \left(\dfrac{G_m}{10^6}\right) \le 0.7 \\ 1.26 - 0.0004p + 0.119\left(\dfrac{10^6}{G_m}\right) + 0.00028p\left(\dfrac{10^6}{G_m}\right) & \text{for } \left(\dfrac{G_m}{10^6}\right) > 0.7 \end{cases} \tag{4.41}$$

In the previous relation G_m in lb/hr ft^2, p in psia.

(2) Convective Coolant Heat Transfer Coefficient Evaluation

The Nusselt number may be interpreted as the ratio between convection heat transfer (proportional to $h\Delta t$) and heat transfer due to internal conduction (proportional to $(k/L)\Delta T$:

$$\mathrm{Nu} = \frac{h.\Delta T}{(\lambda / D_e).\Delta T} = \frac{hD_e}{\lambda} \tag{4.42}$$

Equation (4.42) is widely used in heat transfer correlations for evaluation of the heat transfer coefficient. The following relationship has a general validity: $\mathrm{Nu} = f(\mathrm{Re}, \mathrm{Pr}, \mathrm{Gr}, \mathrm{Br})$, where Re, Renolds number, Pr, Prandtl number, Gr, Grashof number, and Br, Brinkman number. In most practical situations, the effects of viscous dissipation are very small so that the Brinkman number may be neglected [67]. The following correlation was used to characterize the heat transfer in both natural and forced convection in BME-Reactor [68]:

$$\mathrm{Nu} = 0.19\left(\mathrm{Gr}^{*}.\mathrm{Pr}\right)^{0.191}.\mathrm{Re}^{0.266} \tag{4.43}$$

And

$$\mathrm{Gr}^{*} = \frac{\mathrm{g}\beta \mathrm{D}_{\mathrm{e}}^{4}\dot{q}''}{\lambda \nu^{2}}, \tag{4.44}$$

$$\mathrm{Pr} = \frac{\mu c_p}{k}, \tag{4.45}$$

$$\mathrm{Re} = \frac{W.D_e}{\nu}. \tag{4.46}$$

where,

h	Convective heat transfer coefficient [W/m^2 K];
g	Acceleration due to gravity [m^2/sec];
β	Expansion coefficient [1/K];
$\dot{q}''$	Surface heat flux, [W/m^2];
k	Thermal conductivity of water [W/m K];
ν	Kinematics viscosity [m^2/sec];
μ	Viscosity [kg/m sec];
c_p	Specific heat [J/kg K];
W	Velocity [m/sec].

Now, Equations (4.1), (4.2), (4.4), (4.5), (4.25), (4.26), (4.27) together with the constitutive relations (4.24) and (4.38) or their corresponding finite difference forms are defining completely our integrated model sought. A code have been written for radial heat conduction in the fuel and a code of thermal-hydraulics of the moderator realizing the momentum integral model and I have coupled them to the neutronic code POWEX-K to form finally the coupled neutronic/thermal-hydraulic code POWEX-K/MI, see Figure 14 for the horizontal section of the BME-Reactor.

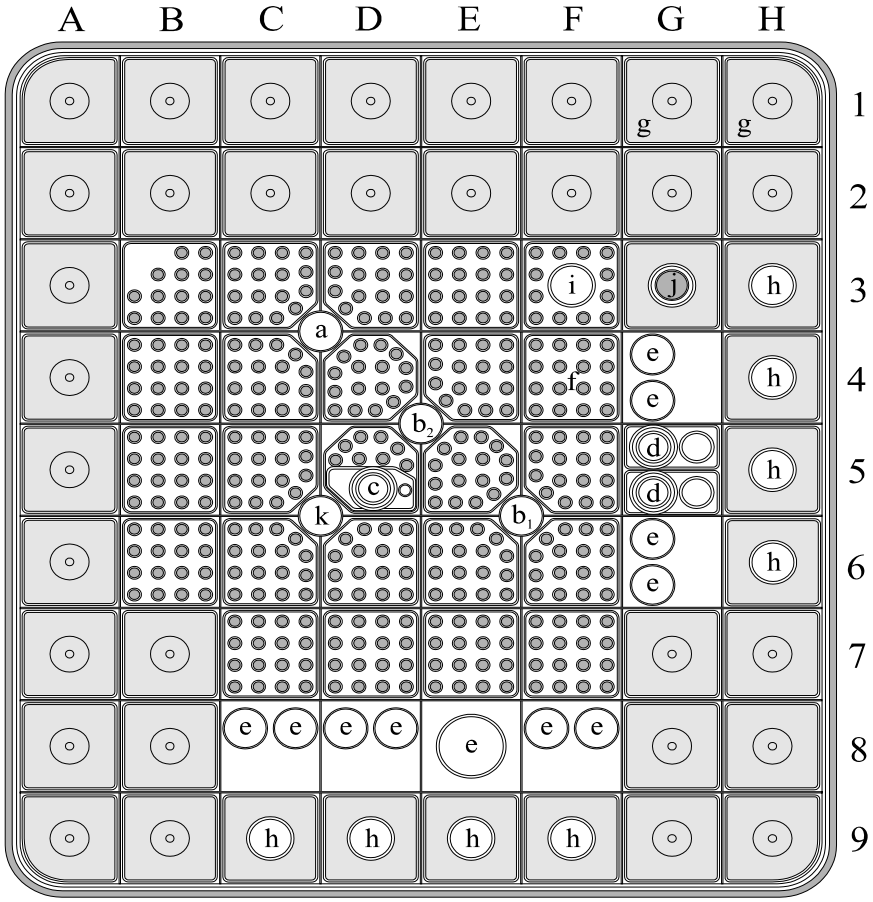

Figure 14. Horizontal section of the BME-Reactor core.
Legend:
f: Fuel Assembly; i: Fuel Assembly with Vertical Irradiation Channel;
g: Graphite Reflector; e: Vertical Irradiation Channel in Water Reflector;
a and k: Automatic and Manual Control Rods; b_1, b_2 : Safety Control Rods; d: Pneumatic Rabbit.

4.3. Group Constant Calculations

The WIMS-D4 code generates the spectral weighted cell averaged cross sections for a wide variety of systems. It uses transport theory for the calculation of the space and energy dependent flux inside the cell and this flux spectrum is used to condense the basic cross sections into group constants. WIMS-D4 is a major software package containing a wide range of lattice and burn-up methods for the design and development of all types of thermal reactor systems including experimental low power facilities as well as commercially operating power reactors. The modular code system is designed for use by all levels of user expertise to solve problems ranging from simple homogeneous systems through the most complex 3D whole core geometries. Central to the aim of WIMS-D4 is use a single physics model treatment of the resonance region that capable to representing all types of reactor within a common framework. It is still one of the few codes capable of dealing with graphite, heavy water and light water

moderated systems as well as problems involving more than one moderator in the reactor [18].

GRACE is a multigroup fast neutron spectrum code which proved to work satisfactorily in generating few-group constants for diffusion calculation. Code GRACE solves the asymptotic neutron transport equation in slab geometry using the Greuling-Goertzel approximation for the slowing down neutron source. It permits the use of both B_1 and P_1 approximations. In the multigroup structure of GRACE a thermal group has been included making possible iteration to criticality of the slab. Group constants as well as energy limits for the thermal energy group must be specified in input. Resonance absorption and fission are taken into account in GRACE, but beside the resonance region, the other energy range in which spectrum variation inside a GRACE microgroups and lattice effects are important is the thermal energy range. These effects are not taken into account by GRACE. Therefore a separate code is needed calculating the same cell average for the thermal energy range. This can be done by THERMOS [19, 20]. For the purpose of feedbacks necessary in power excursion accident of BME-Reactor and by using libraries generated by either WIMS-D4 code or GRACE and THERMOS codes, it is possible to calculate of the group constants as a function of the fuel and moderator temperatures for every particular set of these temperatures. This feedback calculation procedure is implemented into the integrated code POWEX-K/MI. See Appendix A, which show overall strategy flowchart of the whole integrated code.

4.4. Discussion and Conclusion

- Most models for coupled kinetic and thermal-hydraulics consider a point reactor, although, in this thesis a complete description of the 3D-neutronic kinetics is considered.
- A coupled 3D neutronic/thermal-hydraulic integrated code has been developed and, it can simulate the power excursion accidents for a wide range of reactivity insertions of BME-Reactor.
- The simple two phase model, so called momentum integral model is good enough for simulating the thermalhydraulics of the BME-Reactor during power excursions.
- A code has been written for radial heat conduction in the fuel and a code of thermal-hydraulics of the moderator realizing the momentum integral model and they have been coupled with the neutronic code POWEX-K.
- For the feedbacks calculations the cross section libraries generated by using WIMS-D4 code and GRACE and THERMOS codes has been used for calculating the group constants as function of the fuel and moderator temperatures for each node at each time step.

4.5. One Step Forward

Up to now, a complete neutronic/thermal-hydraulic, i.e., POWEX-K/MI, model has been developed for the purpose of simulating power excursion accident in BME-Reactor. Its thermal-hydraulics part is verified for a specific fast transient, although, more verifications and testing for the integrated code POWEX-K/MI will be the subject of the next chapter.

Chapter 5 Nuclear Safety Analysis of the BME-Reactor

The developed POWEX-K/MI) code is verified by two different means: first quantitatively with a BME-Reactor start up experiment, second qualitatively with REMEG point kinetic code. A good agreement was obtained for the former.

This chapter discusses the nuclear safety analysis of the BME-Reactor during power excursions accidents, summarizes the main thesis results of the current work, conclusions, the planned future work that show how to utilize and extend the achieved results.

Up to now this Ph.D. project had investigated the following:

- Comparison between the forward and backward schemes of solution of 2D neutron diffusion equations
- Solution of the 3D time-dependent neutron diffusion and delayed neutron precursor equations.
- Investigating the associated stability and convergence problems for the backward scheme.
- Investigating the coupled neutronic and thermal-hydraulic response during transient.

In this chapter we shall investigate the power excursion accident in BME-Reactor.

5.1. Introduction

For normal reactor operating conditions, it is expected that the rate of heat generation in the fuel will be the same as the rate of removal of heat by the coolant. Any imbalance in this state is likely to bring about a perturbation, which can lead to an accident. Transients induced by reactivity insertions will put the reactor in a super-critical state causing its power to rise suddenly to levels beyond the capabilities of the reactor to remove heat. The transient behavior depends on the design features of the reactor, the rate and magnitude of the reactivity inserted and the operating condition before the initiation of the excursion [69].

The coupled POWEX-K/MI code is used to predict the core behavior under power excursion conditions. Neutron diffusion equations, with four energy groups and six delayed neutrons, are considered to estimate the time-dependent core power. Any mechanism which will cause a decrease in the number of moderating nuclei in the reactor core will lead to a decrease in system reactivity. The mechanisms that may affect the system reactivity are the fuel and moderator expansion by heating only. At the same time, we do not reckon with void production by boiling since we have only a single phase in the actual calculations.

For the calculations performed for BME-Reactor by using the model described in the previous chapter, the input data used are summarized in Table 3 depending on data from reference [7]. In order to have some experimental test of the calculation model, a start-up experiment was simulated: BME-reactor was left alone in a supercritical state with a reactivity of 14 cent and the increase of the neutron flux was observed by means of a neutron detector. The comparison of the experimental and calculated data is discussed in Section 5.2. The calculations simulating power excursion accidents are presented in Sections 5.3 and 5.4. The former is related to a power increase corresponding to the actual excess reactivity (i.e. 0.82 $) of BME-reactor while the latter is related to a real power excursion accident due to a sudden increase of the reactivity from critical to 1.2 $. Since, according to the sense, such reactivities cannot be realized in BME-Reactor, the presented calculated results can not be verified experimentally. In order to have some comparison, the same results are shown for the point kinetics REMEG code. The comparisons give an idea about the improvement brought about by the 3D model with respect to the point kinetics model. A summary of the BME-Reactor core design and thermal-hydraulic parameters used in the following calculations is listed in Table 4.

Table 4. Design and thermal-hydraulic parameters of the BME-Reactor core

Item	Value
Reactor type	Pool type
Reactor power level (kW, thermal)	100
Fuel type	EK-10
Enrichment (% in U-235)	10
Cladding	Aluminum
Moderator and coolant	H_2O
Reflector	Graphite+H_2O
Fuel radius (mm)	3.8
Thickness of the clad (mm)	1.2
Coolant flow rate (m^3/h)	5.8
Coolant inlet temperature ($^\circ$C)	20
Coolant inlet pressure (bar)	1.57
Total number of pins	369

5.2. Start-up Transient Behavior for 14 Cents Reactivity Insertion

The code POWEX-K/MI simulates power excursion accidents. Such a code may not be tested experimentally according to the sense: such a test would destroy the reactor. The only possible test is to simulate a time-dependent reactor state which may be realized under safe conditions. This is a start-up experiment during which the reactor power increases exponentially but slowly. Since such experiments are performed at very low power, no thermal-hydraulic feedbacks need to be taken into account. It follows from this that the thermal-hydraulic module MI of the code was not used in these test calculations i.e., only POWEX-K is used. The group constants were obtained by WIMS-D4 assuming the same temperature for fuel, clad, and moderator (see Section 4.3).

The transient was initiated from a low power of 1 W at ambient temperature of 20 °C without coolant flow. Both safety rods were out and the system was operating at very low power, then the manual and automatic rods were pulled to positions 40 cm and 46 cm, respectively, which assured a slightly supercritical reactor state. The neutron source was in the reactor during the initial phase of the experiment but it was pulled out when the neutron flux reached detectable values. The reactor became supercritical with reactivity equal to 14 cents (approximately) and the doubling time was 44.8 sec. (The uncertainty of the latter value is less than 0.1 sec) Since the POWEX-K/MI code does not allow simulating the presence of the neutron source, the test consists in the calculated value of the doubling time. Now, the code yielded an increasing flux which went over into an exponential with a doubling time of 45 sec. This agreement is excellent. The delayed neutron parameters used in the calculation are given in Table 2 (Section 3.2.1) as calculated by the kinetic version of program GRACE.

Figure 15 illustrates the comparison between the calculations using the POWEX-K/MI code and the measurements. From this plot, one notices the exponential trend of the thermal flux at the measuring channel of BME-Reactor and that the results of simulations performed by POWEX-K/MI are in good agreement with the corresponding experimental data. The small discrepancy at the beginning can be explained by the fact that the code did not simulate the presence of the neutron source which was in the reactor in the initial phase of the experiment.

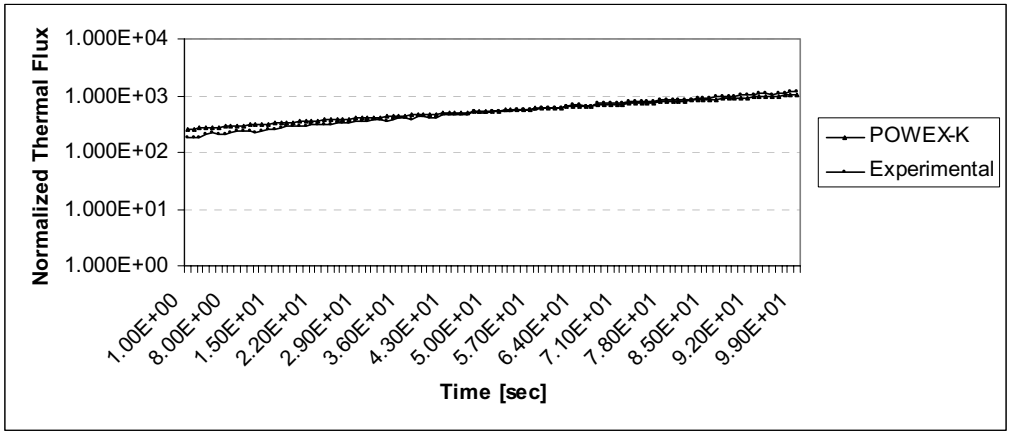

Figure 15. Time dependence of the measured count rate and the thermal flux in the BME-Reactor at 14 cents reactivity

5.3. Power Excursion at the Actual Excess Reactivity

The actual excess reactivity of the BME-Reactor is 0.82 $. We first calculate the consequences of the insertion of this reactivity. In the strict sense of word, this is not a reactivity accident. However, a reactor state with such a reactivity is forbidden by the safety rules. The results of calculations are presented in Figure 16 which shows the power behavior during the transient. The power increases from some 1 W to 1425 W at 4.6 sec. Since the total reactor power was less than 1.5 kW, no temperature increase was

obtained. The corresponding temperature curves are not shown for this reason. The same value for REMEG is 1800 W.

As it can be seen in Figure 16, the reactor power vs. time curve reaches a maximum for 13.48 sec, and it goes down slowly to small values after that. The maximum power is 585 kW. The total energy released during the transient is 17765 kWs for REMEG in the first 75 sec. The fuel, clad, and moderator temperatures rise to 128 °C, 24 °C, and 21 °C, respectively. The reactor power passes through a rather broad maximum, and later, it seems to stabilized a 160 kW. Consequently, this is not an accident having series consequences. The rather time consuming 3D calculations by POWEX-K/MI were not followed over 5 sec for this reason. As it can be seen in Figure 16, REMEG and POWEX-K/MI give nearly the same results for this case.

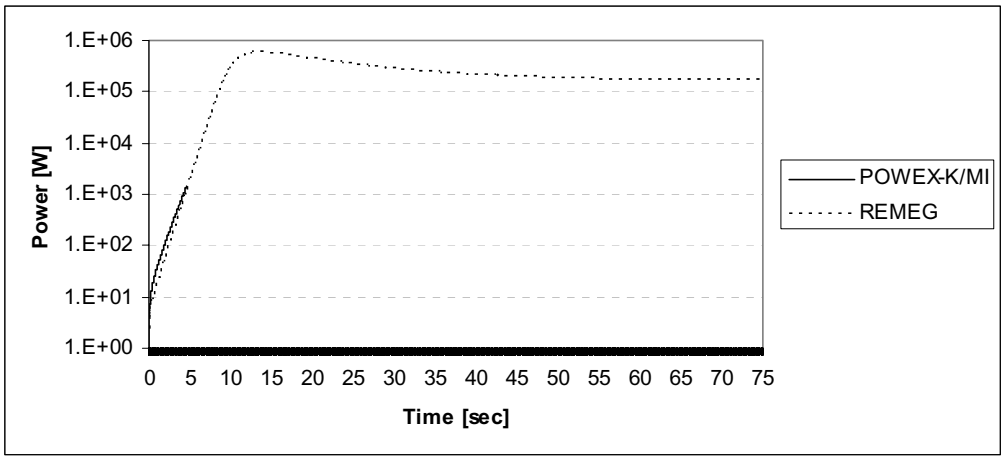

Figure 16. Time behavior of power for ramp reactivity 0.82 $

5.4. Power Excursion at Prompt Supercriticality

The desirable excess reactivity of BME-Reactor is 1.2 $, thus, the power excursion was analyzed for the ramp insertion of this reactivity. In this case, we adjusted a reactor size for which

$$k_{\text{eff}} = 1 + 1.2 * 0.00786 = 1.009432$$

where 0.00786 is the effective delayed neuron fraction for BME-Reactor as calculated by the kinetic version of program GRACE [19]. The adjustment was achieved by adding some fuel rods to the reactor. This is corresponds to the reality because this excess reactivity will be realized in the same way.

Figure 17 shows POWEX-K/MI predictions for the total reactor power. For illustration, the results are compared with the predictions obtained by means of the REMEG code. The figure shows that, starting from 1 W, the power rises following a rapid exponential trend, increasing to 28.9 MW at 0.92 sec then it decreases due to the temperature feedbacks. REMEG increases till 14.7 MW at 0.88 sec, then it decreases. It is remarkable that the two curves deviate from each other very much, namely the 3D

model predicts a power peak which almost two times higher. The shutdown systems would fall in the reactor within 0.5 sec, thus they could reduce the power rise. However, as mentioned in the introduction, we did not assume the operation of the safety rods in order to see the effects of the inherent feedback mechanisms clearly.

The total energy released during the transient is 23687 kW sec, while it is 8256 kW sec for REMEG. If we divide these numbers by the nominal power of BME-reactor, we get 3.9 min and 1.4 min, respectively. This means that the energy released corresponds to the energy released during 3.9 min of nominal operation. In this basis, we do not expect very high temperatures.

Figure 18 shows our model predictions for the fuel temperature while Figure 19 shows the clad and coolant temperatures at a fuel rod located near the core center and in the axial position located at half length of the fuel pin. The fuel temperature goes up to 681 ^{o}C and to 454 ^{o}C according to POWEX-K/MI and REMEG, respectively, for 3.5 sec following the ramp reactivity insertion. The clad temperature increased to 46 ^{o}C according to POWEX-K/MI while only to 28 ^{o}C according to REMEG in 3.5 sec. These figures are much lower than the melting point of aluminum (which is 660.2 ^{o}C). The moderator temperature for both codes is still less than 21 ^{o}C. The calculations were done up to 3.5 seconds until all the heat generated due to the transient went into the moderator and fuel and clad temperatures are stabilized. As in case of the reactor power, the temperatures calculated using POWEX-K/MI model are higher than those calculated by REMEG.

Figure 20 shows the time dependence of the thermal flux during the 1.2 $ transient for three different point inside the core: near the core center (cluster D5), near the reflector (cluster F3) and near a water gap (cluster E7), see Figure 14 for the horizontal section of the BME-Reactor. These three curves are roughly proportional to each other: their ratios are nearly constant in time. This indicates that time dependence and space dependence of the flux are nearly separable from each. Taking into account that this separability is the fundamental assumption of the point kinetic model, the great deviations between the results obtained by POWEX-K/MI and REMEG cannot be explained by the differences of the 3D and point kinetic descriptions. Consequently, the differences are mainly due to a better thermal-hydraulic description of the power excursion by POWEX-K/MI.

Figure 21 shows the development of the normalized mass flux i.e. $G_m(z,t)/G_m(z,0)$ of the hottest channel during the 1.2 $ transient. It can be seen in this figure that the mass flux reaches to more than 16 times its initial value in almost 2 sec. This is a natural convection initiated by the transient. It is an important difference with respect to the REMEG calculation which does not take into account convection.

Figure 22 shows the axial dependence of the thermal flux for the hottest channel during 1.2 $ power excursion. It shows that the flux increase until the time of the power peak (i.e., until 0.92 sec) and it decrease after that due to the thermal-hydraulic feedback effects. (These calculations can be compared with the case which was discussed at the end of Chapter 3 without thermal-hydraulic feedback. i.e., Figure 8.b)

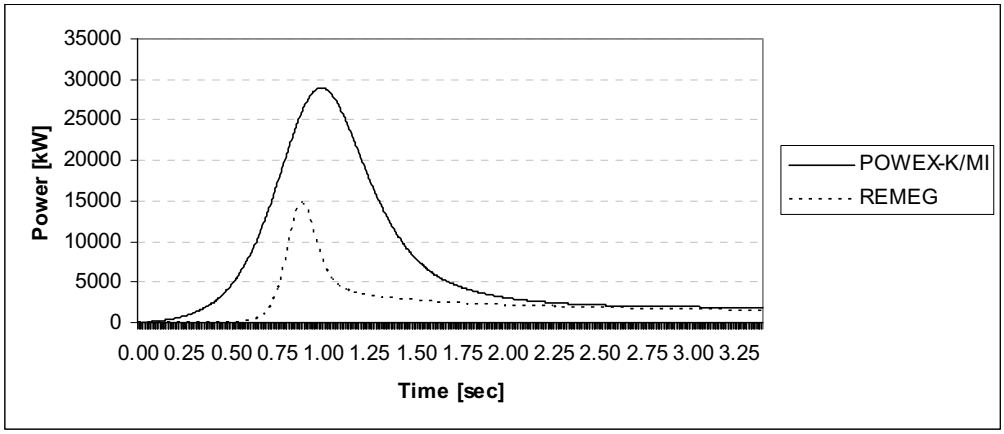

Figure 17. Time behavior of power for ramp reactivity of 1.2 $

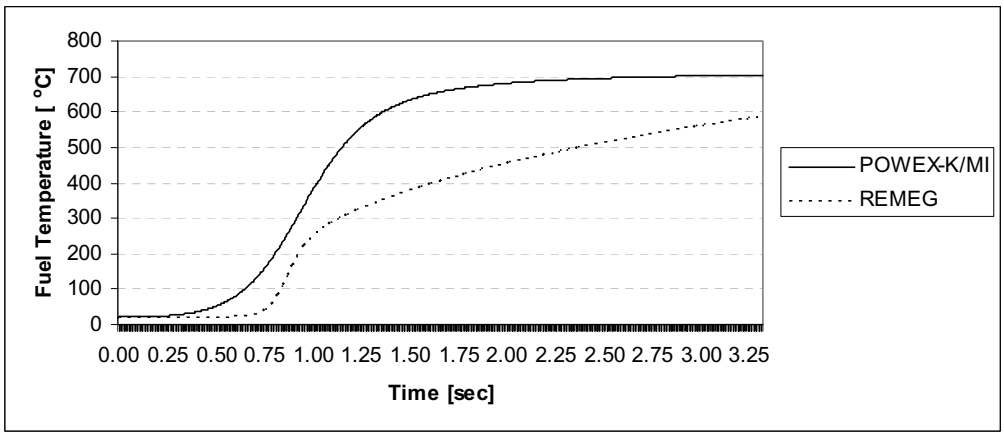

Figure 18. Time behavior of fuel temperature for ramp reactivity of 1.2 $

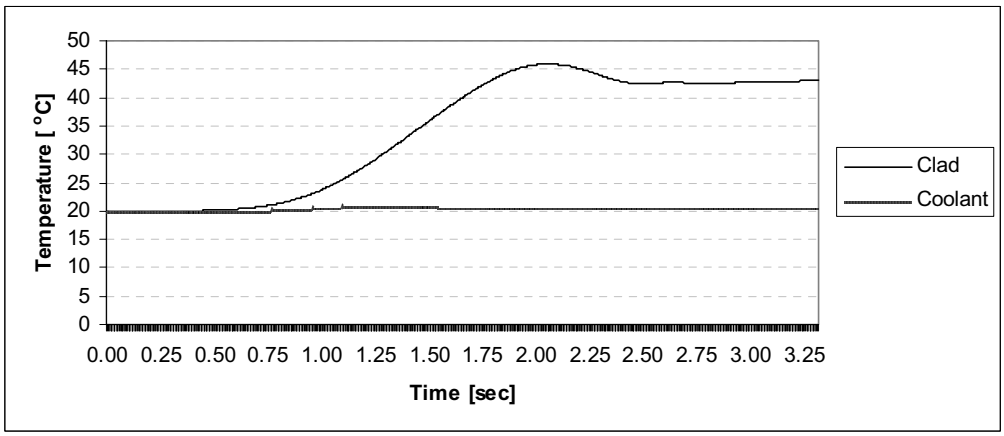

Figure 19. Time behavior of clad and coolant temperature for ramp reactivity of 1.2 $

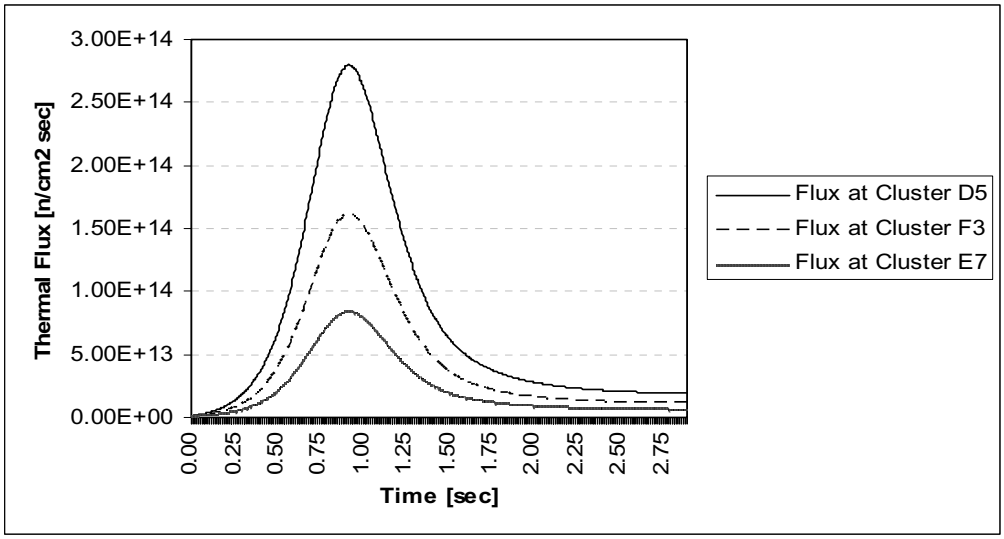

Figure 20. Thermal flux as a function of time in three clusters for 1.2 $

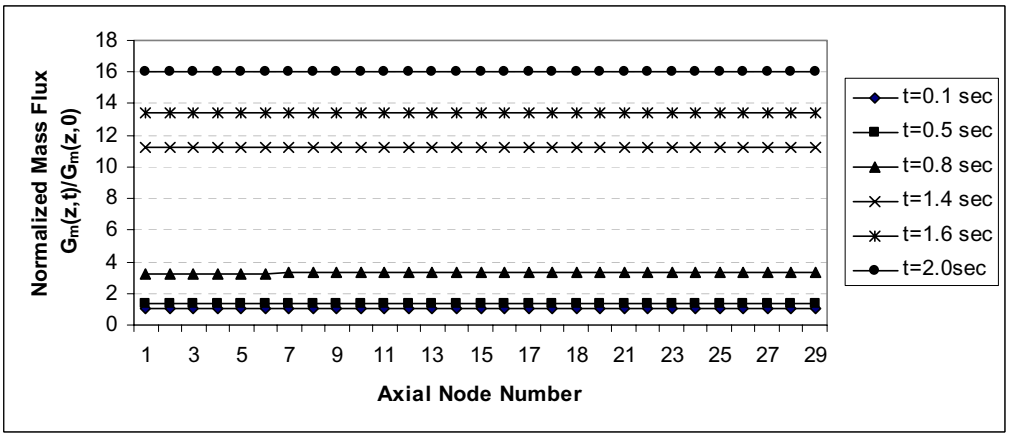

Figure 21. Normalized mass flux of hottest channel for 1.2 $

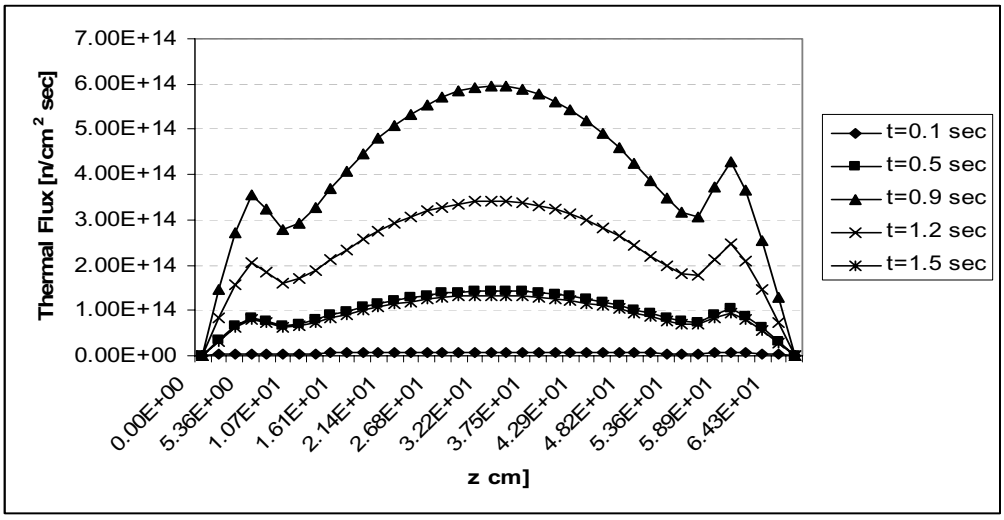

Figure 22. Axial dependence of the thermal flux in the hottest channel for 1.2 $ with feedback

5.5. New Scientific Results

Thesis One

I have written a time dependent 3D-neutron diffusion code adapted for the Training and Research Reactor of Budapest University of Technology and Economics. I have developed a new iteration scheme for solving the discretized neutron group diffusion equations which simplifies the treatment of the delayed neutron precursors and omits the source iteration. In addition, it accelerates the iteration. The method requires a relatively great number of iterations only for the first time steps but, later on, only very few iterations are needed for satisfying the convergent criteria.

Thesis Two

The new iterative scheme deviates from the usual source iteration schemes. Hence, a study of the stability and convergent was needed. Thus, the numerical stability of the new scheme and the convergence of the associated iterative process have been proved. I have proved that the iteration is always convergent for subcritical reactor states while, for supercritical states, it is convergent if the time step Δt sufficiently small:

$$\Delta t < \Delta t_{\max} = \frac{1}{\omega_o}$$

where ω_0 is the asymptotic time constant.

Thesis Three

I have written a code for radial heat conduction in the fuel and the cladding, furthermore a code of thermal-hydraulics of the moderator realizing the so called momentum integral model. I have coupled them to the neutronic part of the POWEX-K/MI code.

Thesis four

By the aid of WIMS-D4 program, for one hand, and GRACE and THERMOS programs, for the other hand, I have calculated the 4-group constants as functions of the fuel, clad, and moderator temperatures for describing the feedbacks necessary in power excursion accidents. For any set of values of this temperature, the actual 4-group constants can be calculated by an interpolation procedure (also included in the POWEX-K/MI code).

Thesis five

I have checked the neutronic part of the program by comparing the calculated results with experimental values measured during a start up experiment for about 14 cents of super-critical reactivity. The agreement was excellent. I have checked the thermal-hydraulic model by comparing the results with values taken from literature.

Thesis six

I have simulated the power excursion accidents for positive reactivity insertions 1.2 $ and 0.82 $ with reactivity feedback calculations. I could conclude that no fuel damage is to be expected for these reactivity insertions. The results were compared with those obtained from the point kinetic program REMEG.

5.6. Future Work

At this point of my research, it becomes visible to me that in this framework, two research programs would be interesting:

- Including the control rods effects inside the neutronic module.
- Changing the core geometry, coolant properties to be applied for power plants which have good benchmark problems.

5.7. Discussion and Conclusions

From the results presented in this chapter, we can draw the following conclusions:

- The comparison of the POWEX-K/MI model predictions with the data measured during the start up experiment at about 14 cents reactivity shows a very good agreement. This is a strong argument in favor of the neutronic part of the model.
- From the comparisons with the results of the point kinetic REMEG code, we may conclude that the 3D model predicts the reactivity accident more severe both as far as peak powers and temperatures are concerned. This is due to a better thermal-hydraulic description by POWEX-K/MI.
- Even for 1.2 $ reactivity insertion, we need not reckon with the melting of the clad and boiling of the moderator.

Appendices

Appendix A The Iterative Scheme Flow Chart

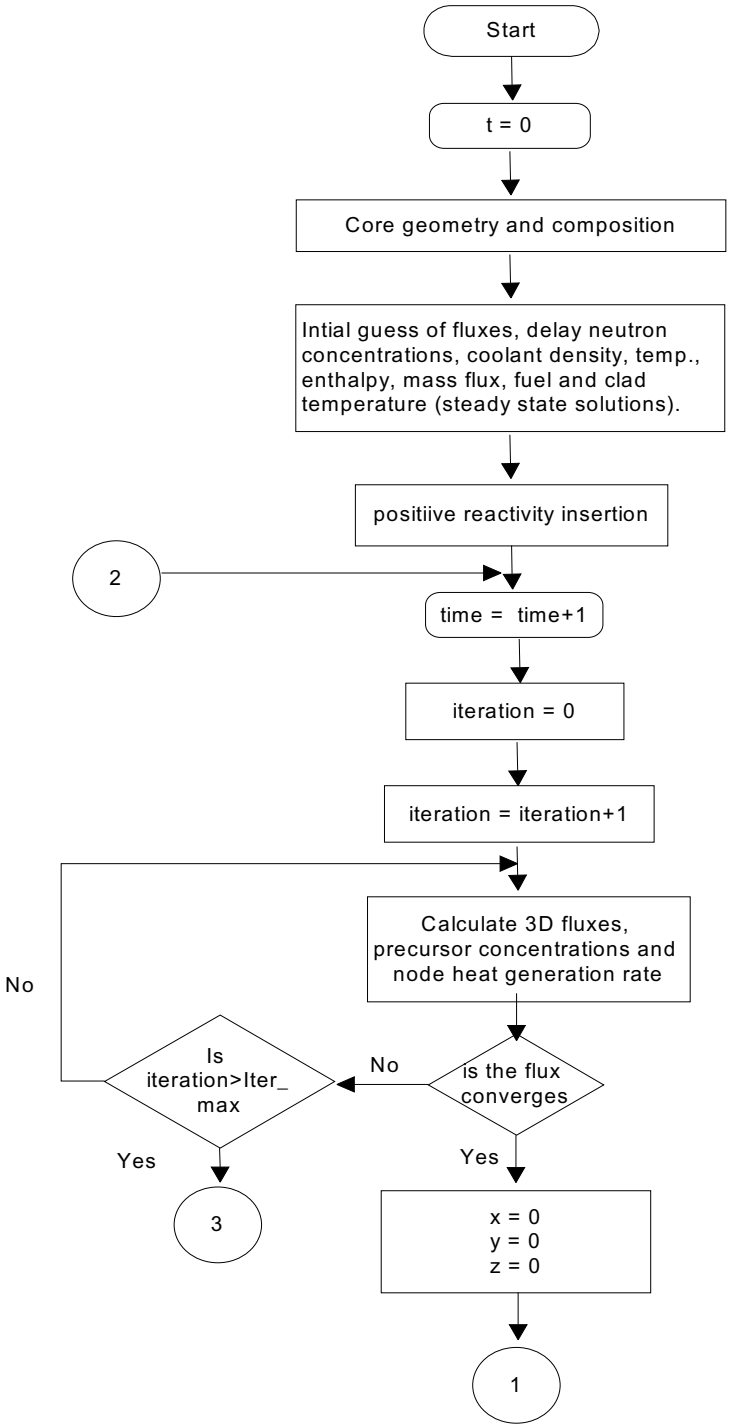

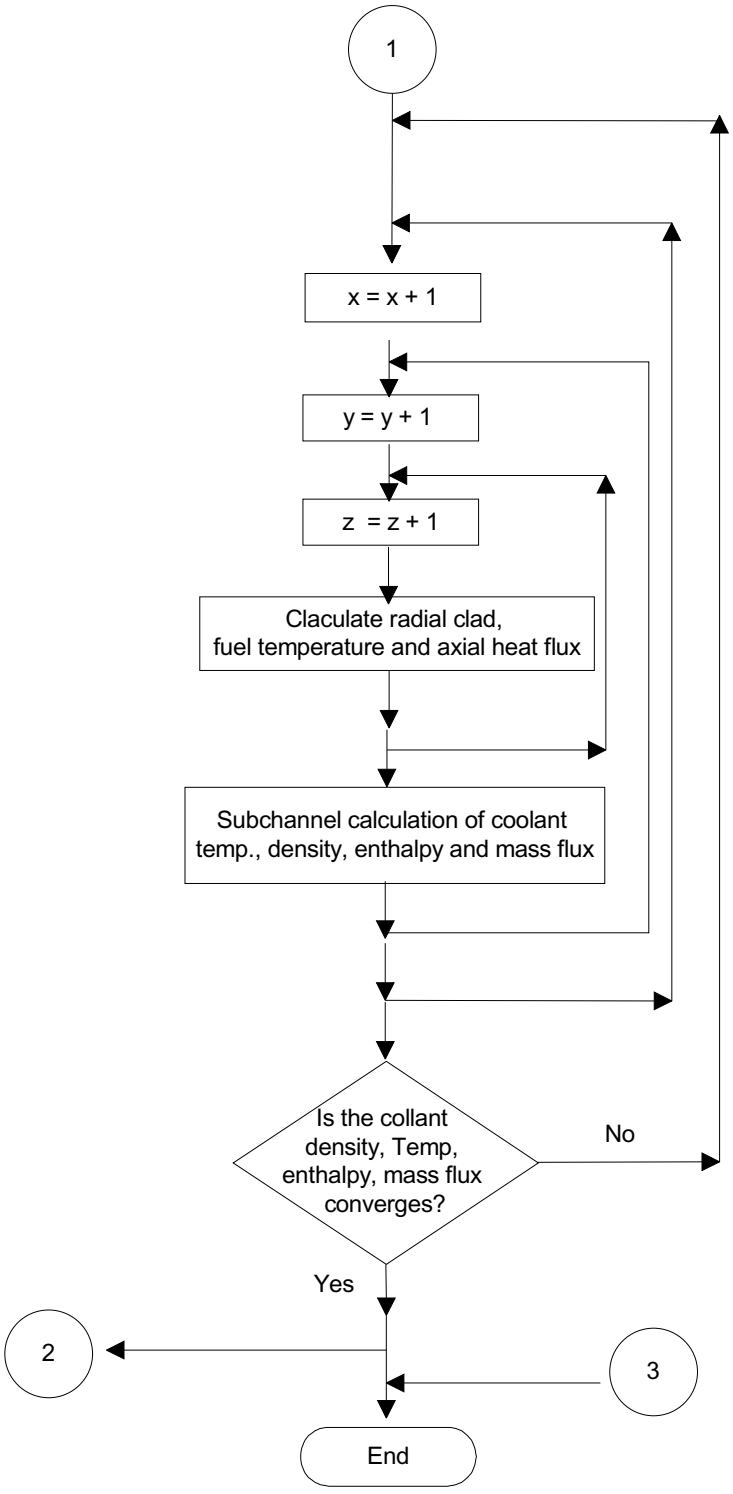
1
x = x + 1
y = y + 1
z = z + 1
Claculate radial clad,
fuel temperature and axial heat flux
Subchannel calculation of coolant
temp., density, enthalpy and mass flux
Is the collant
density, Temp,
enthalpy, mass flux
converges?
No
Yes
2
3
End

References

[1] B. Pershagen, in: Light Water Reactor Safety, Pergamon Press, Oxford, 1989.
[2] D. Ginestar, J. Marín, G. Verdú, Multilevel Methods to Solve the Neutron Diffusion Equation, Applied Mathematical Modelling 25, 463-477, 2001.
[3] R . Bru, D. Ginestar and J. Marín, Iterative Schemes for the Neutron Diffusion Equation, Computers and Mathematics with Applications 44, 1307-1323, 2002.
[4] T. J. Thompson and J. G. Beckerly, The Technology of Nuclear Reactor Safety, Vol. 1, Reactor Physics and Control, The M.I.T. Press, Cambridge, Massachusetts, 1964.
[5] Technical Documentation of the Training Reactor of the Budapest University of Technology and Economics.
[6] G. Legradi, A. Aszodi and G. Por, Investigation of Slightly Forced Buoyant Flow in a Training Reactor, The International conference of Nuclear Energy in Central Europe, Portoroz, Slovenia, Sep.10-13, 2001.
[7] Z. Szatmáry, Nuclear Safety Report of BME-Training Reactor, Budapest University of Technolgy, Institute of Nuclear Techniques, 1996.
[8] J.J. Duderstadt and L.J. Hamilton, Nuclear Reactor Analysis, John Wiley & Sons, New York, 1976.
[9] S.M. Ghiaasiaan, A.T. Wassel and J.L. Farr, Heat Conduction in Nuclear Fuel Rods, Nuclear Engineering and Design 85, 89-96, 1985.
[10] Neil E. Todreas, and Mujid S. Kazimi, Nuclear Systems II: Elements of Thermal-hydraulic Design, Hemisphere Publishing Coordination, New York, 1990.
[11] M. Lee, and M. S. Kazimi, Transient Response of a Single Heated Channel, MITNE-271, July 25, 1985.
[12] J. E. Meyer, Hydrodynamic Models for the Treatment of Reactor Thermal Transients, Nucl. Sci. & Eng., 10, 269-277, 1961.
[13] S. Nakamura, Computational Methods in Engineering and Science, 93-95, 1977.
[14] R. S. Varga, Matrix Iterative Analysis, Prentice-Hall, Englewood Cliffs, N.J., 1962.
[15] Eugene L. Wachspress, Iterative Solution of Elliptic Systems and Applications to the Neutron Diffusion Equation of Reactor Physics, Prentice-Hall, Englewood Cliffs, N.J, 1966.
[16] T.M. Sutton & B.N. Aviles, Diffusion Theory for Spatial Kinetics Calculations, Progress in Nuclear Energy, 30, 119-182, 1995.
[17] Gy.Csom, F.Lévai, S.Fehér and J.Szondi, Development of the Emergency Response Procedures Plan for the BME-Training Reactor, Part II, Budapest, BME-NTI-178/89, 1988.
[18] T.D. Newton, and J.I. Hutton, The Next Generation WIMS-D4 Lattice Code, PHYSOR, October 7 10, Seoul, Korea, 2002.
[19] Z. Szatmáry, J. Valkó, GRACE- A Multigroup Fast Neutron Spectrum Code, Central Research Institute for Physics, Budapest, KFKI-70-14-RPT, 1977.
[20] J. Valkó, RJT1-THERMOS
[21] F. M. Bsebsu, Thermal-hydraulic Analysis of Water Cooled Nuclear Research Reactors, Thesis, Budapest University of Technology and Economics, Department of Energy, 2001.
[22] C. Housiadas, Lumped Parameters Analysis of Coupled Kinetics and Thermal-hydraulics for Small Reactors, Annals of Nuclear Energy, 29, 1315-1325, 2002.
[23] Rubina Nasir, Nasir M. Mirza, and Sikander M. Mirza, Sensitivity of Reactivity Insertion Limits with respect to Safety Parameters in a Typical MTR, Ann. Nucl. Energy, Vol. 26, pp.1517-1535, 1999.
[24] D.E. Cullen, et al., Applications in Nuclear Data and Reactor Physics. World Scientific, Vienna, Austria; 765-819, 1986.

[25] A.F. Henry, Space-time Reactor Kinetics, 22.243 Course notes, Massachusetts Institute of Technology, 1969.
[26] W.M. Stacey, Jr., Nucl. Sci. Eng., 34, 45, 1968.
[27] K. Ott, Nucl. Sci. Eng., 26, 563, 1966.
[28] W.R. Cadwell, A.F. Henry, and A.J. Vigilotti, WIGLE-A Program for the Solution of the Two-group, Space-time Diffusion Equations in Slab Geometry, WAPD-TM-416, Bettis Atomic Power Laboratory, 1964.
[29] A.F. Henry, and A.V. Vota, WIGL2-A Program for the Solution of the One-dimensional, Two group, Space-time Diffusion Equations accounting for Temperature, Xenon, and Control Feedback. Bettis Atomic Power Laboratory Report WAPD-TM-532, 1965.
[30] J.B. Yasinky et.al., TWIGL-A Program to Solve the Two-dimensional, Two-group, Space-time Neutron Diffusion Equations with Temperature Feedback, WAPD-TM-743, Bettis Atomic Power Laboratory, 1968.
[31] V.G. Zimin, H. Ninokata, Nodal Neutron Kinetic Model based on Nonlinear Iteration Procedure for LWR Analysis. Ann. Nucl. Energy 25, 507–528, 1998.
[32] P.J. Turinsky, M.K. Al-chalabi, et al., NESTLE: A Few-Group Neutron Diffusion Equation Solver Utilizing the Nodal Expansion Method for Eigenvalue, Adjoint, Fixed-Source Steady-state and Transient Problems. EGG-NRE-11406, 1994.
[33] C.W. Stewart, C.A. Mcmonagle, et al., Core Thermal Model: COBRA-IV Development and Applications. BNWL-2212, NRC-4. Pacific Northwest Laboratories, 1977a.
[34] C.W. Stewart, C.A. Mcmonagle, et al., COBRA-IV-I: The Model and the Method. BNWL-2214, NRC-4. Pacific Northwest Laboratories, 1977b.
[35] Chengkui Liao, Zhongsheng Xie, The Coupled Kinetic and Thermal-hydraulic Three Dimensional Code System NLSANMT/COBRA-IV for PWR Core Transient Analysis, Annals of Nuclear Energy 30, 405–412, 2003.
[36] H. Finnemann, A. Galati, NEACRP 3-D LWR Core Transient Benchmark, Final Specification, NEACRP-L-335 (Revision 1), October 1991 (January 1992).
[37] H. Finnemann, H. Bauer, A. Galati, R. Martinelli, Results of LWR Core Transient Benchmark, OECD Nuclear Energy Agency Report, NEA/NSC/DOC(93)25, October 1993.
[38] M.P. Knight, P. Bryce, Derivation of a Refined PANTHER Solution to the NEACRP PWR Rod Ejection Transient. In: Proceedings of the Joint International Conf. on Mathematical Methods and Supercomputing for Nuclear Applications, Vol. 1, Saratoga Springs, 5–9, October, p. 302, 1997.
[39] C.K. Liao, Study on Numerical Method for Three Dimensional Nodal Space-Time Neutron Kinetic Equations and Coupled Neutronic/Thermal-Hydraulic Core Transient Analysis. PhD Thesis, Xi'an Jiaotong University, China, 2002.
[40] Ri Keresztu´, A. Jakob, L., A Nodal Method for Solving the Time-depending Diffusion Equation in the IQS Approximation. FKI-1991-5/Greport, 1991.
[41] A. Keresztúri, et.al., Development and Validation of the Three-dimensional Dynamic Code—KIKO3D, Annals of Nuclear Energy 30 93–120, 2003.
[42] AGNES Project Executive Summary, Budapest, 1994.
[43] J. Gado´, et al., VVER Reactor Physics code Applications. In: Proc. of the International Conference on Reactor Physics and Reactor Computations, Tel-Aviv, Israel, 1994.
[44] G. Lerchl, H. Austregesilo, The ATHLET Code Documentation Package, GRS-P-1/Vol. 1.: User's Manual, 1995.

[45] N. Kostadin Ivanov, Features and Performance of a Coupled Three-dimensional Thermal-hydraulic/kinetics TRAC-PF1/NEM Pressurized Water Reactor (PWR) analysis code, Annals of Nuclear Energy 26 1407-1417, 1999.
[46] N.M. Schnurr, et al., TRAC-PF1/MOD2: Volume 1. Theory Manual, Los Alamos National Laboratory Report LA-12031-M, Vol. I, NUREG/CR-5673, 1992.
[47] B.R. Bandini, A Three Dimensional Transient Neutronics Routine for the TRAC-PF1 Reactor Thermal-hydraulic Computer Code, Ph.D. thesis, The Pennsylvania State University, 1990.
[48] K.N. Ivanov, A.J. Baratta, B.R. Bandini, Three-dimensional NEM/TRAC-PF1 Rod Ejection Benchmark Analyses. TANSAO 72, 343, 1995a.
[49] A.F. Henry, Refinements in Accuracy of Coarse-Mesh Finite-Difference Solution of the group diffusion equations, 447, Vienna, 17-21 January, 1972.
[50] A.F. Henry, Nuclear Reactor Analysis, MIT Press, Cambridge, Massachusetts, 1975
[51] Weston M. Stacey, Nuclear Reactor Physics, John Wiley & Sons, Inc., Canada, 2001.
[52] K. F. Hansen & S. R. Johnson, GAKIN – A One Dimensional Multigroup Kinetics Code, GA-7543, General Atomic, 1967.
[53] M. R. Buckner & J. W. Stewart, Multidimensional Space-time Nuclear Reactor Kinetics Studies–Part I, Nucl. Sci. and Eng, 59, p.289-297, 1976.
[54] C.H. Adams, Current Trends in Methods for Neutron Diffusion Calculations, Nucl. Sci. Eng., 64, 552-562, 1977.
[55] L.A. Hageman and D.Young, Applied Iterative Methods, Academic Press, New York, 1981.
[56] Zbigniew I. Woznicki, The Numerical Analysis of Eigenvalue Problem Solutions in the Multigroup Neutron Diffusion Theory, Progress in Nuclear Energy, Vol. 33, No. 3, 301-391, 1998.
[57] S. M. Khaled, Z. Szatmáry, Time Dependent Calculations for the Training Reactor of Budapest University of Technology and Eonomics, 4th International Conference of PHD Students, University of Miskolc, Hungary, pp. 69-74, 11-17 August 2003.
[58] S. M. Khaled, Z. Szatmáry, Two-dimensional Time Dependent Calculations for the Training Reactor of Budapest University of Technology and Economic, Romanian Reports in Physics, Vol. 57, no. 1, 53–60, 2005.
[59] Z. Szatmary, Introduction to Reactor Physics. Hungarian Academy of Science, ISBN 9630577348, 2000.
[60] S. M. Khaled and Z. Szatmáry, Numerical Method for Solving the Three-dimensional Time-dependent Neutron Diffusion Equation, Int. J. Nuclear Energy Science and Technology, Vol.1, 4, 297-311, 2005
[61] Atul A. Karve, Rizwan uddin, and J.J. Dorning, Stability Analysis of BWR Nuclear-coupled Thermal-hydraulics using a Simple Model, Nuclear Engineering and Design 177, 155–177, 1997.
[62] S. M. Khaled, Power Excursion of the Training and Research Reactor of Budapest University, (Submitted).
[63] J.P. Holman, Heat Transfer. McGraw-Hill Companies. IAEA Safety Guide on the Assessment of Research Reactors and Preparation of the Safety Analysis Report, 1992. Safety Series 35-G1, 1990.
[64] A. Gourdin, M. Boumahart, Méthods Numériques Appliquées. Office des Publications Universitaires, Alger, 1991.
[65] R. C., Martinelli and D. B. Nelson, Prediction of Pressure Drop During Forced Circulation Boiling of Water, Trans. ASME 70:695, 1948.

[66] A. B. Jones, Hydrodynamic Stability of Boiling Channel, KAPL-2170, Knolls Atomic Power Laboratory, 1961.
[67] M. Cumo and A. Naviglio, Thermal-hydraulics, Vol. I, CRC Press, Inc., Boca Raton, Florida, 1988.
[68] S. Konczol, Investigation of Heat Transfer for Nuclear Power Plant Fuel Element, Diploma Work, Dept. of Heat Energy, Budapest University of Technology, 1973.
[69] E.H.K. Akaho, B.T. Maakuu, Simulation of Reactivity in Miniature Neutron Source Reactor Core, Nuclear Engineering and Design 213, 31-42, 2002.

Index

B

C

D

E

F

G

H

I

K

M

N

P

R

S

T

W